Development, Characterization and Electrochemical Behavior of Lanthanum and Cerium Incorporated Zeolite-Modified Electrodes

BY

ISMAIL ABDULAZEEZ

A Thesis Presented to the

DEANSHIP OF GRADUATE STUDIES

KING FAHD UNIVERSITY OF PETROLEUM & MINERALS

DHAHRAN, SAUDI ARABIA

In Partial Fulfillment of the

Requirements for the Degree of

MASTER OF SCIENCE

In

CHEMISTRY

MAY 2015

KING FAHD UNIVERSITY OF PETROLEUM & MINERALS

DHAHRAN- 31261, SAUDI ARABIA

DEANSHIP OF GRADUATE STUDIES

This thesis, written by **Ismail Abdulazeez** under the direction of his thesis advisor and approved by his thesis committee, has been presented to and accepted by the Dean of Graduate Studies, in partial fulfillment of the requirements for the degree of **MASTER OF SCIENCE in CHEMISTRY**

Thesis committee

Dr. A. Al-Betar (Advisor)

Dr. A. Kawde (Co-Advisor)

Dr. Oki Muraza (Member)

Dr. Tawfik Saleh (Member)

Dr. Nisar Ullah (Member)

Dr. Abdulaziz Al-Saadi

Department Chairman

Dr. Salam A. Zummo

Dean of Graduate Studies

عمادة الدراسات العليا

DEANSHIP OF GRADUATE STUDIES

19/5/15

Date

Dedicated to my beloved parent and my beloved wife whose continuous prayers and inspiration led to the accomplishment of this study

ACKNOWLEDGEMENT

I would like to begin by expressing my sincere gratitude to my creator, the sustainer of the universe and master of the Day of Judgement, Subhanahu Wa Ta'ala who created me and gave me the strength and wisdom to accomplish this yet another goal in my life. May His peace and blessings be upon the last of His messengers, Muhammad (SAW), his family, his companions and upon those who follow them in piety until the Day of Judgement.

My profound gratitude goes to the following individuals who contributed immensely towards the accomplishment of this work. First, I will like to acknowledge my advisor Dr. Abdul-Rahman Al-Betar for his constant help, patience and guidance throughout this work. I don't know what I would have done without you sir. I want to say thank you for everything. I also want to thank my co-advisor Dr. Abdel-Nasser Kawde who played the role of a father, a mentor and a guardian throughout this work. I cannot find the words to express my gratitude to you sir. I also appreciate the support received from the other committee members, Dr. Oki Muraza, Dr. Tawfik Saleh and Dr. Nisar Ullah.

I also wish to appreciate the entire faculty and staff of chemistry department too numerous to mention, particularly the chairman Dr. Abdulaziz Al-Saadi and the graduate coordinator Prof. Bassam El-Ali for their support always.

Finally, to the university, the kingdom and my fellow Nigerians and friends from other nationalities at KFUPM I wish to say a big thank you for giving me the opportunity to undertake this study and for making my stay at KFUPM a worthy one. Thank you all.

TABLE OF CONTENTS

LIST OF TABLES

LIST OF FIGURES

LIST OF EQUATIONS

LIST OF ABBREVIATIONS

AAS:	Atomic absorption spectrometry
ASV:	Anodic stripping voltammetry
CV:	Cyclic voltammetry
CSV:	Cathodic stripping voltammetry
CME:	Chemically-modified electrode
DPV:	Differential pulse voltammetry
DME:	Dropping mercury electrode
DDW:	Double de-ionized water
EPA:	Environmental protection agency
EDX:	Energy dispersive x-ray spectrometry
FCC:	Fluid catalytic cracking
GFAAS:	Graphite furnace atomic absorption spectrometry
ICP-OES:	Inductively coupled plasma-Optical emission spectrometry
ICP-MS:	Inductively coupled plasma-Mass spectrometry
IZA:	International zeolite association
LSV:	Linear sweep voltammetry

LOD:	Limit of detection
MCL:	Maximum contaminant level
MOR:	Mordenite
MAS:	Magic angle spinning
NPV:	Normal pulse voltammetry
NMR:	Nuclear magnetic resonance spectrometry
ppm:	Parts per million
ppb:	Parts per billion
RE:	Rare earth
rpm:	Revolutions per minute
SWV:	Square wave voltammetry
SEM:	Scanning emission microscopy
SWASV:	Square wave anodic stripping voltammetry
WE:	Working electrode
XRD:	X-ray diffraction spectrometry
ZME:	Zeolite-modified electrode
ZMCPE:	Zeolite-modified carbon paste electrode

Abstract

Name **Ismail Abdulazeez**

Title **Development, Characterization and Electrochemical Behavior of La and Ce - Incorporated Zeolite Modified Electrodes**

Major Field **Chemistry**

Date **May 2015**

Rare earth impregnated zeolite-modified carbon paste electrode (RE-ZMCPE) has been investigated as an alternative electrode for the anodic stripping voltammetric detection of Pb (II) and Cd (II) ions. The RE-ZMCPE which was produced-in-house by first carrying out the synthesis of mordenite zeolite with molar composition $6Na_2O:Al_2O_3:30SiO_2:780H_2O$ and characterized by XRD, SEM, EDX and NMR before La and Ce-impregnation, displays comparable results to those of other modified electrodes for similar analyses. Deposition of the metal onto the surface of the electrodes was accomplished by holding the electrode at a potential of -1.2 V (vs Ag/AgCl) for 120 sec followed by a square wave stripping scan from -1.6 to 0 V. Calibration plots obtained by carrying out a stripping analysis of Pb (II) and Cd (II) shows a good linearity over the metal ion concentrations with detection limits 0.225 µg L^{-1} and 0.122 µg L^{-1} at the La-ZMCPE for Pb (II) and Cd (II) detection, and 0.07 µg L^{-1} and 0.046 µg L^{-1} at Ce-ZMCPE for Pb (II) and Cd (II) detection, respectively. The electrodes displayed good reproducibility with RSD 3.02% and 2.23% for both La-ZMCPE and Ce-ZMCPE. Overall, the electrode exhibits a potential to be used for analyzing environmental samples due to their inexpensiveness, ease of fabrication and lack of toxicity compared to mercury-based electrodes.

Master of Science Degree

King Fahd University of Petroleum and Minerals

Dhahran – Saudi Arabia

Abstract (Arabic)

خلاصة الرسالة

الاســــــــــم إسماعيل عبدالعزيز

عنوان الرسالة تطوير وتشخيص التصرف الالكتروكيميائي لأقطاب الزيوليت المشوبة بالعناصر La و Ce

التخصــــــص كيمياء

التاريـــــــخ مايو 2015

تم التحقيق من أثر العناصر الأرضية النادرة عند تشويبها بالزيوليت وعملها مع قطب عجينة الكربون (RE-ZMCPE)باعتبارها قطب بديل للكشف عن أيونات الرصاص (II) والكادميوم (II) . والتي تم إنتاجها في المعمل داخليا بواسطة تصنيع الزيوليت موردينايت والذي له التكوين المولي المحدد $(6Na_2O:Al_2O_3:30SiO_2:780H_2O)$. وقد تم التوصيف بواسطة عدة أجهزة (XRD ، SEM، EDX ، NMR) قبل التشويب بالعناصر الارضية النادرة (La, Ce). وكانت النتائج قابلة للمقارنة مع نتائج أقطاب أخرى معدلة لتحليلات مماثلة. كما تم ترسب المعادن على سطح الأقطاب من خلال عقد القطب عند فرق الجهد (-1.2 V) لمدة 120 ثانية تبعتها فرق جهد رباعية الموجة الكشطية من (-1.6 V) الى (0V) . المعايرة التي حصلت عليها من إجراء تحليل التجريد من الرصاص (II) والكادميوم (II) يظهر إستقامة خطية جيدة خلال تركيزات أيونات المعادن مع حدود الكشف بين 0.225 ميكروغرام لكل لتر و 0.122 ميكروغرام لكل لتر على سطح القطب المعدل بواسطة (La). بالنسبة للقطب المعدل بواسطة (Ce) فقد أظهر حدود الكشف بين 0.07 ميكروغرام لكل لتر و 0.046 ميكروغرام لكل لتر. الأقطاب المعدلة لها إمكانية تكرار النتائج مع تباعد بنسبة % 3.02 للقطب المعدل بواسطة (La) اما القطب المعدل بواسطة (Ce) فقد اظهر تباعد بمقدار % 2.23 . وعموما، فقد أظهرت الأقطاب المعدلة إمكانية استخدامها لتحليل العينات البيئية بسبب الرخص، وسهولة التصنيع وعدم وجود سمية مقارنة مع الأقطاب المحتوية على الزئبق.

درجة الماجستير في العلوم

جامعة الملك فهد للبترول والمعادن

الظهران- المملكة العربية السعودية

CHAPTER 1

INTRODUCTION AND LITERATURE REVIEW

1.1 Introduction

Heavy metals are naturally occurring elements, which are found in various concentrations in all ecosystems. Over the years, human activities through technological development and industrial events results in the discharge of heavy metals into the environment which have today become a matter of great concern. While there is still no clear definition of what a heavy metal is, it is sometimes referred to as any metallic element with a high relative density (> 5 g/cm^3) and is toxic or fatal even at low concentrations [2]. In addition to the density, it has also been established that the chemical properties of the metals is an influencing factor when classifying heavy metals. They include metals such as chromium, lead, cadmium, cobalt, nickel, mercury, iron, silver, arsenic, as well as the platinum group elements. The major risks associated with heavy metals comes with exposure to lead, cadmium, mercury and arsenic [3].

Cadmium is an extremely toxic metal whose toxicity presents a number of health issues, including the major killer diseases such as heart disease, cancer, and diabetes [4]. It accumulates in the kidney, liver and various other organs and is considered more harmful than either mercury or lead. In fact, it is harmful even at levels one tenth that of mercury, lead, aluminum, or nickel. Exposure to this metal is increasing today as a result of its use as a coating for steel, iron and copper. Cadmium is also used in stabilizers, copper alloys, in rubber and plastics, fungicides, cigarette papers, and in many other products. Oftentimes these industries pollute water, air and food with this metal.

Another frequently encountered toxic pollutant in the environment is lead as a result of its use in paints, gasoline and car batteries. Lead is known for its manifestation of several health problems, such as cardiac, mental and neurological disorders. As a matter of fact, about thirty important health conditions have been linked to lead, many of which affects children and the unborn. It has been reported to have unknown function in the body. Lead substitutes for calcium in the bones and hence delays osteoporosis (a medical condition which causes the bones to become weak and brittle). However, lead causes other metabolic problems in the body, and hence calcium is the preferred element. Symptoms of lead toxicity may appear years after exposure, as a result of sudden release of stored lead due to illness, alcoholism, stress or other metabolic changes. Sources of lead include paints, radioactive disintegration of uranium, car batteries, lead pipes, hair colorings, and so on.

Mercury is one of the members of the class of toxic metals which have been recognized since pre-historic times. It is poisonous in any form, with its toxicity commonly affecting the neurologic, gastrointestinal and renal organ systems. Poisoning from mercury can occur as a result of vapor inhalation, injection, ingestion, and penetration through the skin. It exists in three forms: elemental, organic and inorganic forms. The three forms are inter-convertible, and can all produce systemic toxicity. Mercury is widely used in the industry and in a variety of products, such as fungicides, algaecides used in swimming pools, in the manufacture of adhesives, floor waxes, fabric softeners, and in the production of chlorine.

Another harmful carcinogen to both humans and animals is arsenic. Its toxicity has been linked with cancers of the bladder, skin and lung. An estimation of tens of millions of people are at risk of exposure to enormous levels of arsenic as a result of exposure to contaminated water and arsenic-containing coal from natural sources [5]. Chronic arsenic exposure may lead to skin cancer, diabetes, black foot disease, papillary and cortical necrosis, and so on. Table 1.1 summarizes the maximum contaminant level (MCL) allowed of some inorganic contaminants in domestic water, their common sources, and their potential health effects; adapted from EPA National Primary Drinking Water Standards tables [6].

1.2 Methods for the Detection of Heavy Metals

1.2.1 Optical Methods

Optical methods includes spectroscopic techniques such as atomic absorption spectrometry (AAS), graphite furnace atomic absorption spectrometry (GFAAS), inductively coupled plasma-optical emission spectrometry (ICP-OES), inductively coupled plasma-mass spectrometry (ICP-MS), and so on.

1.2.1.1 Atomic Absorption Spectrometry (AAS)

AAS is a common spectroscopic technique for the qualitative determination of chemical elements using the absorption of optical radiation by free atoms in the gaseous state. The atoms absorb ultraviolet or visible light and make transitions to higher energy levels. A detector measures the wavelengths of light transmitted by the sample, and compares them to the wavelength which originally passed through the sample. A signal processor then integrates the change in wavelength absorbed, which appear in the read-out as peaks of energy absorption at discrete wavelengths. Fig. 1.1 shows an atomic absorption spectrophotometer.

All atoms have their distinct pattern of wavelengths at which they will absorb energy, due to the unique configuration of electrons in their outer shells. The concentration of the analyte is then calculated based on the Beer-Lambert law as follows;

$$A = \varepsilon\ b\ C \qquad \text{Eqn. 1.1}$$

Where A = absorbance, Ɛ = molar absorptivity coefficient, b = path length, and C = concentration

Table 1.1 Maximum Contaminant Levels of Inorganic Chemicals Allowed in Drinking Water

S/N	Contaminant	MCL (ppm)	Common Source	Potential Health Effect
1	As	0.01	Drainage from glass and electronic production waste	Skin damage; prospect of getting cancer
2	Ba	2	Release of drilling wastes, and metal refineries	Increase in blood pressure
3	Cd	0.005	Decay of galvanized pipes; release from metal refineries, drainage from waste batteries and paints	Kidney impairment
4	Cr	0.1	Release from steel and pulp mills	Allergic dermatitis
5	Pb	0.015	Decay of household plumbing systems	Kidney diseases and high blood pressure in adults
6	Hg (Inorganic)	0.002	Release from refineries and factories	Kidney damage
7	Selenium	0.005	Release from petroleum and metal refineries,	Hair or fingernail loss, circulatory problems
8	Tl	0.002	Seep from ore-processing sites, release from electronics, glass, and drug factories	Loss of hair, kidney, intestine or liver complications
9	CN^- (as free cyanide)	0.2	Release from steel factories, discharge from plastic and fertilizer factories	Nerve damage or thyroid complications
10	F^-	4.0	Water supplement which enhances strong teeth	Bone infections (pain and tenderness of bones

1.2.1.2 Graphite Furnace Atomic Absorption Spectrometry (GFAAS)

This technique possesses the same working principle as AAS. The difference between the two is the way in which sample is injected into the instrument. In GFAAS, an electrothermal graphite furnace is used. The sample is heated gradually (up to 3000 ^{o}C) until it dries before being atomized and subsequently analyzed. The advantage of the GFAAS over AAS is that the limit of detection in GFAAS is about two orders of magnitude better than that of AAS.

1.2.1.3 Inductively Coupled Plasma-Optical Emission Spectrometry

ICP-OES is among the most robust analytical tools for the measurement of trace elements in a numerous sample types. Its working principle relies upon the rapid release of photons from atoms and ions that have been excited in a RF discharge. One major advantage of this technique is the fact that it can analyze samples of any form (solid, liquid or gaseous). The sample solution is transformed to an aerosol and sent into the central channel of the plasma. At its core the plasma sustains a temperature of approximately 10,000 K, so the aerosol is quickly vaporized. Analyte elements are released as free atoms in the gaseous state. Ample amount of energy is often available to transform the atoms to ions and later to promote the ions to excited states. Both the atomic and ionic excited state species may then return to the ground state with the emission of a photon. These photons possess characteristic energies that are determined by the quantized energy level structure for the atoms or ions. Hence, the wavelength of the photons can be used to identify the elements from which they were emitted. The total number of emitted photons is directly proportional to the concentration of the element in the sample.

Fig. 1.1 Atomic Absorption Spectrophotometer

One major disadvantage of optical techniques listed above is that they require highly sophisticated instrumentation, and are not suitable for on-site monitoring. Alternatively, electroanalytical techniques offer a simple approach with several advantages, such as rapid analysis, portability, good selectivity and sensitivity. Voltammetric techniques, and stripping techniques in particular are suited for the determination of trace amounts of heavy metals due to their speed, remarkable analytical sensitivity, simplicity, low cost, and minimum sample pre-treatment [4, 7].

1.2.2 Electroanalytical Techniques

These are among the most powerful and popular techniques used in analytical chemistry. The techniques offer a remarkable sensitivity, accuracy, and precision in addition to a large linear dynamic range, with relatively low cost instrumentation, and have found applications in areas such as environmental studies, industrial quality control, biomedical analysis, and so on. They include techniques such as; cyclic voltammetry (CV), linear sweep voltammetry (LSV), normal pulse voltammetry (NPV), differential pulse voltammetry (DPV), square wave voltammetry (SWV), anodic stripping voltammetry (ASV), cathodic stripping voltammetry (CSV), and so on.

1.2.2.1 Cyclic Voltammetry (CV)

CV is an electrochemical technique where the potential at a working electrode is changed linearly with time while measuring the resulting current. This give rise to voltammograms which provides information about the reactivity and mass transport properties of an electrolyte. CV is one of the most widely used electroanalytical methods because of its ability to study and characterize redox systems from macroscopic scales down to nanoelectrodes as well as composite electrodes. A typical CV voltammogram is shown in Fig. 1.2.

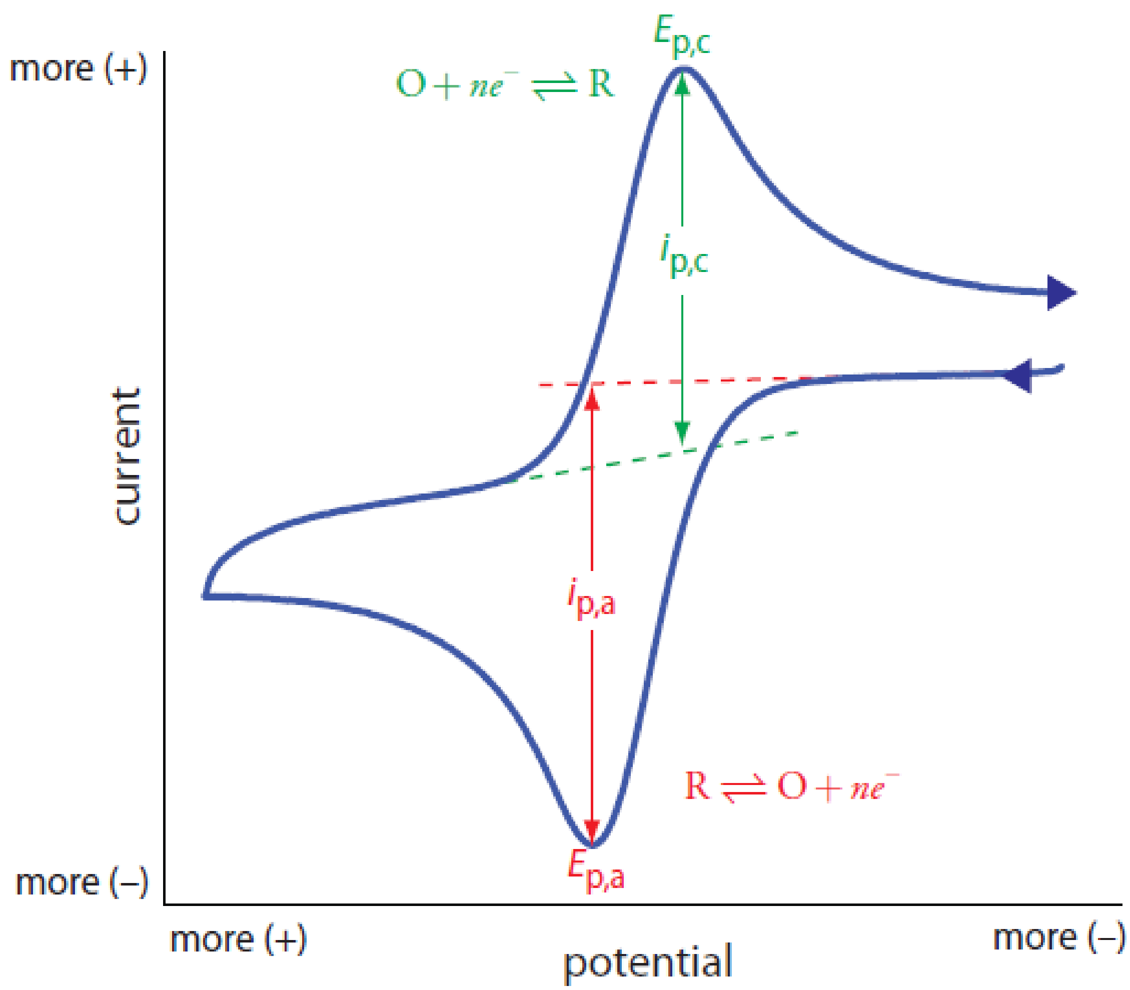

Fig. 1.2 The Corresponding Voltammogram of a Single Electron Redox System [1]

Where $E_{p,c}$ and $E_{p,a}$ are the peak potentials at the cathode and anode, respectively, and $i_{p,c}$ and $i_{p,a}$ are the peak currents at the cathode and anode, respectively.

The peak current in CV is given by the Randles-Sevcik equation

$$i_p = (2.69 \times 10^5) n^{3/2} A D^{1/2} v^{1/2} C \qquad \text{Eqn. 1.2}$$

Where n is the number of electrons in the redox system, A is the area of the working electrode, D is the diffusion coefficient of the electroactive species, v is the scan rate and C is the concentration of the electroactive specie at the electrode.

Cyclic Voltammetry provides qualitative information about electrochemical processes under different conditions, which include the presence of intermediates in redox reactions and the reversibility of a reaction. It is also used to determine the electron stoichiometry of a system, the diffusion coefficient of an analyte, and the formal reduction potential, which can be used as an identification tool. Also, because concentration is proportional to current in a reversible, Nernstian system, concentration of an unidentified solution can be found by generating a calibration curve of current versus concentration.

1.2.2.2 Linear Sweep Voltammetry (LSV)

In LSV, potential is varied at constant rate while the current is measured. The rate of change of the potential is called the scan rate (v). Traditionally, the potential is plotted on the x-axis with more negative (reducing) potentials to the right. Currents, on the other hand, are graphed on the y-axis with currents due to reduction assigned positive values.

In LSV, it is common practice to measure the peak current (i_p), the largest current; peak potential (E_p), the potential at the peak current and the half-peak potential ($E_{1/2}$), which is the potential when the current is half of the peak current.

The potential at the peak is characteristic of the system being investigated. It is mainly a thermodynamic measurement, but may be affected by the kinetics of the system. The value of the peak current depends on several factors including the analyte concentration, kinetics of electron transfer and the mass transport of the analyte. Fig. 1.3 shows a typical LSV voltammogram of ferrocene. In a diffusion-controlled system, reversible electron transfer, the relationship is

$$i_{\mathrm{p}} = (2.69 \times 10^5)\mathrm{n}^{3/2}\,\mathrm{A}\mathrm{D}^{1/2}v^{1/2}\mathrm{C}^* \qquad \text{Eqn. 1.3}$$

where C* is the bulk concentration of analyte (mol analyte/cm^3) and all other symbols same as the previous equation. The dependence on bulk concentration (rather than concentration at the electrode surface) allows peak current to be used for quantitative purposes.

1.2.2.3 Normal Pulse Voltammetry (NPV)

NPV consists of stages of pulses of rising amplitude applied to successive drops at a pre-selected time close to the end of each drop lifetime, while the electrode is maintained at a base potential between pulses where no reaction occurs. Current is measured at around 40 ms after each pulse is applied and is graphed as a function of potential. The resulting voltammogram has a sigmoidal shape, with a limiting current represented by a modified Cottrell equation as:

$$i_l = \frac{nFACD^{1/2}}{\sqrt{\pi t_m}} \qquad \text{Eqn. 1.4}$$

where t_m is the time after application of the pulse where the current is measured. A typical signal for normal pulse voltammetry is shown in Fig. 1.4.

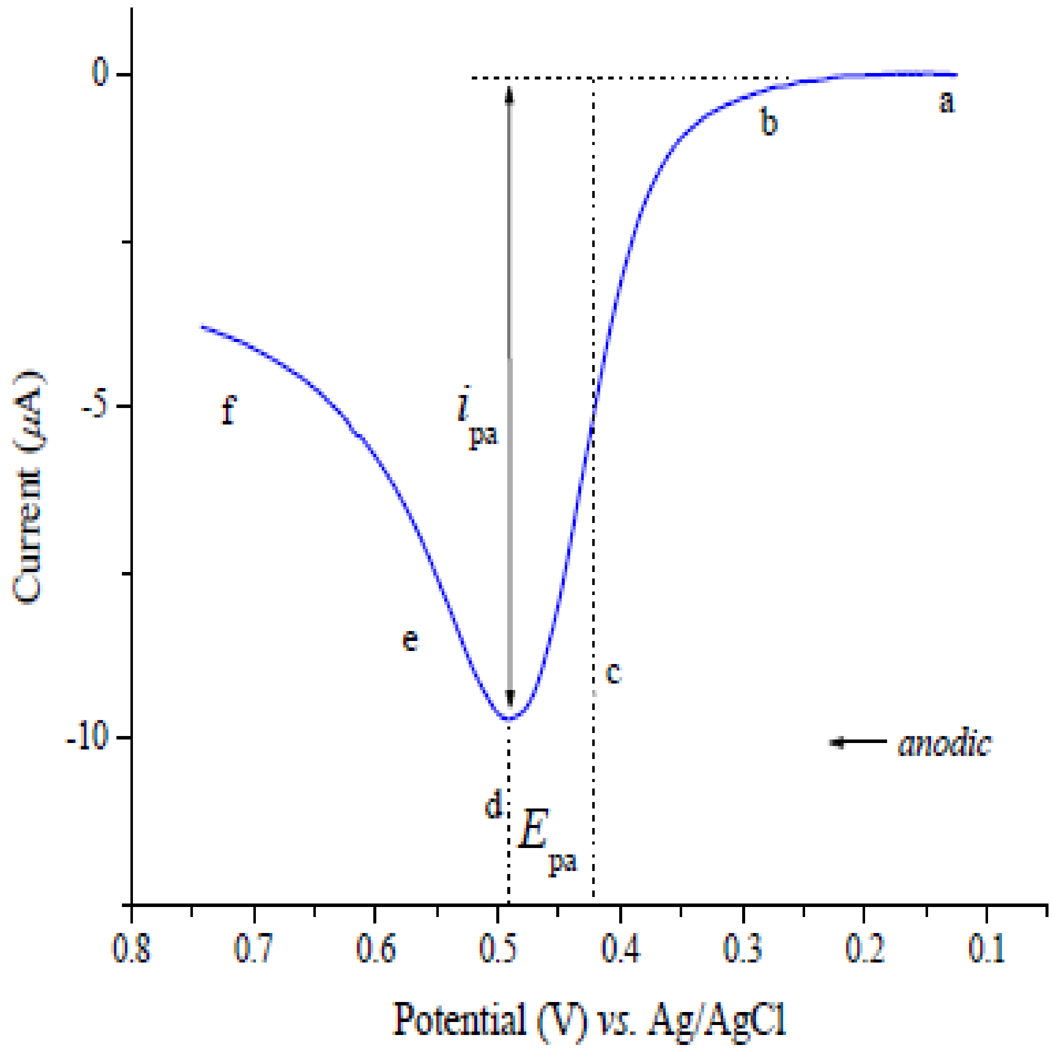

Fig. 1.3 Linear Sweep Voltammogram of Ferrocene [1]

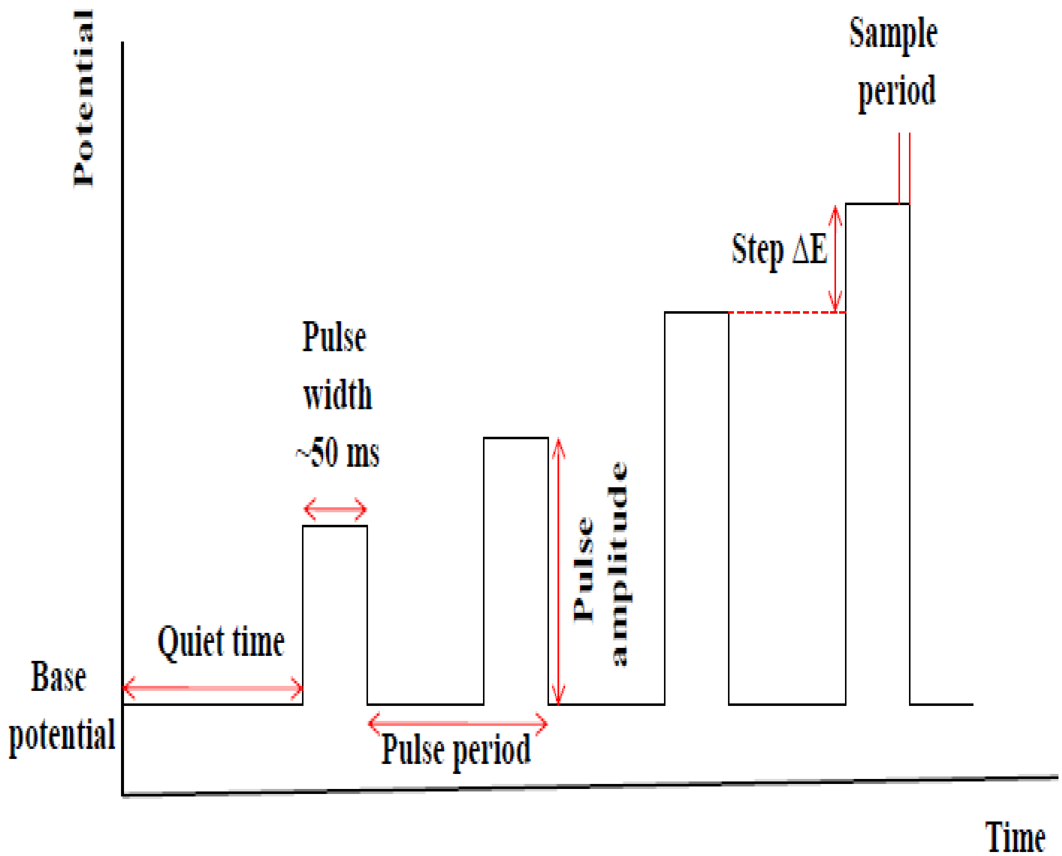

Fig. 1.4 Normal Pulse Voltammetry Signal [1]

1.2.2.4 Differential Pulse Voltammetry (DPV)

DPV is a very useful technique for detecting trace amounts of organic and inorganic species. In DPV, fixed magnitude pulses-superimposed on a linear potential ramp are applied to the working electrode just before the end of the drop (Fig. 1.5). The current is measured twice, before the pulse application and after pulse (after ~40 ms, when the charging current goes down). The first current is instrumentally deducted from the second, and this current difference is graphed against the applied potential. The resulting differential pulse voltammogram consists of current peaks, whose height is directly proportional to the concentration of the corresponding analyte. The peak potential (E_p) appears close to the polarographic half-wave potential and can be used to identify the species. This technique is useful for analysing mixtures with very low detection limits. It is also used to yield information about chemical nature of the analyte.

1.2.2.5 Square Wave Voltammetry (SWV)

SWV is a robust electrochemical technique suitable for analytical applications, mechanistic study of electrode processes and electrokinetic measurements [8]. In this technique, current is measured twice during each square wave cycle, once at the completion of the forward pulse, and once at the completion of the reverse pulse. Because the square wave modulation amplitude is very large, the reverse pulses leads to the reverse reaction of the product (of the forward pulse). Thus, the difference between the two measurements is graphed versus the base staircase potential. This is shown in Fig. 1.6.

A plot of the theoretical forward, reverse, and difference currents is given in Fig. 1.7 for a reversible redox system. The resulting peak-shaped voltammogram is symmetric about the half-wave potential, and the peak current is proportional to the concentration. The major advantage of this technique over other electrochemical techniques is its speed, sensitivity, and the fact that it can reach very low limits of detection.

1.2.2.6 Anodic Stripping Voltammetry (ASV)

ASV is one of the most common of a class of techniques known as stripping electroanalytical methods. The distinguishing property of this technique is the deposition of analyte at the surface of the electrode, and thus to lower the detection limit for the analyte. ASV involves the deposition of electroactive species at the electrode surface by the application of a negative potential. In most cases a mercury drop electrode or mercury thin film electrode is used under forced convective conditions (stirred solution). The deposition step is followed by a short time period in which the solution is allowed to quiet (no stirring), after which a potential scan is initiated from the deposition potential in the anodic direction. From the resulting voltammogram, the current magnitude (peak height) or charge (peak area) is then used to quantify unknown amounts of analyte. For a mercury film deposited on the surface of an inert substrate, the stripping peak current is given by:

$$i_p = \frac{n^2 F^2 \nu^{1/2} A\, I\, C_M}{2.7RT} \qquad \text{Eqn. 1.5}$$

Where F represents the Faraday (9.65×10^4 C), I the mercury film thickness in cm, and other symbols remain as defined earlier.

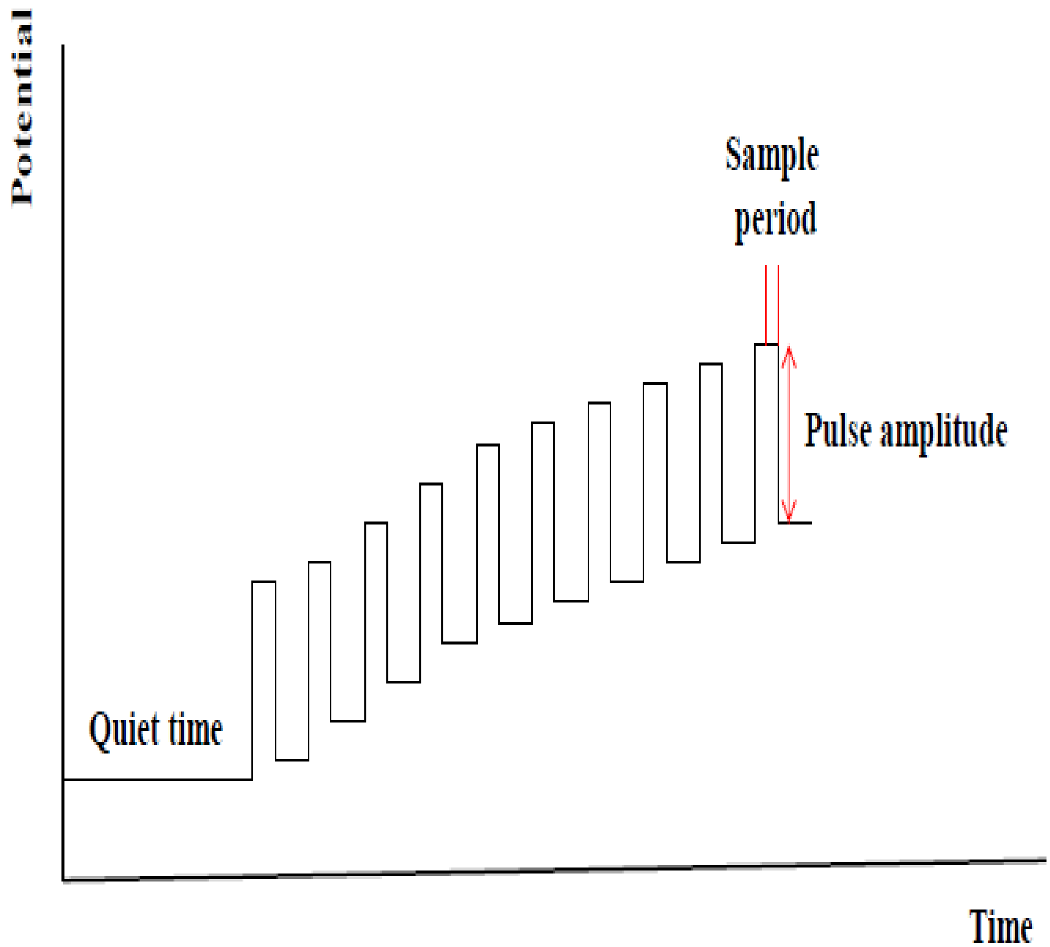

Fig. 1.5 Differential Pulse Voltammetry Signal [1]

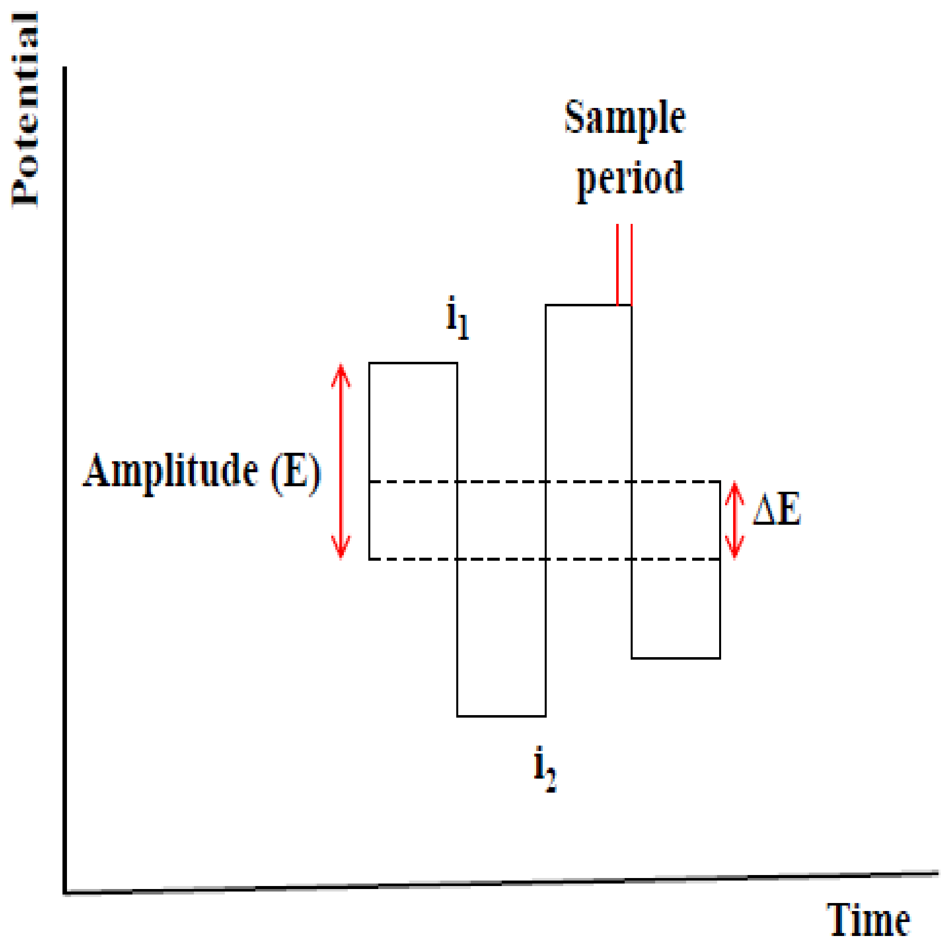

Fig. 1.6 Square Wave Waveform [1]

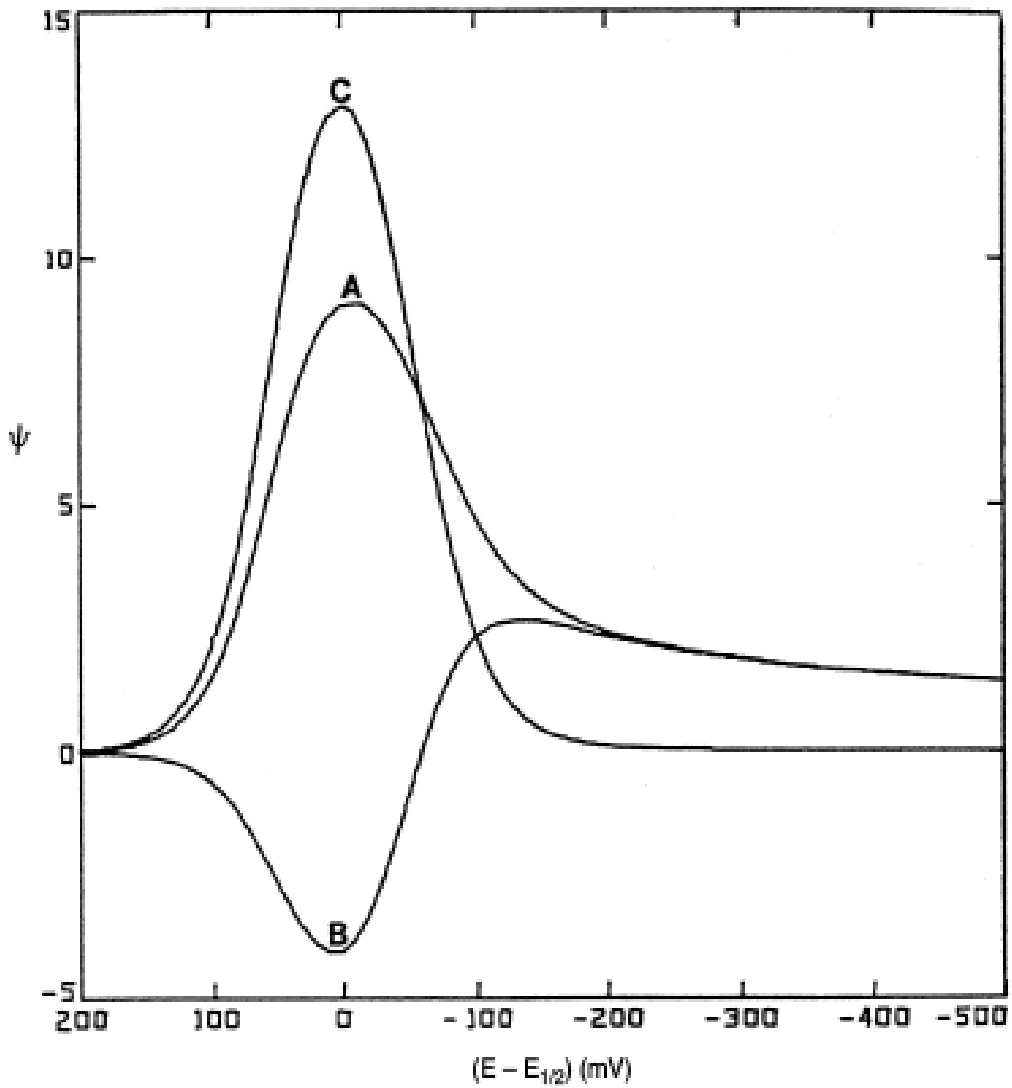

Fig. 1.7 Square Wave Voltammograms for a Reversible Electron Transfer. A: Forward Current. B: Reverse Current. C: Net Current [1]

1.2.2.7 Cathodic Stripping Voltammetry (CSV)

CSV is the mirror image of ASV. It involves anodic deposition of the analyte, followed by stripping in the negative potential scan:

$$A^{n-} + Hg \leftrightarrow HgA + ne^{-}$$

The resulting peak current provides the desired quantitative information. CSV is used to measure a wide range of organic and inorganic compounds, capable of forming insoluble salts with mercury. Examples are thiols or penicillin, as well as halide, cyanide, and sulfide ions.

1.3 Working Electrodes Employed in Electroanalytical Techniques

The working electrode (WE) is a crucial component of an electrochemical cell. This is because the electron transfer of interest occurs at its surface. The selection of the material for this electrode is therefore a critical issue to the analyst. Several factors are considered when selecting the material for the working electrode. First, it should possess favorable redox behavior with the analyte i.e. it should enable reproducible electron transfer without electrode contamination. Second, the potential window over which the electrode works in a given electrolyte solution should be as wide as possible to allow for the greatest degree of analyte characterization. Other factors are cost of the material, its ability to be tuned into useful geometries, the ease of surface renewal after analysis, and its toxicity [9].

The most commonly used working electrode materials are Pt, Au, C, and Hg. Fig. 1.8 shows examples of working electrodes employed in electroanalytical chemistry.

1.3.1 Platinum Electrode

Due to its inertness, platinum is one of the most preferred electrodes in electroanalytical studies. However, the major drawback to the use of this electrode, aside from its high cost is that the presence of little amounts of water or acid in the electrolyte leads to the reduction of hydrogen ion to form hydrogen gas at fairly modest negative potentials. This reduction interferes with any useful analytical signal.

1.3.2 Gold Electrode

Gold electrode has limited application in the positive potential range due to the ease of oxidation of its surface. Hence this electrode is not generally preferred in electrochemical studies.

1.3.3 Carbon Electrode

Carbon electrodes have advantage over platinum and gold electrodes because they enable scans to more negative potentials, and possess good anodic potential windows. The most prevalent form of carbon electrode is glassy carbon, which is relatively costly and difficult to machine. Carbon paste electrodes have also found usefulness in several applications. These electrodes are made from a paste of finely granulated carbon mixed with an oil substrate (usually Nujol or paraffin). The resulting paste is then packed into the cavity of an inert electrode body. These electrodes have drawbacks of being susceptible to mechanical damage during use.

1.3.4 Mercury Electrode

Mercury is a classic type of electrode material. Due to its high hydrogen overvoltage, it can extend the cathodic potential window. In addition, mercury electrodes possess highly reproducible, renewable and smooth surface, which is very beneficial in electrochemical analyses. Among the mercury electrodes, dropping mercury electrode (DME) is the most commonly preferred. This is because in these electrode drops of mercury forms and fall off continuously during a potential scan, and this yields the advantage of self-renewal, so it does not need to be cleaned or polished before each experiment. However, the toxic nature of mercury has restricted the use of this electrode for electroanalytical studies.

Fig. 1.8 Examples of Working Electrodes (from left: empty tip, platinum, gold, silver, glassy carbon)

1.3.5 Zeolite-Modified Electrodes (ZMEs)

Zeolite-modified electrodes belong to a class of the so called “chemically-modified electrode” (CMEs). From the electrochemical perspective, zeolites offers a nanostructured domain, where the physical structure and the chemical nature of the zeolite affects electron-transfer reactions and influences known chemical steps couple with the electron transfer at the electrode-solution interfaces. This results to the fabrication of electrodes with high sensitivity, high selectivity and a wide dynamic range.

The advent of zeolite-modified electrodes (ZMEs) has over the past 15 years attracted the attention of researchers in the field of electrochemistry and other similar fields [10]. This is because ZMEs encloses in a single device the peculiarity of charge transfer reactions coupled with the intrinsic properties of the aluminosilicates, such as molecular sieving and ion-exchange [10]. In addition, the incorporation of zeolites into carbon electrodes imparts a number of chemical, physical and structural features of high interest in the design of electroanalytical systems. These include shape, size and charge selectivities, physical and chemical stabilities, high ion-exchange capacity as well as hydrophilic character [11].

Zeolites are crystalline materials that afford molecular sized frames and pores for excellent steric control of reaction paths [12]. The major building units of zeolites are $[SiO_4]^{4-}$ and $[AlO_4]^{5-}$ tetrahedra. These units can link in several ways, resulting in arrays producing three-dimensional anionic networks. The extra negative charge on $[AlO_4]^{5-}$

tetrahedra is counter balanced by a cation, maintaining the overall neutrality of the zeolite.

Zeolites have been used for various industrial and catalytic purposes, the most important of which is their use in fluid catalytic cracking (FCC) which supplies about 45% of the global gasoline pool by the cracking of larger hydrocarbons into the gasoline fractions [13]. Today, over 200 zeolite and zeotype structures are recognized by the International Zeolite Association (IZA), which includes MFI, BEA, MEL, MTW, MOR, FER, FAU, etc. [14].

In the past, the composition of zeolites was limited to aluminosilicate polymorphs [15]. However, in recent years heteroatoms such as Ta, Ge, Fe, V, Sn, P, Ti and B, among others are now incorporated (into zeolite structure) alongside silicon and aluminum [15]. This large chemical utility has enabled the control of the physicochemical activities of zeolites (such as acidity, redox properties, or hydrophobic-hydrophilic nature), and as a consequence, there has been an increased number of applications of these materials. [16]. Also more recently the introduction of additional rare earth (RE) elements such as La and Ce into zeolite composition with the aim of improving the stability and enhancing the zeolite activity has been investigated [17].

Several authors have reported the improvement in the stability of zeolites after the addition of RE such as La, Ce, Nd, Sm and Pr, and such properties have been attributed to the formation of hydroxyl rare earth cation species in zeolite channels [18]. It was also found that the incorporation of RE ions into zeolite frameworks tends to alter the Lewis acid sites in the framework, and this in turn enhances the zeolite's catalytic activity [19].

Zeolites are made catalytically more active and thermally more stable at the operating temperatures by incorporating RE ions in them [20]. Introduction of RE is used to adjust the amount and intensity of distribution of the acid sites [21]. For example in FCC, catalysts are generally used at high temperature and in hydrothermal environments. These conditions usually induce a decline in the degree of crystallinity, deterioration of the aluminum leaching framework and consequent collapse in the zeolite structure, which result in the deactivation of the catalyst. The introduction of RE ions into the zeolite framework was therefore reported to help stabilize the zeolite framework [21].

Mordenite is an industrially important member of the zeolite family with ideal composition $Na_8Al_8Si_{40}O_{96}.nH_2O$ [22]. Its framework is built on 5-membered rings arranged in columns parallel to the [001] axis. Hence, the framework includes elliptical micropore (6.7 x 7.0 Å) tunnels parallel to the c-axis and (2.6 x 5.7 Å) tunnels parallel to the b-axis Fig. 1 [22, 23]. By virtue of the small nature of the latter axis, molecules are unable to pass through and as such mordenite is generally regarded as a one-dimensional zeolite [24]. Due to its high thermal and acid stabilities, mordenite has been used in several applications, such as in the separation of gas or liquid mixtures and in catalysis such as hydrocracking, hydro-isomerization, alkylation, reforming, dewaxing and in the synthesis of dimethyl amines [25, 26]. Also more recently, it has been considered for use in semiconductors, chemical sensors, and non-linear optical materials [22]. Fig. 1.9 shows the framework of mordenite zeolite.

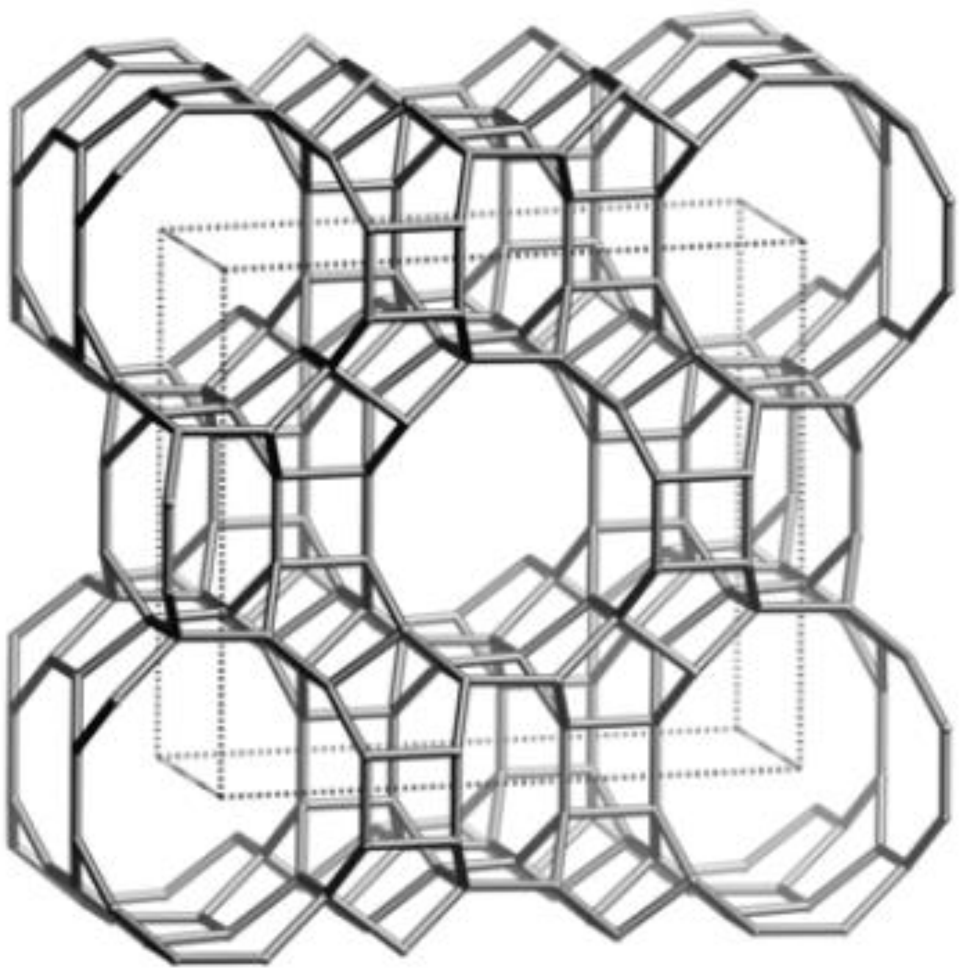

Fig.1.9 Mordenite Framework [27]

1.4 Literature Review

Several reports have been published on the role played by metals in enhancing the electrocatalytic activity of zeolites [12, 28-34] some of which are summarized in Table 1.3. Li et al [32], studied the electrochemical performance of Ag ion-incorporated zeolite Y-modified electrode in aqueous solution containing different anions. It was shown that the Ag ion-exchanged zeolite Y-modified electrode has a high selectivity for Cl^- and Br^- anions.

In another research, Kaur et al [28] investigated the role played by various transition metals in the electrocatalytic oxidation of glucose on ZSM-5 modified electrode. Metals studied include Cu, Ni, Co, Fe and Mn. It was found that a non-enzymatic electrochemical sensor based on Ni^{2+} exchanged nanocrystalline ZSM-5-modified electrode exhibits the highest sensing ability oxidation whereas the corresponding Cu^{2+} exchanged electrode exhibits the highest current sensitivity for glucose oxidation. It was therefore concluded that the enhancement in the electrocatalytic activities of nanocrystalline ZSM-5-modified electrodes is due to the enhanced accessibility of glucose/methanol to M^{2+} active centers in the nanocrystalline ZSM-5 owing to its large specific surface area and inter-crystalline mesopores.

Guzman, V. et al [30] also studied the effect of Cu (II) ion incorporation into ZSM-5 modified electrode for the reduction of nitrite species. It was found that the Cu (II) ion-incorporated modified electrode exhibits good electrocatalytic activity towards the reduction of nitrite species. It was also found that the activity increases as the Si/Al ratio of the zeolite decreases.

The influence of incorporating Ni (II) ion into the framework of zeolite Y for the electrocatalytic oxidation of methanol was also investigated by Ojani et al [12]. It was found that the modified electrode prepared by both methods of cation exchange and open circuit accumulation of Ni ion on the surface of the electrode displayed the best catalytic activity in alkaline solution. They also studied the effect of the ratio of graphite to zeolite on electrocatalytic current and found that the ratio 3:1 of graphite to zeolite was the optimum ratio for best electrocatalytic activity.

In another study, the analytical performance of Bi-modified zeolite doped carbon paste electrode for trace analysis of Cd and Pb was investigated [33]. Bi ion was incorporated into a commercial zeolite (synthetic zeolite) and this was used in the preparation of modified electrode by mixing with graphite and silicone oil (binder). The electrochemical behavior of this electrode was studied by stripping technique in 0.10 M sodium acetate buffer solution (pH 4.5) before its application for the determination of Cd and Pb. It was found that the in situ plated (zeolite/graphite powder/silicone, 10/190/80 w/w) exhibited the most sensitive response to Cd and Pb in 0.10 M acetate buffer, and the detection limits of 0.08 μgL^{-1} and 0.10 μgL^{-1} were obtained for Cd (II) and Pb (II), respectively. The results obtained were found to agree with those obtained by atomic absorption spectroscopy (AAS).

The role played by metals such as Zr, Ti and Al when incorporated into zeolite-modified electrodes was also studied by Kaur et al [34], using nano-ZSM-5 zeolite. The electrochemical behavior of this electrode studied by cyclic voltammetry revealed that nano-Zr-ZSM-5/carbon paste electrode exhibits excellent stability, high sensitivity and selectivity. This electrode was applied in the determination of nano-molar concentrations of aminophenol isomers and the detection limits found were 26 nM, 30 nM and 30 nM for *p*-aminophenol, *o*-aminophenol and *m*-aminophenol, respectively.

However, not much has been done on the application of zeolite-modified electrodes for trace metal analysis. Therefore, we investigate for the first time the incorporation of La and Ce metal ions into zeolite-modified carbon paste electrode for electroanalytical determination of Cd and Pb ions in water samples.

Table 1.2 Summary of Literature

S/N	Zeolite	Metal Impregnated	Characterization Technique	Application	Ref
1	Zeolite Y	Ni	Cyclic voltammetry	Electrocatalytic oxidation of methanol in alkaline solution	[12]
2	ZSM-5	Cu, Ni, Co, Fe and Mn	Cyclic voltammetry	Electrochemical oxidation of glucose and methanol	[28]
3	Zeolite X	Pt and Pt/Ru	Cyclic voltammetry	Carbon monoxide electrooxidation	[29]
4	ZSM-5	Cu	Cyclic voltammetry	Electrocatalytic reduction of nitrite species	[30]
5	ZSM-5	Ni	Cyclic voltammetry	Electrocatalytic oxidation of methanol	[31]
6	Zeolite Y	Ag	Cyclic voltammetry	Electroactivity in aqueous solutions of different anions	[32]
7	Synthetic zeolite	Bi	Differential pulse square wave voltammetry	Determination of trace amounts of Cd and Pb	[33]
8	ZSM-5	Zr	Cyclic voltammetry	Simultaneous electrochemical determination of nano-molar concentrations of aminophenol isomers	[34]

1.5 Objectives of the Current Study

The current study aims at the following objectives:

I. Synthesis and characterization of La and Ce incorporated mordenite zeolite.

II. Electrochemical characterization of the zeolite-modified electrodes.

III. Application of the fabricated electrodes for the electroanalytical determination of Cd (II) and Pb (II) ions in water samples.

CHAPTER 2

EXPERIMENTAL

2.1 Reagents and Chemicals

All solvents and reagents used in this research were of standard purity and of analytical grade. The chemicals include: NaOH (PRS codex, Panreac Quimica), silica gel (pore size 60 Å, 70 – 230 mesh, Sigma-Aldrich), colloidal silica (LUDOX, 40 wt%, Sigma Aldrich), sodium silicate (reagent grade, Lot: MKBG3583, Sigma Aldrich), fumed silica (175-225 m^2/g surface area, 99.8%, Sigma-Aldrich), $NaAlO_2$ (anhydrous, Sigma-Aldrich), NaH_2PO_4 and Na_2HPO_4 (fluka), $K_4Fe(CN)_6$ (BDH chemicals), KCl (anhydrous, Sigma-Aldrich), phosphoric acid (BDH, analar grade), NH_4OH (Fisher scientific), H_2SO_4 (Panreac Quimica), glacial acetic acid and ammonium acetate (Fisher scientific). Solutions of Pb (II) and Cd (II) were prepared from 1000 ppm stock solutions (spectroscopic grade, BDH chemicals). All solutions were freshly prepared with double distilled water obtained from labstrong nanopure water distiller (Thermoscientific).

2.2 Instruments

Powder X-ray diffraction pattern (XRD) of the crystal was recorded on Rigaku miniflex II X-ray diffractometer using CuKα radiation (λ = 1.5418 Å) with 2θ from 5° to 50° and a scanning step of 0.02. Morphology of the crystal was obtained by field emission scanning electron microscopy (FESEM) LYRA 3 dual beam, Tescan. Samples were coated with gold prior to analysis. Solid state ^{27}Al and ^{29}Si MAS NMR were carried out on JEOL Lamda-500 Multi Nuclear Magnetic Resonance spectrometer with solid state MAS probe. The ^{29}Si MAS spectra were taken at a pulse interval of 10 s with 20,000 scans per sample and a spin of 4 kHz. The spectra were processed with 40 Hz line broadening and chemical shifts were determined relative to TMS as external reference. Electrochemical experiments were performed on CHI 760E electrochemical workstation (CH instruments, USA). An Ag/AgCl electrode was used as reference electrode and a platinum wire as the auxiliary electrode. Working electrode was carbon paste electrode modified/un-modified with zeolite.

2.3 Synthesis of Mordenite Zeolite (MOR)

A gel having the molar composition $6Na_2O:Al_2O_3:30SiO_2:780H_2O$ was synthesized according to the following procedure; 2.10 g NaOH was dissolved in 20 g double deionized water (DDW). To this solution, 0.63 g $NaAlO_2$ was added and the mixture stirred until dissolution. Thereafter, 34.13 g DDW was added while stirring. Finally, 6.95 g SiO_2 was added and the mixture stirred for 1 h (aging time). The resulting gel was then transferred to a Teflon-lined stainless steel autoclave and crystallization was carried out under hydrothermal condition at 180 ^{o}C for 48 h.

2.3.1 Product Recovery After 48 h

The material resulting after crystallization was centrifuged and washed with DDW until the pH drops below 9. The sample was allowed to dry overnight at room temperature in order to obtain the crystal powder. The crystal was calcined at 550 ^oC to expel all organic matter present.

2.4 Metal Impregnation

An appropriate amount of the metal precursors ($La(NO_3)_3.6H_2O$ and $Ce(NO_3)_3.6H_2O$) required to make 2 wt%, 5 wt% and 10 wt% of La and Ce-impregnated zeolites was dissolved in ethanol (40 g) and was mixed with 2 g zeolite under vigorous stirring. The resulting slurry was dried overnight in a fume hood and was later calcined at 550 ^oC for 4 h in static air (temperature ramp 20 ^oC/min).

2.5 Electrode Fabrication

Zeolite-modified carbon paste electrode (ZMCPE) was prepared by mixing an appropriate amount of graphite, zeolite and paraffin oil in order to form a paste according to various ratios which will be explained in subsequent chapters. The paste was packed into the end of the tip of a micropipette (40 mm long, 0.1 mm diameter) with copper wire as electrical contact. The electrode was renewed after every experiment by packing in a fresh paste and smoothening by polishing the surface on a weighing paper. Bare carbon paste electrode was prepared the same way without the addition of zeolite (graphite and paraffin oil only) and was used for comparison. Fig. 2.1 and 2.2 shows the electrode preparation process and a finished composite electrode, respectively.

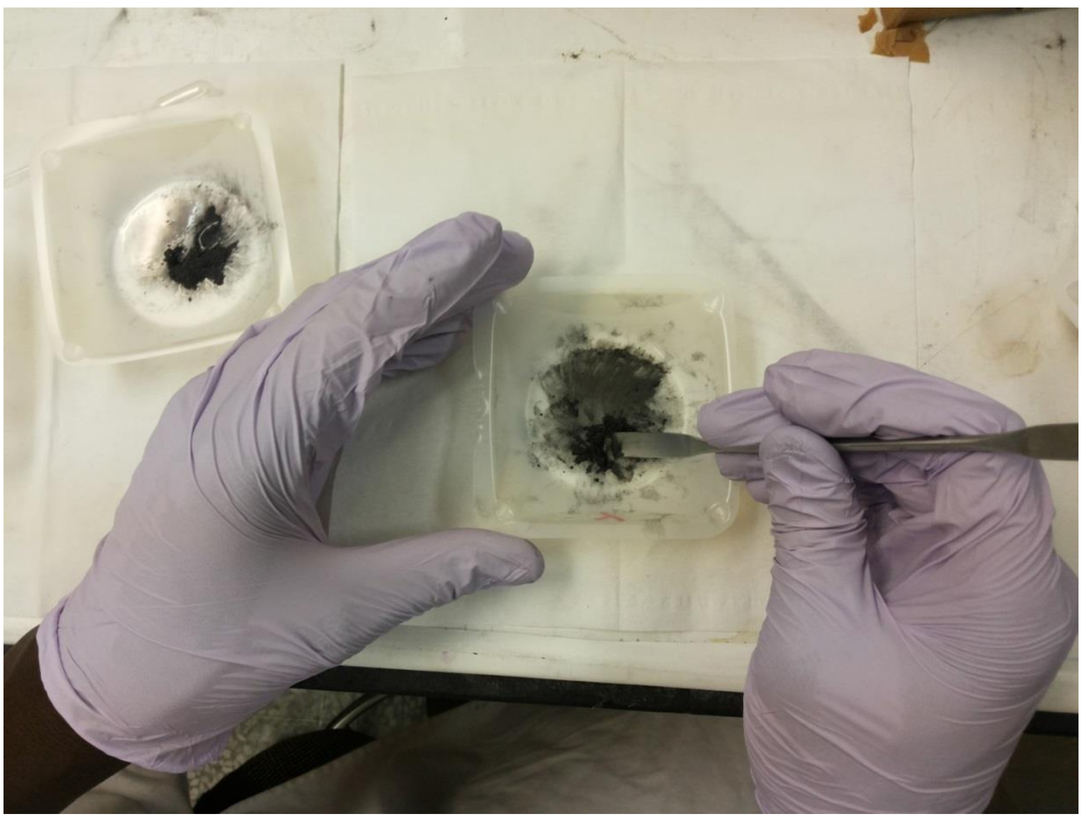

Fig. 2.1 Carbon Paste Electrode Preparation Process

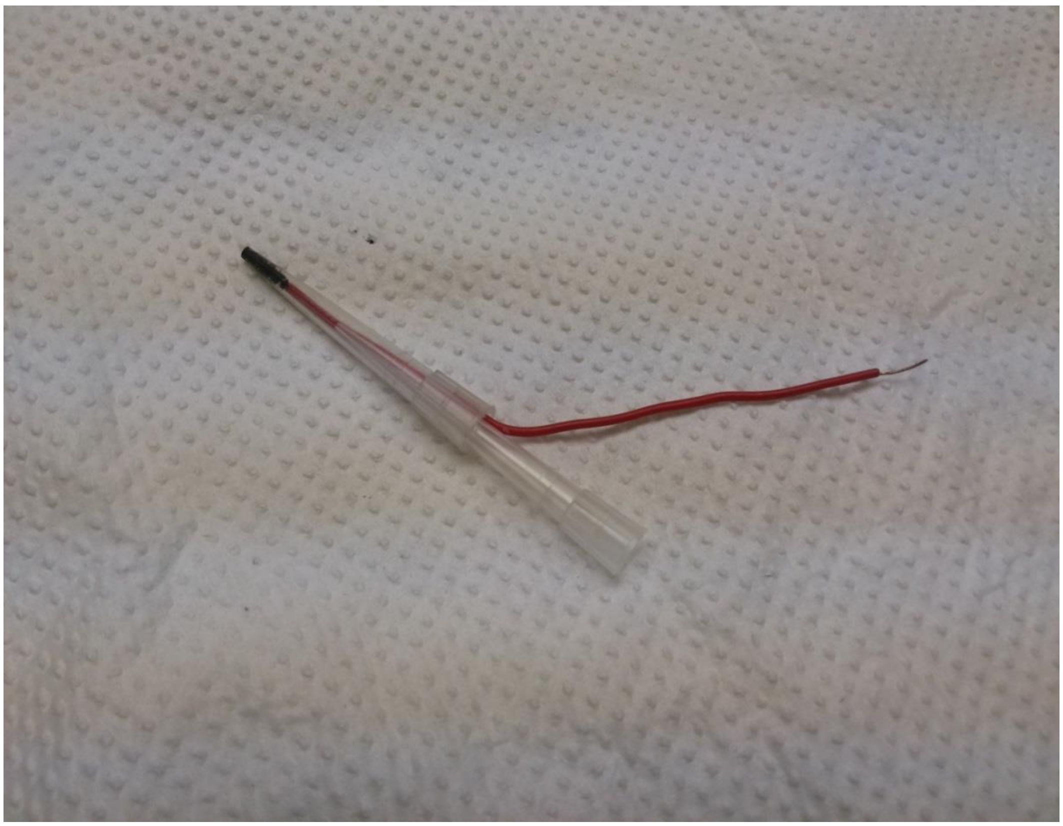

Fig. 2.2 Composite Electrode Used as Working Electrode

CHAPTER 3

SYNTHESIS, SPECTROSCOPIC CHARACTERIZATION AND VOLTAMMETRIC DETERMINATION of Cd (II) at La-IMPREGNATED ZEOLITE-MODIFIED CARBON PASTE ELECTRODE (La-ZMCPE)

3.1 Summary

We report the synthesis of mordenite zeolite hydrothermally in the absence of organic template. The zeolite whose molar composition was $6Na_2O:Al_2O_3:30SiO_2:780H_2O$ was characterized by XRD, SEM, EDX and NMR. It was further impregnated with lanthanum and was used in the construction of zeolite modified carbon paste electrode by mixing with various amount of graphite and paraffin oil in order to form a paste. It was found that the composite with the ratio 65:5:30 (graphite:zeolite:paraffin) displayed the best electrochemical behavior in the cyclic voltammetry of 10 mM $K_4Fe(CN)_6$ in the presence of 0.1 M KCl at a scan rate of 100 mV s^{-1}. The electrode whose electroactive surface area was calculated as 25.9 mm^2 was applied in the square wave voltammetric determination of Cd (II) ions. The results of the electroanalysis show linear response over the range 50 – 500 ppb and 5 – 50 ppb with correlation coefficient 0.999 and 0.998 respectively, and a detection limit of 0.12 ppb. The electrode displayed good reproducibility with RSD 2.7%.

This electrode demonstrates a potential to be used as a sensor for analyzing environmental samples due to its inexpensiveness and easy fabrication as well as lack of toxicity, compared to mercury-based electrodes used in stripping analysis.

3.2 Synthesis and Characterization of La-MOR-15

Mordenite with different silica to alumina ratio was synthesized hydrothermally and investigated by XRD as shown in the XRD pattern (Fig. 3.1). The figure shows the XRD pattern of samples synthesized with silica to alumina ratio 10 – 30, which reveals that an amorphous material was obtained for the sample with silica to alumina ratio 10, while the rest gave crystalline materials. At higher silica to alumina ratio (higher than 20), another phase which was confirmed to be analcime appears along with the mordenite crystal. The formation of analcime along with mordenite at higher silica to alumina ratio has been reported by Hincapie et al [35]. It was also observed that the area of the XRD peaks for prepared mordenite samples was higher than that of standard mordenite reported in the literature. This could be attributed to the high crystallinity of the prepared samples as can be seen from the size of the crystals obtained.

Several morphologies of this crystal have been synthesized in the literature which includes; spherical, circular pie, flat prismic, ellipsoidal, hexagonal star-like prism and so on [36]. The result of SEM (Fig. 3.2) reveals that a flat prismic crystal was formed in the current work. The formation of analcime growing phase at higher silica to alumina ratios was also confirmed from the result of the SEM. Since the silica to alumina ratio which gave a relatively pure form of mordenite was 15, it was adopted for the purpose of this study, and hence will subsequently be referred to as MOR-15.

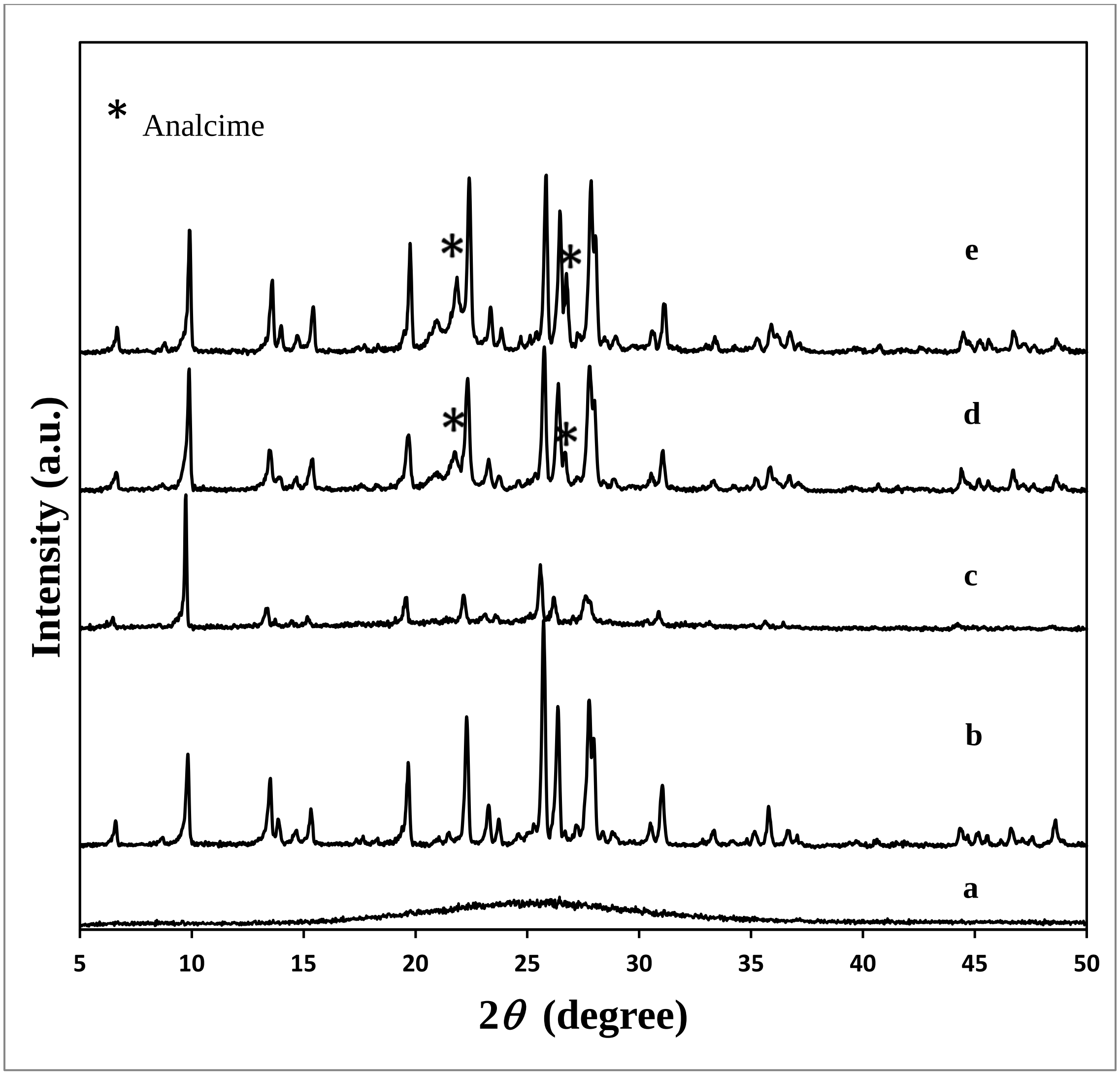

Fig. 3.1 XRD Pattern of Mordenite Synthesized at 180 °C for 48 h with Different Silica to Alumina Ratios; (a) 10, (b) 15, (c) 20, (d) 25, and (e) 30

After characterization of MOR-15, it was impregnated with 2 wt% La and the EDX results (Table 3.1 and Fig.3.3) show that an average of 1.68 wt% of the metal exists on the surface of the zeolite. The incorporation of La into the framework of the zeolite was also supported by ^{27}Al MAS NMR (Fig. 3.4), which shows two distinct peaks at around 50 ppm and 0 ppm. The peak at around 50 ppm could be assigned to the tetrahedral coordinated framework of Al atoms, while the peak at around 0 ppm is due to the octahedral coordinated extra framework [37]. From Figure 5, the intensity of the peak corresponding to the tetrahedral coordinated Al atoms decreases after La impregnation. This implies that some of the Al atoms have been replaced by La in the framework of the zeolite. The metal impregnated zeolite will henceforth be denoted as La-MOR-15.

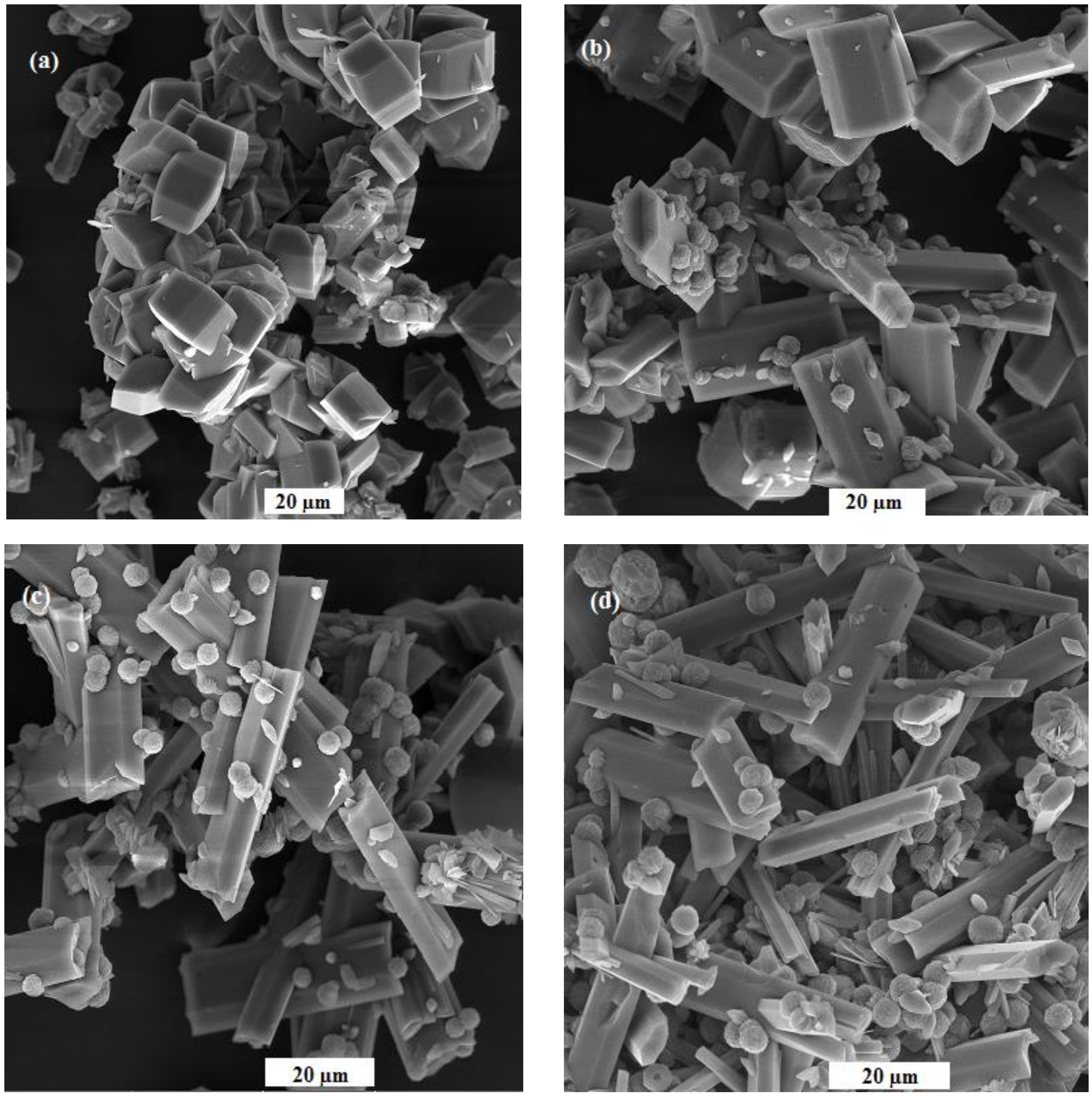

Fig. 3.2 SEM Images of Mordenite Crystal with Silica to Alumina Ratio (a) 15, (b) 20, (c) 25 and (d) 30

Table 3.1 EDX Results of La-MOR-15

Spectrum	Oxygen (wt %)	Aluminum (wt %)	Silicon (wt %)	Lanthanum (wt %)	Total (wt %)
Mean	56.48	4.39	37.45	1.68	100

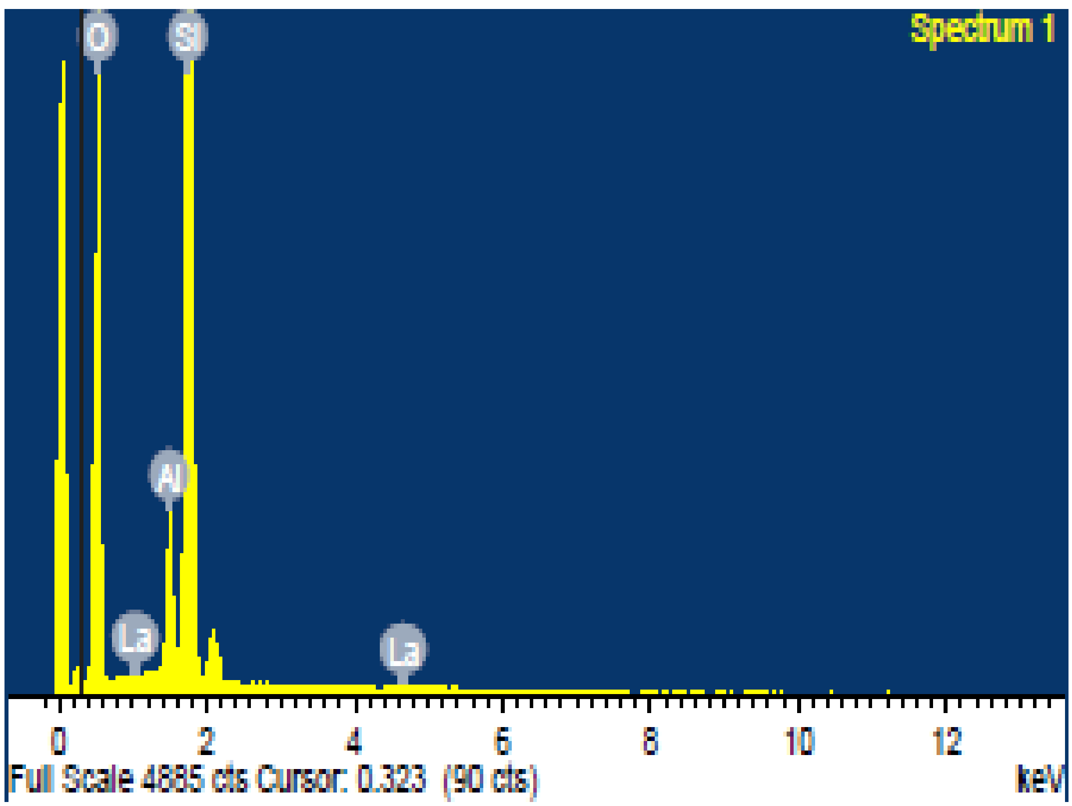

Fig. 3.3 EDX Spectrum of La-MOR-15

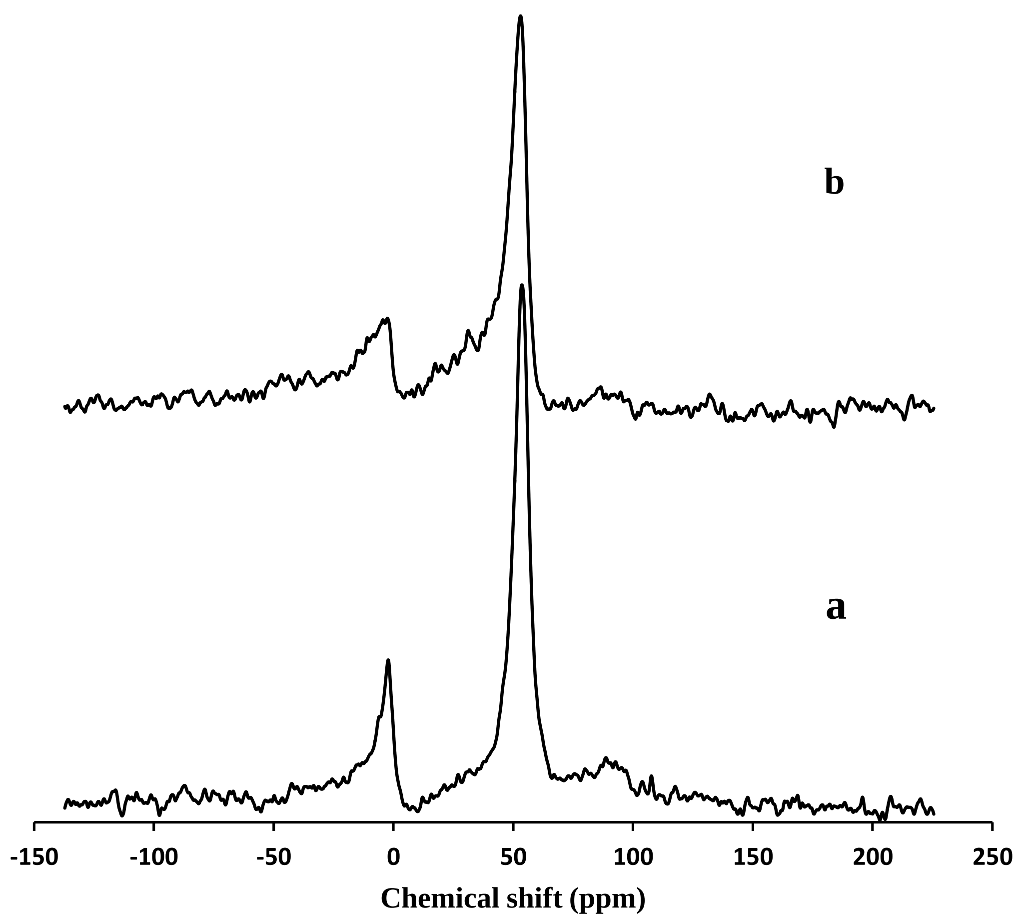

Fig. 3.4. ^{27}Al MAS NMR of MOR-15 (a) Before Impregnation, and (b) After La-Impregnation

3.3 Electrochemical Characterization

Cyclic voltammetry was employed for the investigation of the electrochemical properties of the zeolite modified carbon paste electrode (ZMCPE) synthesized in the current work, where 10 mM potassium ferrocyanide ($K_4Fe(CN)_6$) and 0.1 M KCl were used as the electroactive specie and the supporting electrolyte, respectively. The La-impregnated zeolite (La-MOR-15) and the un-modified zeolite (MOR-15) were mixed separately with carbon graphite and paraffin oil in the ratios shown in Table 2 to obtain five composite electrodes (A – E). The resulting homogeneous paste was packed into the tip of a micropipette and cyclic voltammetry was carried out in potassium ferrocyanide. The cyclic voltammograms shows that composite B with the ratio 65:5:30 (graphite:zeolite:paraffin) has the highest anodic peak current as shown in Fig. 3.5.

The results obtained shows reproducible anodic and cathodic peaks ascribed to $Fe(CN)_6^{3-}$/$Fe(CN)_6^{4-}$ redox couple at the surface of the ZMCPE. This was confirmed to be a quasi-reversible system since the peak separation potential, ΔEp ($Ep_a – Ep_c$) is equal to 163 mV (0.294 – 0.131) which is greater than 59 mV expected for reversible systems [38].

To determine the electroactive surface area of the composite electrodes, scan rate was varied from 5 to 400 mV s^{-1} for both the bare carbon paste (composite A) and the La-MOR-15 (composite B). An approximately linear relationship was found between the anodic peak current and the square root of the scan rate (R^2 = 0.9992) for composite B as shown in Fig. 3.6. While for composite A, a less linear relationship was obtained between the anodic peak current and the square root of scan rate (R^2 = 0.9881) as shown in Fig.

3.7. It can be concluded from such relationship that ion accessibility to electrode surface can be enhanced by La-impregnation.

Table 3.2 Composite Ratio of Prepared Electrodes

Designation	Graphite (wt %)	Zeolite (wt %)	Paraffin (wt %)
A	70	0	30
B	65	5	30
C	60	10	30
D	55	15	30
E	50	20	30

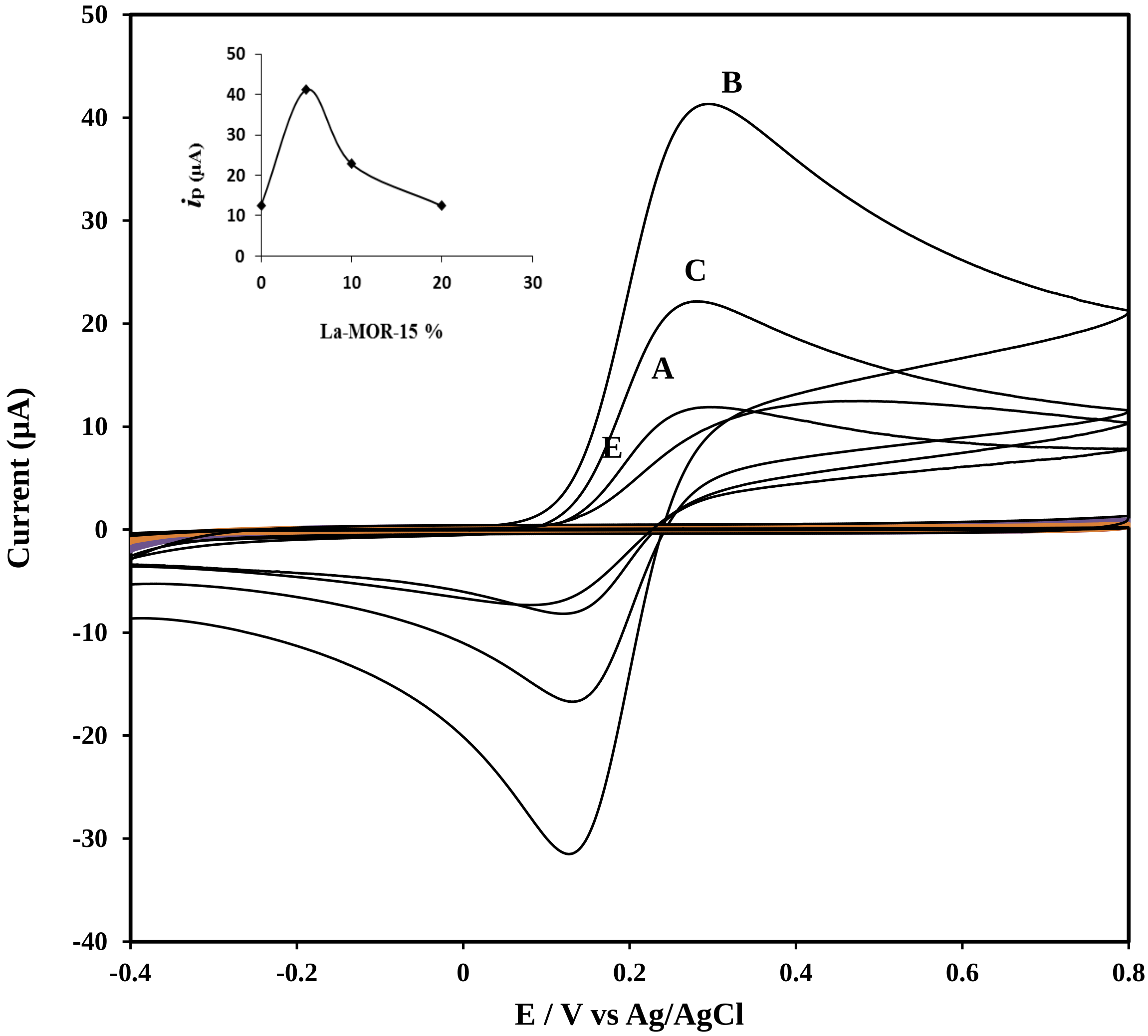

Fig. 3.5 CVs of 10 mM $K_4Fe(CN)_6$ Solution in 0.1 M KCl at a Scan Rate of 100 mV s^{-1} (pH 7) at Composites A – E. Inset: Plot of Peak Current vs La-MOR Percentage

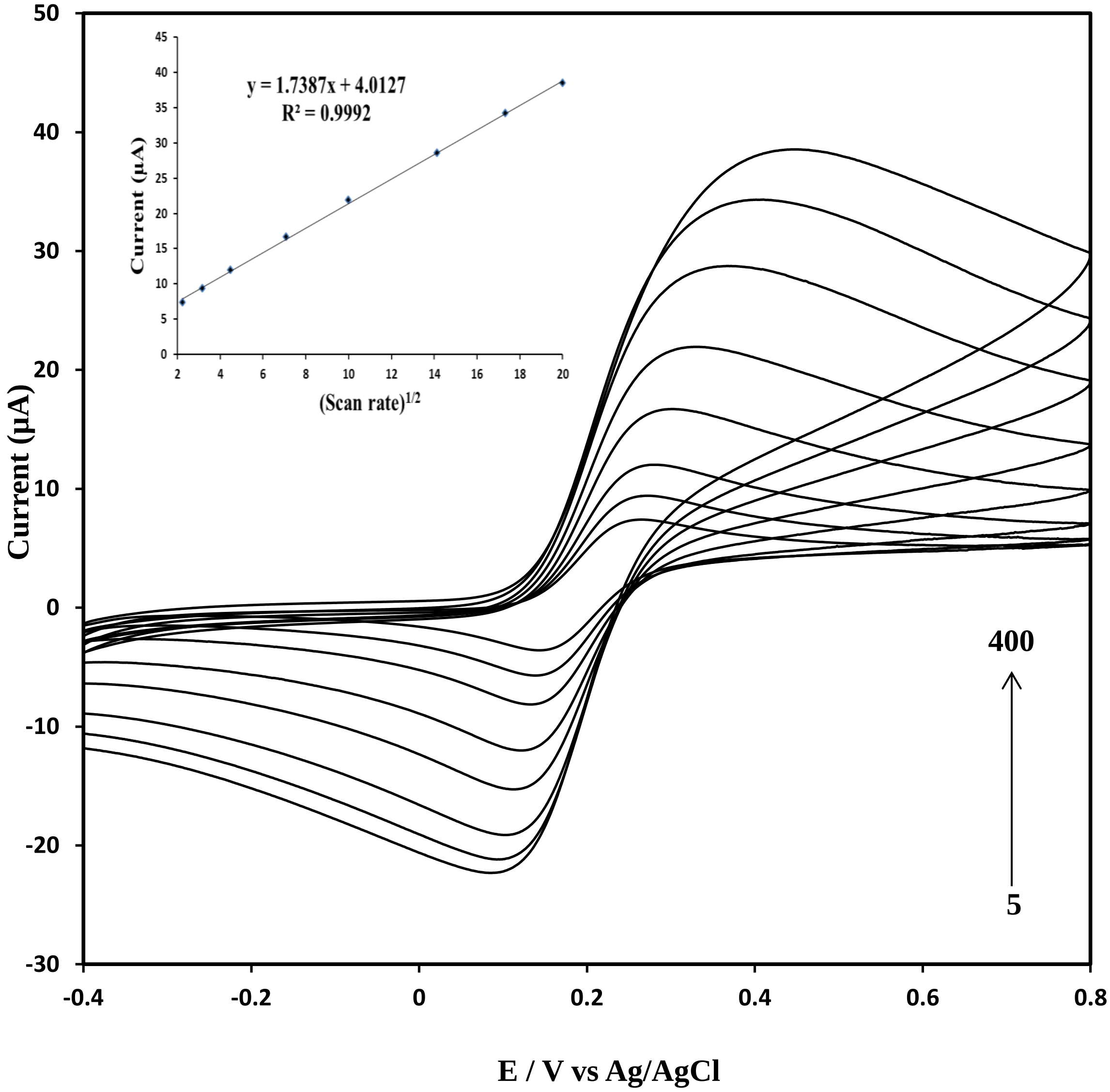

Fig. 3.6 Effect of Scan Rate on the Peak Current in the Presence of 10 mM $K_4Fe(CN)_6$ Solution and 0.1 M KCl (pH 7) at Composite B. Inset: Plot of Peak Current vs Square Root of Scan Rate

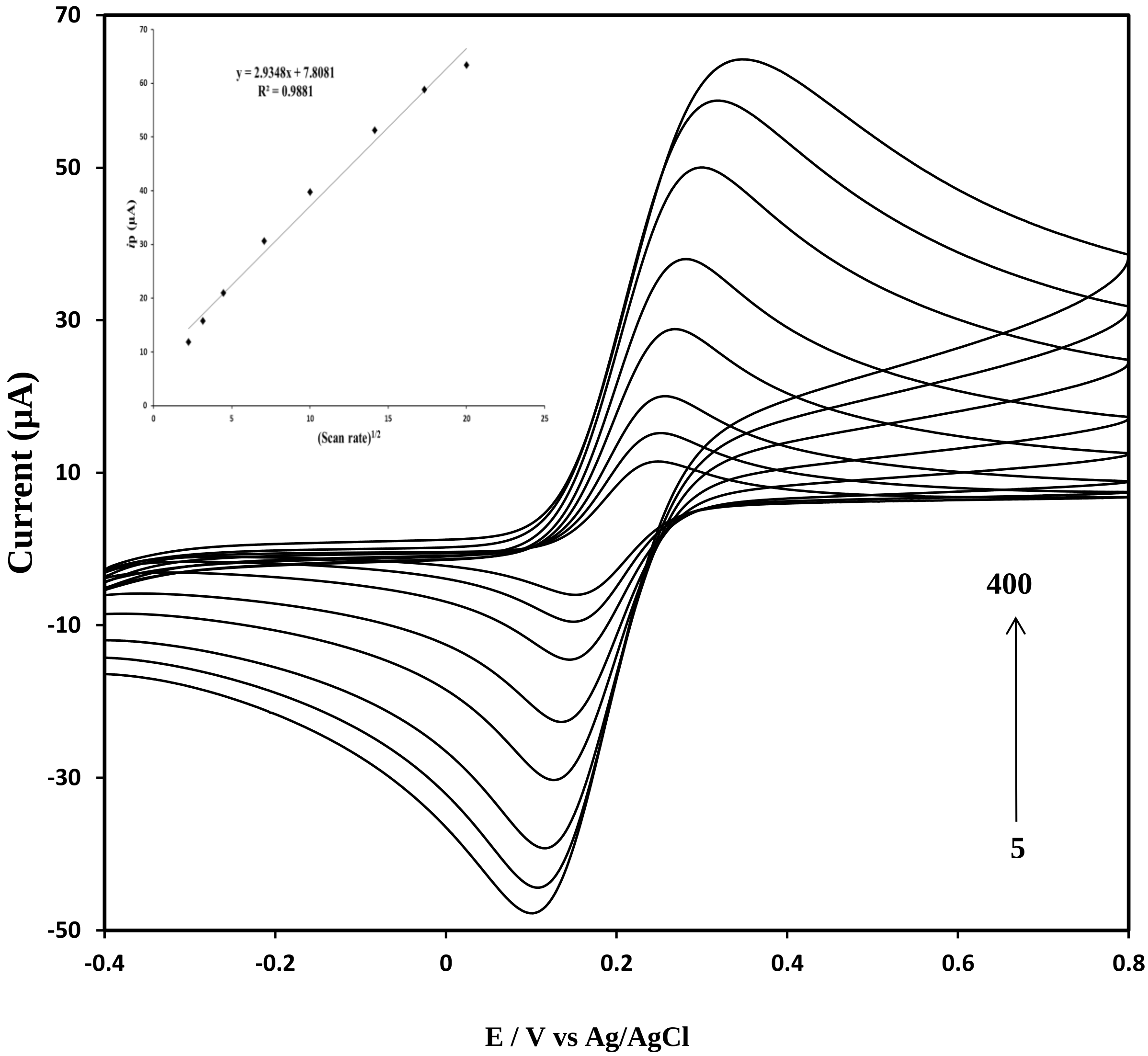

Fig. 3.7 Effect of Scan Rate on the Peak Current in the Presence of 10 mM $K_4Fe(CN)_6$ Solution and 0.1 M KCl (pH 7) at Composite A. Inset: Plot of Peak Current vs Square Root of Scan Rate

The electroactive surface area of the composite electrodes was estimated from the slope of the above plots using the Randles-Sevcik equation given in Eqn. 1.2 as:

$$i_p = 2.69 \times 10^5 n^{3/2} v^{1/2} D^{1/2} AC$$

Where n is the number of electrons, v is the scan rate, D is the diffusion coefficient (cm^2 s^{-1}), A is the area of the electrode and C is the electrolyte concentration in mol L^{-1}. The electroactive surface area estimated for the composite electrodes are 21.4 and 25.9 mm^2 for composites A and B, respectively. The results show that modifying the carbon paste electrode with lanthanum impregnated zeolite (La-MOR-15) led to an increase in the electroactive surface area of the electrode.

3.4 Voltammetric Determination of Cd (II)

The composite electrode B i.e. La-MOR-15 was applied for the determination of Cd (II) ions in 0.1 M phosphate buffer (pH 4) using square wave anodic stripping voltammetry with constant stirring at 600 rpm during the accumulation of the analyte. Accumulation parameters i.e. accumulation potential and accumulation time were optimized before carrying out Cd determination.

3.4.1 Optimization of Accumulation Potential and Time

Accumulation potential and time are crucial parameters while carrying out anodic stripping voltammetric determination of metal ions such as Cd (II) ion. This is because unless an appropriate potential is applied to enable the reduction and pre-concentration of the metal ions onto the surface of the working electrode prior to stripping, the sensitivity of the electrode is greatly affected. The effect of accumulation potential was studied by Kokkinos et al [39]. They demonstrated that choosing a high potential (in the negative direction) leads to background hydrogen evolution. In addition, accumulation potential which is too low is not enough to reduce the metal onto the surface of the electrode before being stripped.

In the current study, optimization was carried out in 500 ppb Cd (II) solution in 0.1 M phosphate buffer (pH 4) and the accumulation potential was varied from -1.4 V to -0.6 V. The resulting square wave voltammograms are presented in Fig. 3.8. As can be seen from the inset plot of current vs accumulation potential, the maximum peak current was obtained at -1.0 V. However, when it was adopted for subsequent detection along with other parameters such as amplitude (0.2 V) and frequency (40 Hz), a very broad peak was obtained. Hence, a balance has to be struck between obtaining a maximum peak current and a less broad peak. As such, accumulation potential of -1.2 V was adopted for the purpose of the current study.

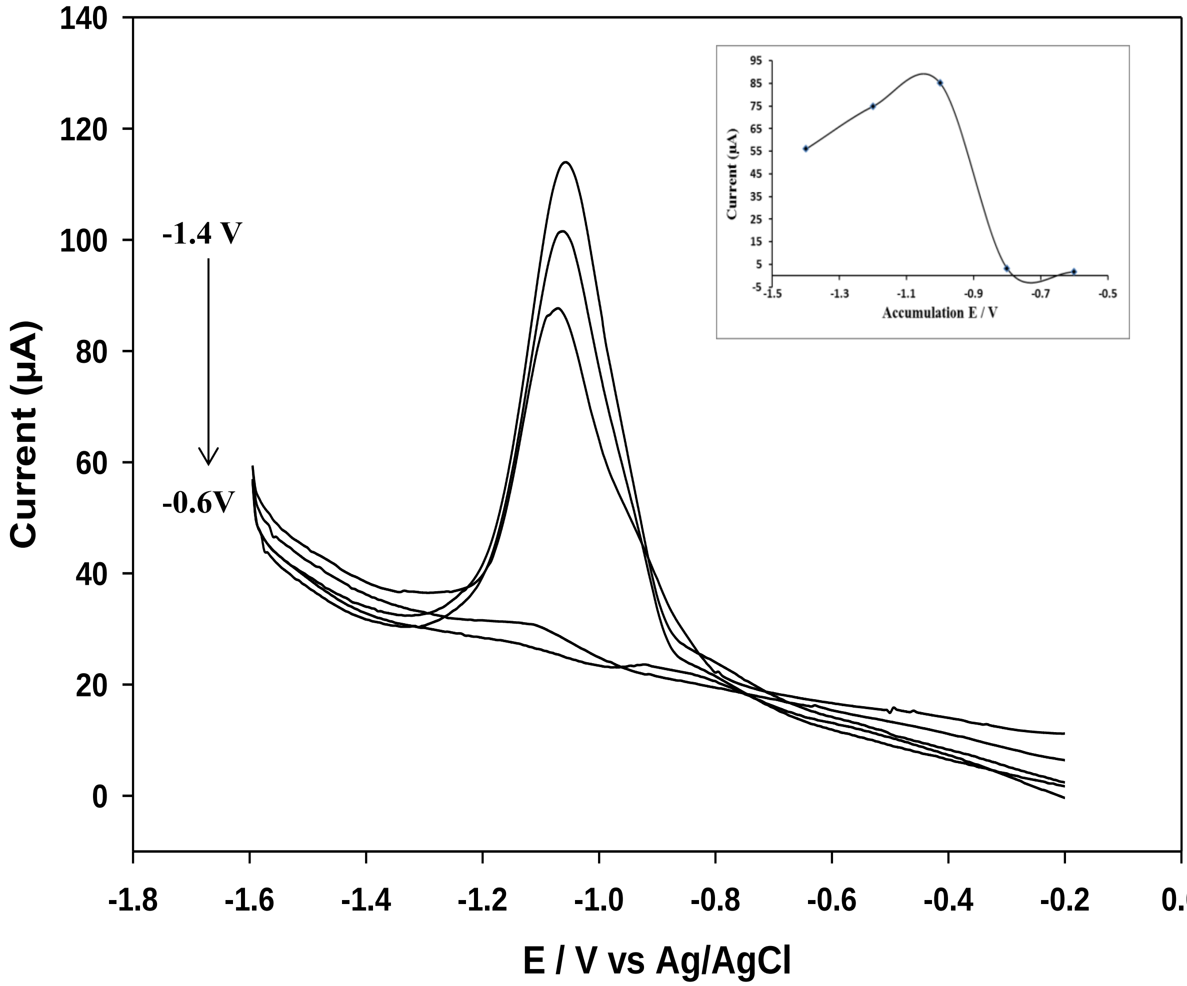

Fig. 3.8 SWASV of 500 ppb Cd (II) in 0.1 M Phosphate Buffer (pH 4) at La-ZMCPE with Varying Accumulation Potential: -1.4 V to -0.6 V. [Accumulation Time: 120 s; Amplitude: 0.2 V; Frequency: 40 Hz; Potential Step: 5 mV; Inset: Plot of Current vs Accumulation Potential]

In the same manner, accumulation time was varied from 20 sec – 200 sec, and the results are shown in Fig. 3.9. Accumulation time is the time during which the analyte is reduced at the working electrode (WE). It is generally believed that lower detection limits can be obtained with longer accumulation time [40]. However, longer accumulation time can alter the electrode's surface thereby affecting its performance. As a result, accumulation time of 120 sec was adopted for the purpose of the current study. In summary, the following conditions were employed for the subsequent construction of calibration curve for Cd (II) detection using the ZMCPE prepared in the current study; amplitude: 0.2 V, frequency: 40 Hz, accumulation potential: -1.2 V, accumulation time: 120 s, potential increment: 0.005 V.

3.4.2 Construction of Calibration Curve

After the optimization of the different parameters, stripping of Cd (II) over two different concentration ranges of 50 – 500 ppb and 5 – 50 ppb was investigated as shown in Fig. 3.10 and Fig. 3.11 respectively. The stripping current was found to be linear with various concentrations of Cd (II) at both higher and lower concentration ranges with correlation coefficient of 0.999 and 0.998 for the higher and lower ranges, respectively. The limit of quantitation was found as 5 μg/L and the limit of detection (S/N = 3) was 0.12 μg/L. It can be concluded from the results of the analytical performance parameters that the La-impregnated zeolite modified carbon paste electrode constructed in the current study has a wide determination range with a low detection limit.

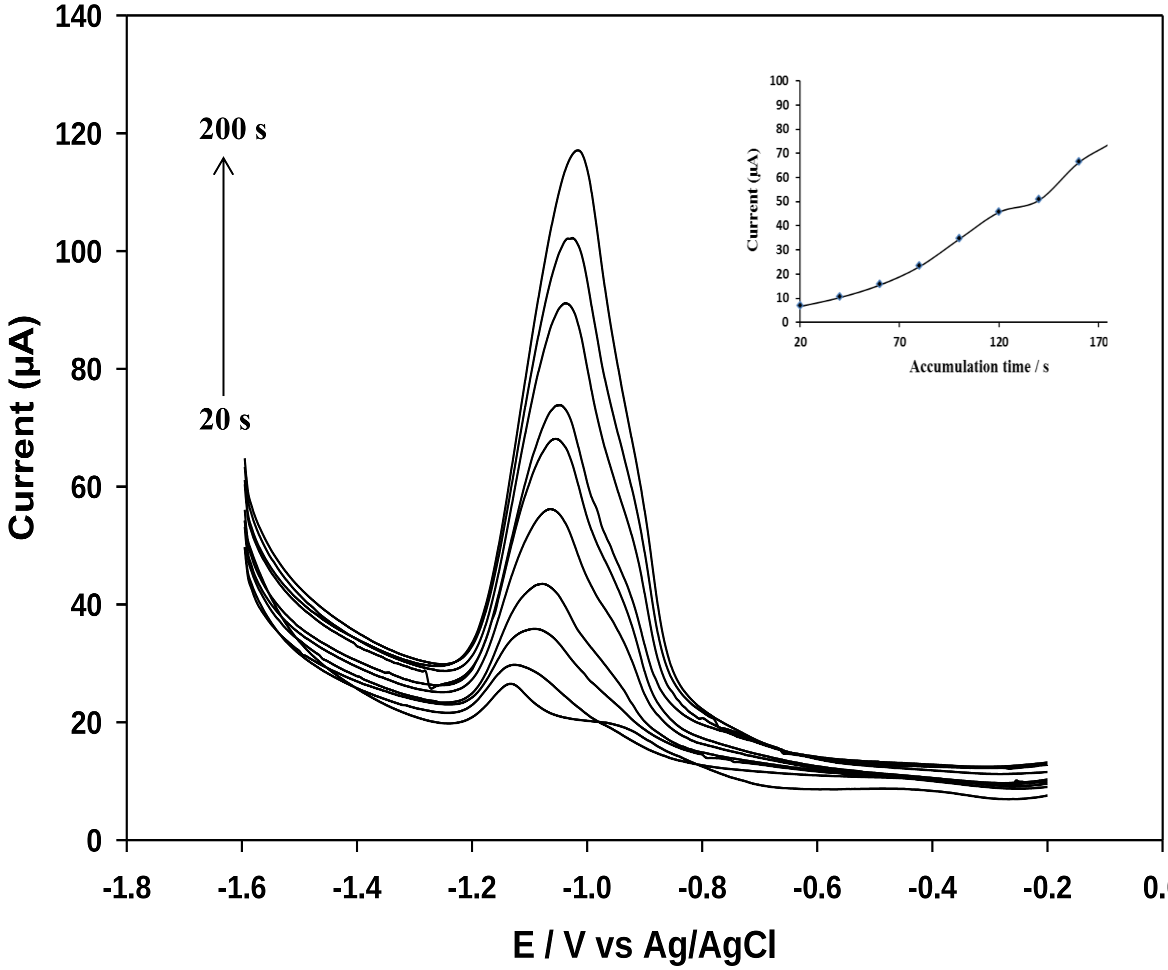

Fig. 3.9 SWASV of 500 ppb Cd (II) in 0.1 M Phosphate Buffer (pH 4) at La-ZMCPE with Varying Accumulation Time: 20 – 200 s. [Accumulation Potential: -1.2 V; Amplitude: 0.2 V; Frequency: 40 Hz; Potential Step: 5 mV; Inset: Plot of Current vs Accumulation Time]

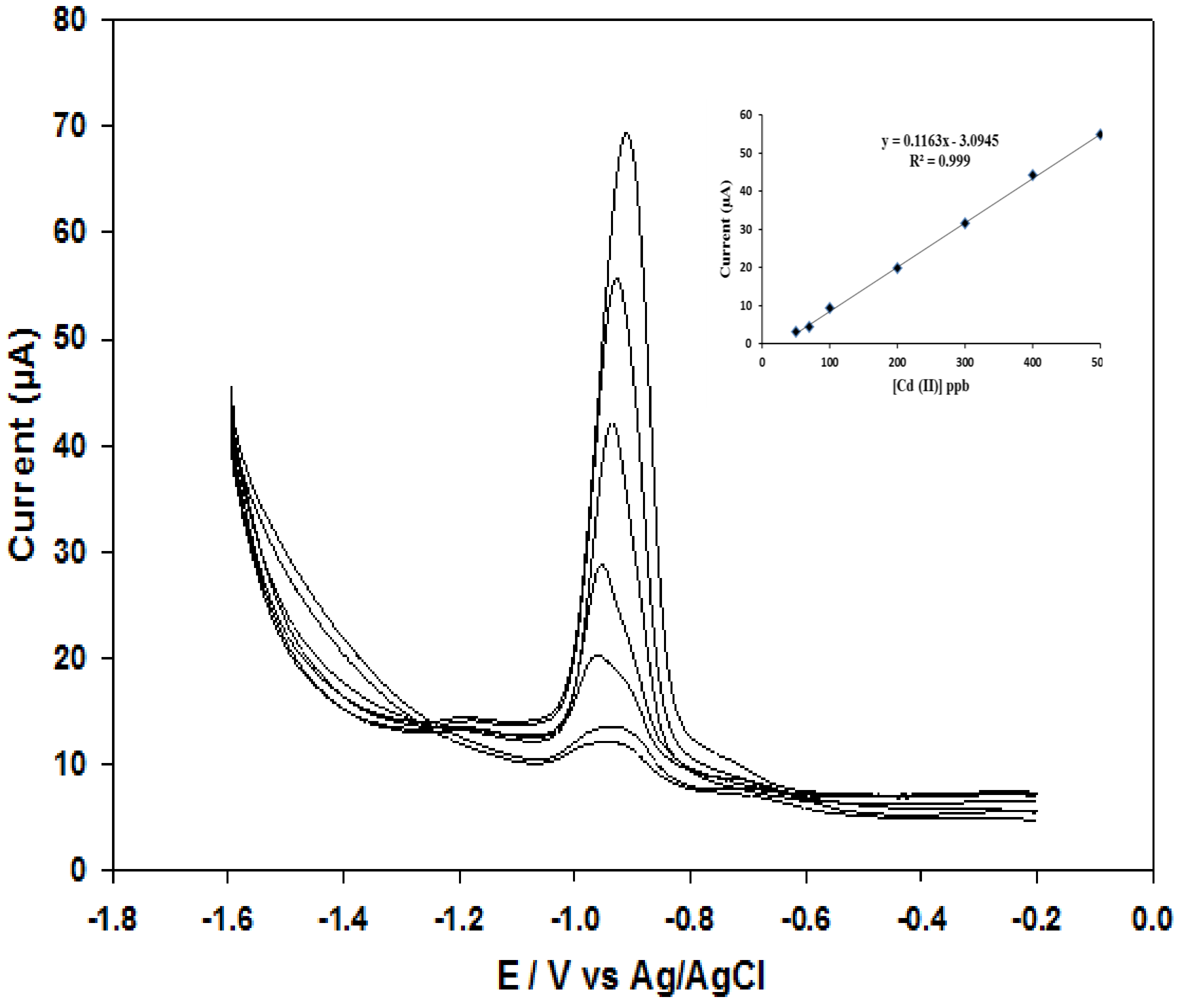

Fig. 3.10 SWASV of Cd (II) (50 – 500 ppb) in 0.1 M Phosphate Buffer (pH 4) at La-ZMCPE. [Accumulation Potential: -1.2 V; Accumulation Time: 120 s; Potential Step: 5 mV; Amplitude: 100 mV; Frequency: 40 Hz; Inset: Calibration Plot of Cd (II)]

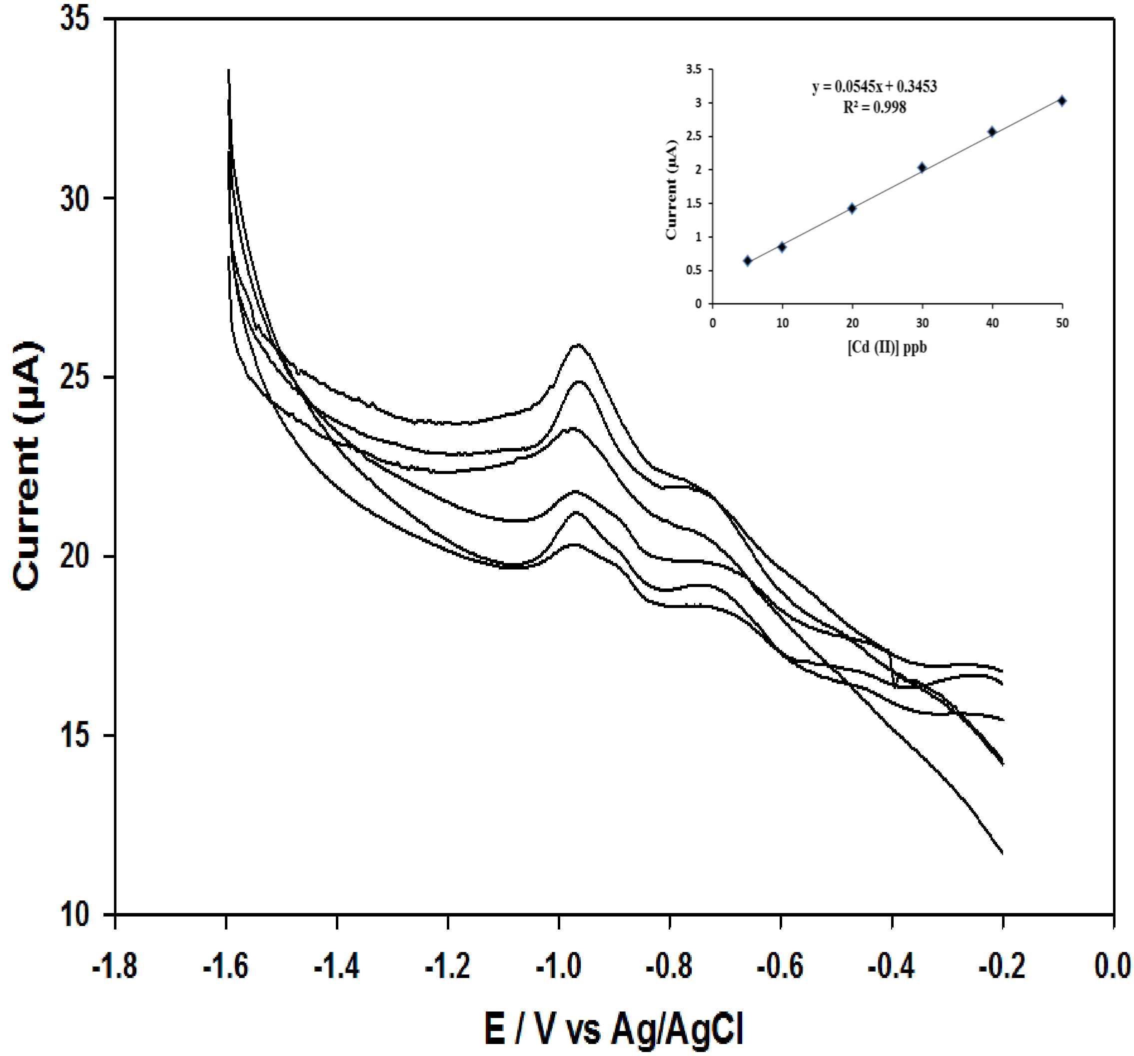

Fig. 3.11 SWASV of Cd (II) (5 – 50 ppb) in 0.1 M Phosphate Buffer (pH 4) at La-ZMCPE. [Accumulation Potential: -1.2 V; Accumulation Time: 120 s; Potential Step: 5 mV; Amplitude: 100 mV; Frequency: 40 Hz; Inset: Calibration Plot of Cd (II)]

Comparing the performance of the current electrode with other electrodes for the detection of Cd (II) reported previously (Table 3.3), the current electrode compares well and in fact it has one of the lowest detection limits for Cd (II) detection.

The reproducibility of the stripping analysis of 50 ppb Cd (II) at the La-ZMCPE was also checked by carrying out 5 consecutive measurements with a single electrode. The RSD was found as 2.7% implying that the electrode is stable with reproducible Cd (II) detection ability, Fig. 3.12.

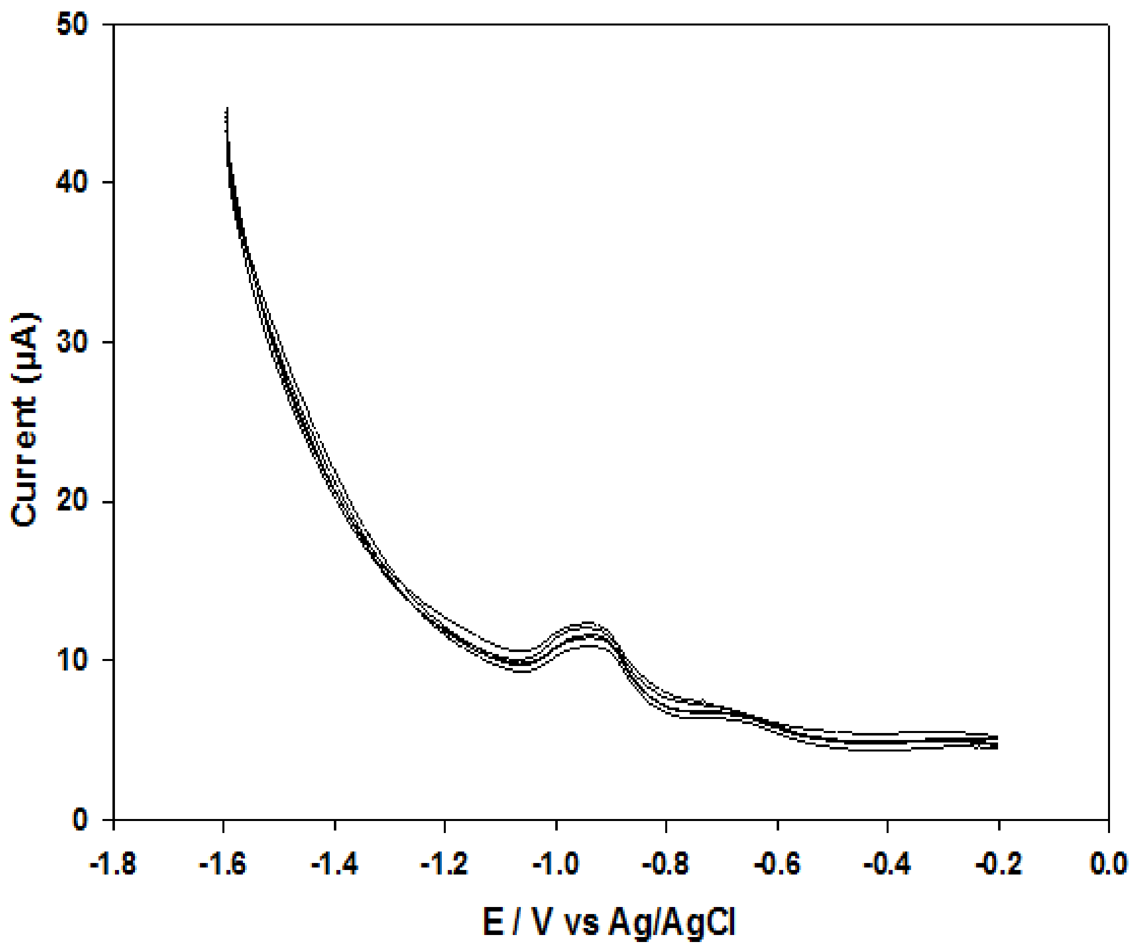

Fig. 3.12 SWASV of 50 ppb Cd (II) in 0.1 M Phosphate Buffer (pH 4) at La-ZMCPE, After Five Consecutive Runs. (Conditions Same as Fig. 3.10)

Table 3.3 Detection Limits of Some Reported Electrodes

Electrode Type	**Analyte**	**Technique**	**Accumulation Potential (V)**	**Accumulation Time (s)**	**Detection Limit (μg/L)**	**Ref**
Carbon screen-printed electrode modified by Bi-nanoparticle	Cd (II)	SWASV	-1.4	120	1.3	[41]
Boron-doped diamond electrode	Cd (II)	DPASV	-1.7	60	0.36	[42]
Bi-modified carbon paste electrode	Cd (II)	SWASV	-0.95	120	1.0	[43]
Bi-film electrode	Cd (II)	SWASV	-1.10	90	1.4	[44]
Nafion-coated Bi-film electrode	Cd (II)	SWASV	-1.4	-	2.0	[45]
Bi nano-powder electrode	Cd (II)	SWASV	-1.2	180	0.07	[46]

CHAPTER 4

TRACE LEVEL DETECTION OF Pb (II) AND Cd (II) AT RARE EARTH-IMPREGNATED ZEOLITE MODIFIED CARBON PASTE ELECTRODE (RE-ZMCPE)

4.1 Summary

Rare earth impregnated zeolite-modified carbon paste electrode (RE-ZMCPE) has been investigated as an alternative electrode for the anodic stripping voltammetric determination of Pb (II) and Cd (II) ions. The RE-ZMCPE which was produced-in-house by first carrying out the synthesis of La and Ce-impregnated zeolite before fabrication, displays comparable results to those of other modified electrodes for similar analyses. Deposition of the metal onto the surface of the electrodes was accomplished by holding the electrode at a potential of -1.2 V (vs Ag/AgCl) for 120 sec followed by a square wave stripping scan from -1.6 – 0 V. Prior to the stripping analyses, experimental conditions such as choice of electrolyte, pH, amplitude, frequency, deposition potential and deposition time were optimized. Calibration plots obtained by carrying out a stripping analysis of Pb (II) and Cd (II) shows a good linearity over the metal ion concentrations with detection limits 0.225 µg L^{-1} and 0.122 µg L^{-1} at the La-ZMCPE for Pb (II) and Cd (II) detection, and 0.07 µg L^{-1} and 0.046 µg L^{-1} at Ce-ZMCPE for Pb (II) and Cd (II)

detection, respectively. The electrodes displayed good reproducibility with RSD 3.02% and 2.23% for both La-ZMCPE and Ce-ZMCPE. Comparing the limits of detection and sensitivities of the metals when detected alone and when detected simultaneously in a mixture reveals that Ce-impregnated zeolite modified carbon paste electrode (Ce-ZMCPE) is suitable for simultaneous trace level detection of Pb (II) ions. Overall, the electrodes exhibits potential to be used for analyzing environmental samples due to their inexpensiveness, ease of fabrication and lack of toxicity compared to mercury-based electrodes.

4.2 Synthesis and Characterization of La/Ce-MOR

In this study, mordenite zeolite with silica to alumina ratio 15 was synthesized by the sol-gel method. The resulting crystal was investigated by XRD in order to ascertain its crystallinity. The result of the XRD as shown in Fig. 4.1 present the Na and H-forms of the crystal prior to and after ion-exchange, with diffraction peaks corresponding to the typical structure of mordenite [47]. The average crystal size of the synthesized material was obtained using the Scherer equation [48] as 6.8 µm. The size of crystals obtained using Scherer equation is usually interpreted as an average crystal dimension, perpendicular to the reflection plane [49], the accuracy of which is usually no better than 20 – 40% because the sample analyzed usually do not have crystals of uniform size. The morphology of the mordenite indicates that a flat-prismic crystal was formed as shown in the SEM image in Fig. 4.2. The EDX result of the prepared sample (Fig. 4.3) showed the presence of O, Al and Si. The weight percent of each element is summarized in Table 4.1

After impregnation of the zeolite with La (III) and Ce (III) ions, the XRD pattern, the SEM images and the EDX spectrum of the crystal was carried out to ensure that the crystallinity was not lost. The results of the XRD pattern (Fig. 4.4 and Fig. 4.5) showed that the crystallinity of the MOR zeolite was not damaged, and the results of the SEM (Fig. 4.6) also showed that the crystal morphology was retained. We could however see several spots on the metal impregnated zeolites indicating the binding between the zeolite crystal and the impregnated metals. Tables 4.2 and 4.3 summarize the weight percent of the elements present in the zeolite after La (III) and Ce (III) impregnation respectively obtained from their corresponding EDX spectra.

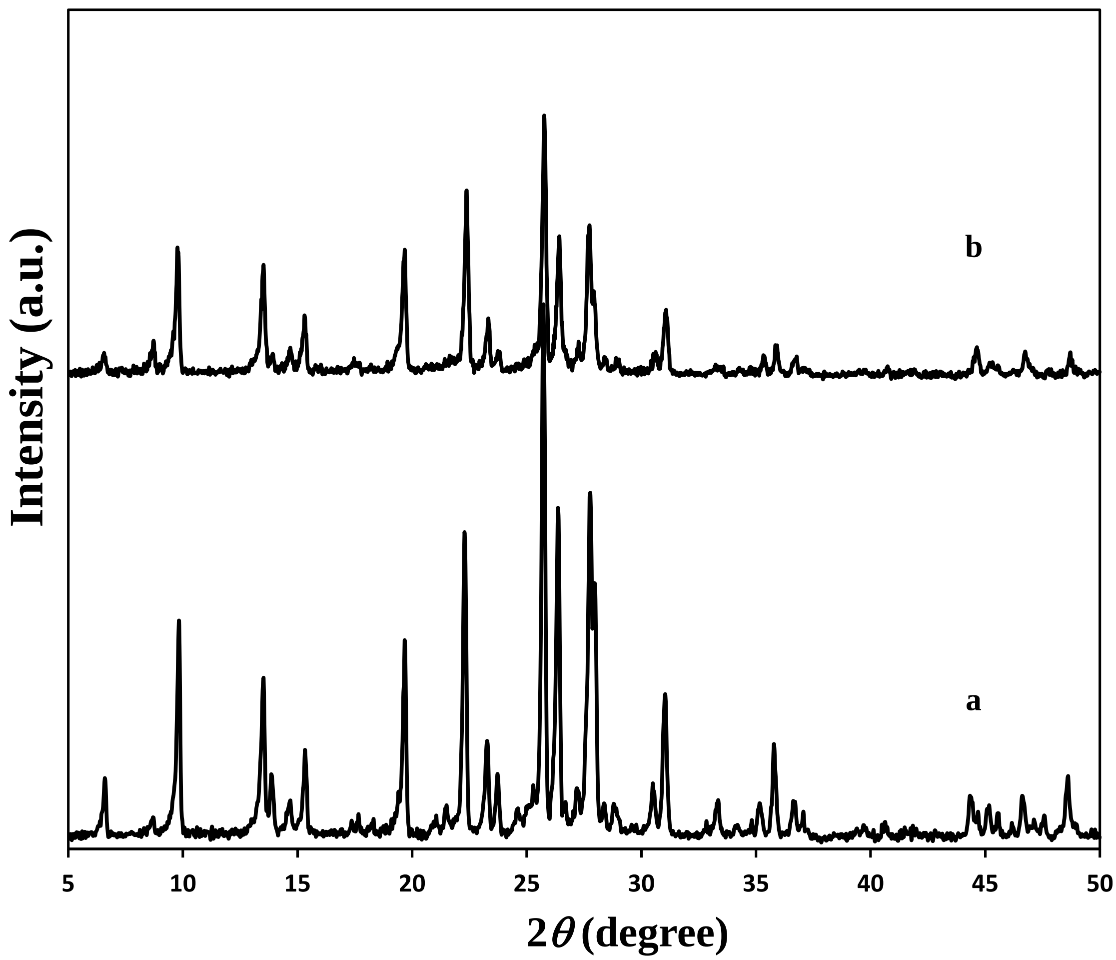

Fig. 4.1 XRD Pattern of (a) Na-MOR, and (b) H-MOR

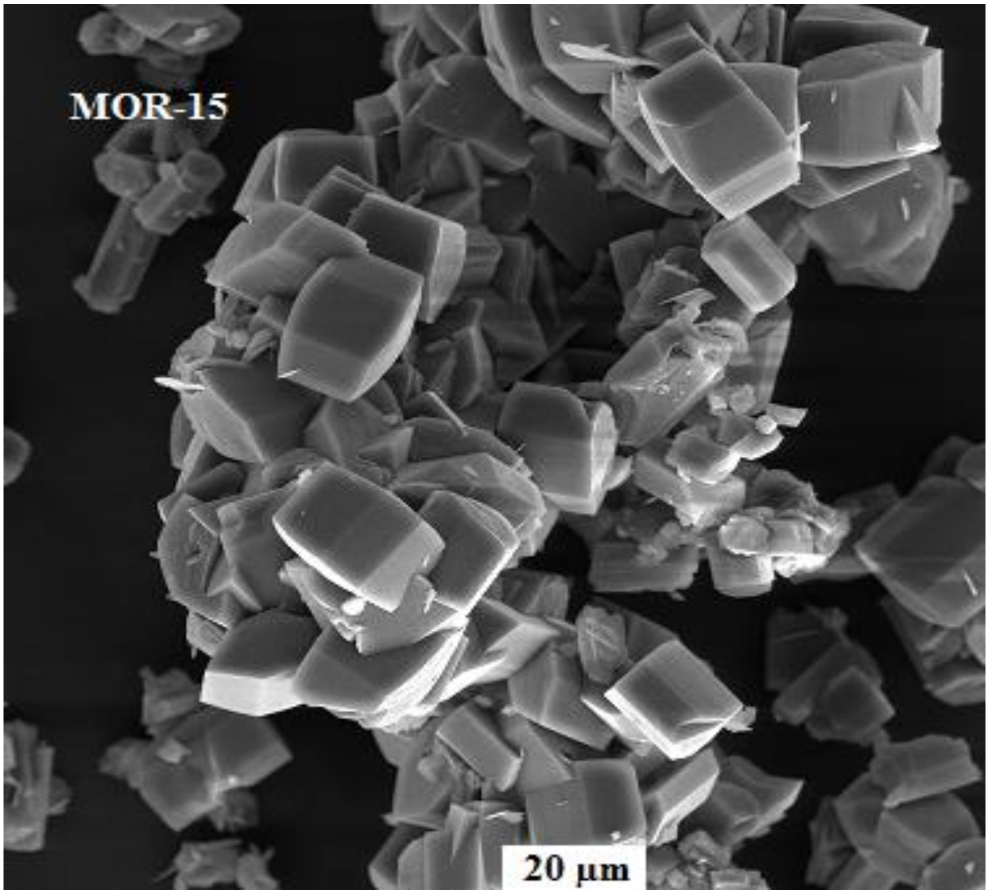

Fig. 4.2 SEM Image of MOR

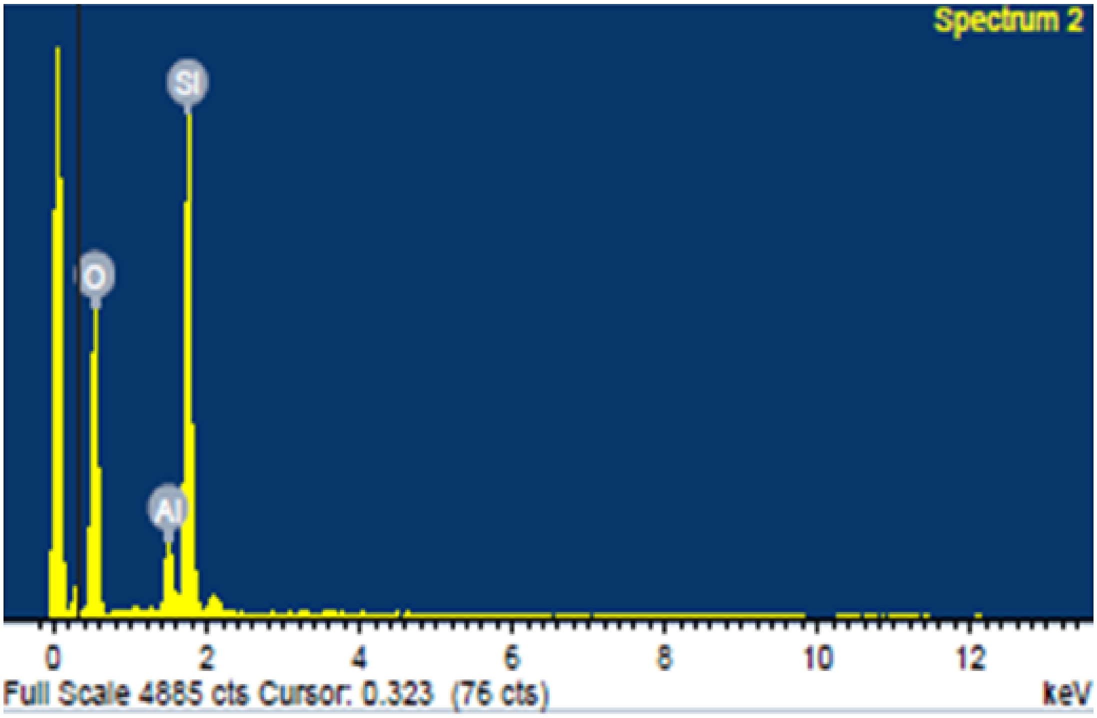

Fig. 4.3 EDX Spectrum of MOR

Table 4.1 Weight Percent of Elements of MOR

Element	**Oxygen (wt. %)**	**Aluminum (wt. %)**	**Silicon (wt. %)**	**Total (wt. %)**
Mean	55.87	4.68	39.45	100

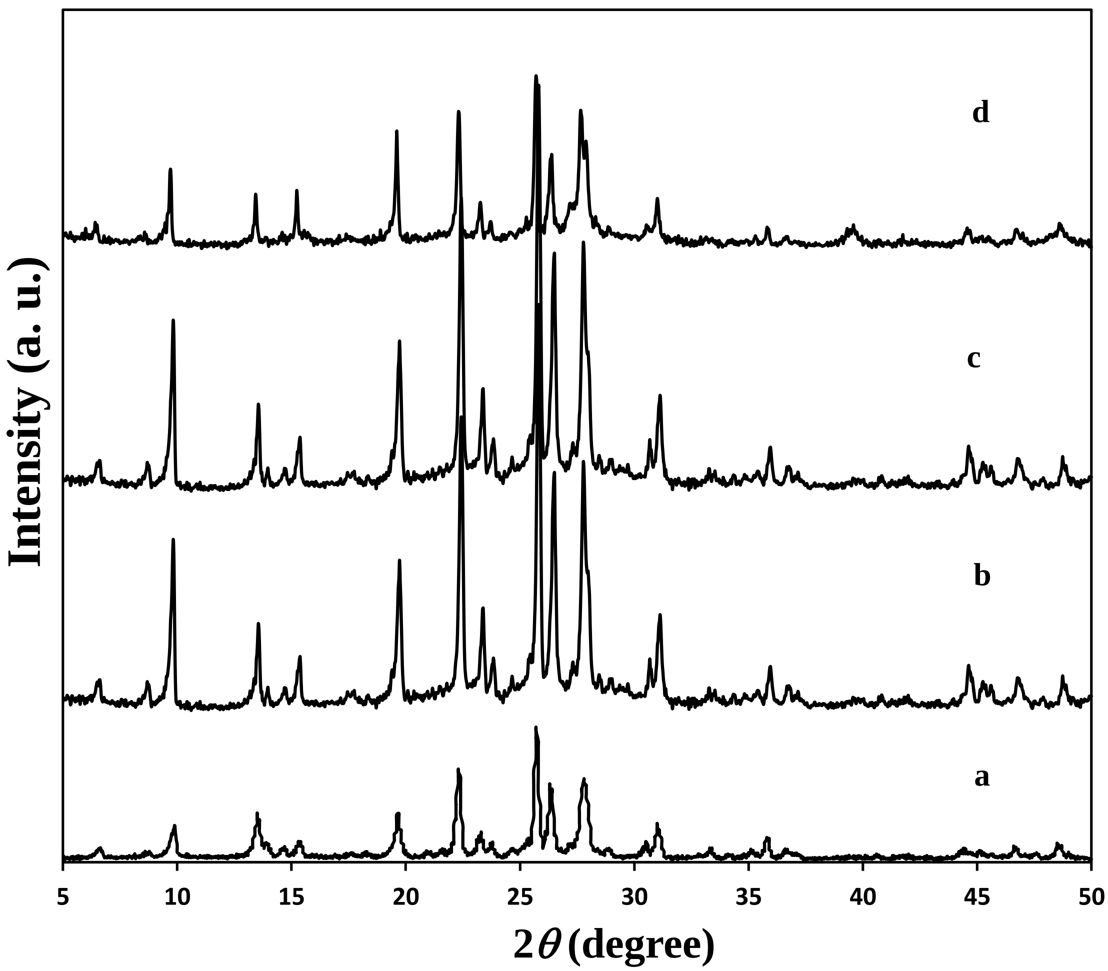

Fig. 4.4 XRD Pattern of (a) H-MOR, (b) 2 wt% La-MOR, (c) 5 wt% La-MOR, and (d) 10 wt% La-MOR

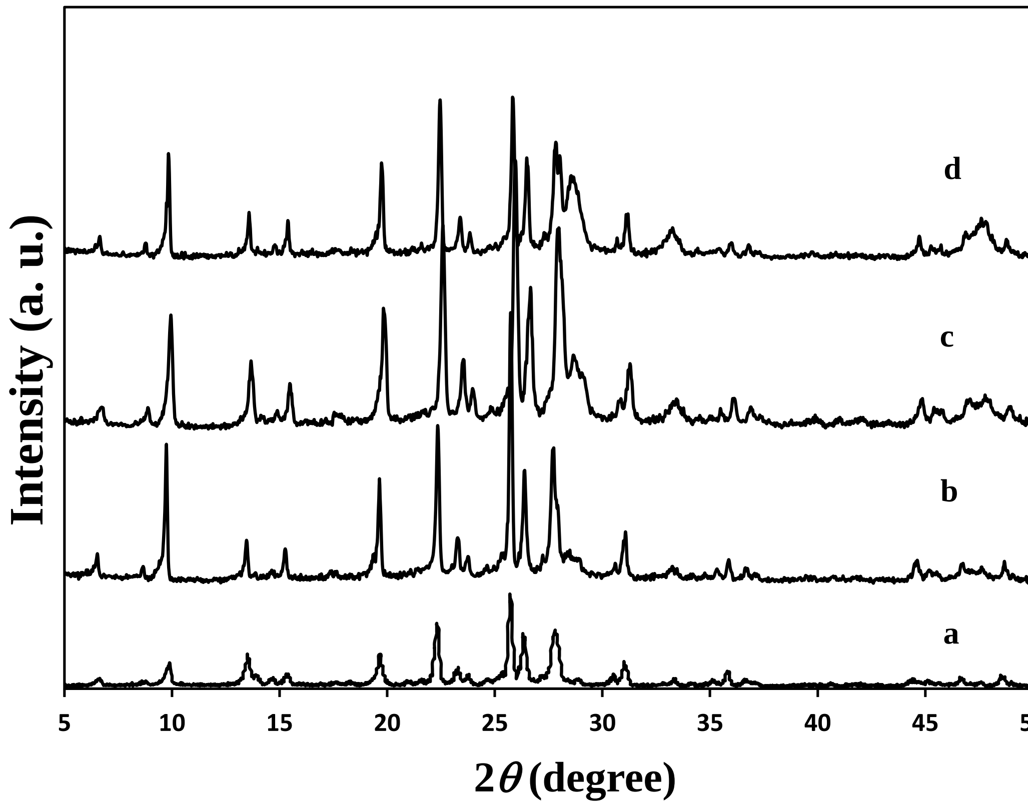

Fig. 4.5 XRD Pattern of (a) H-MOR, (b) 2 wt% Ce-MOR, (c) 5 wt% Ce-MOR, and (d) 10 wt% Ce-MOR

Table 4.2 Weight Percent of Elements of La-MOR

Material	Oxygen (wt. %)	Aluminum (wt. %)	Silicon (wt. %)	Lanthanum (wt. %)	Total (100 %)
2 wt% La-MOR	56.48	4.39	37.45	1.68	100
5 wt% La-MOR	55.99	4.82	36.67	2.51	100
10 wt% La-MOR	51.28	4.38	36.00	8.34	100

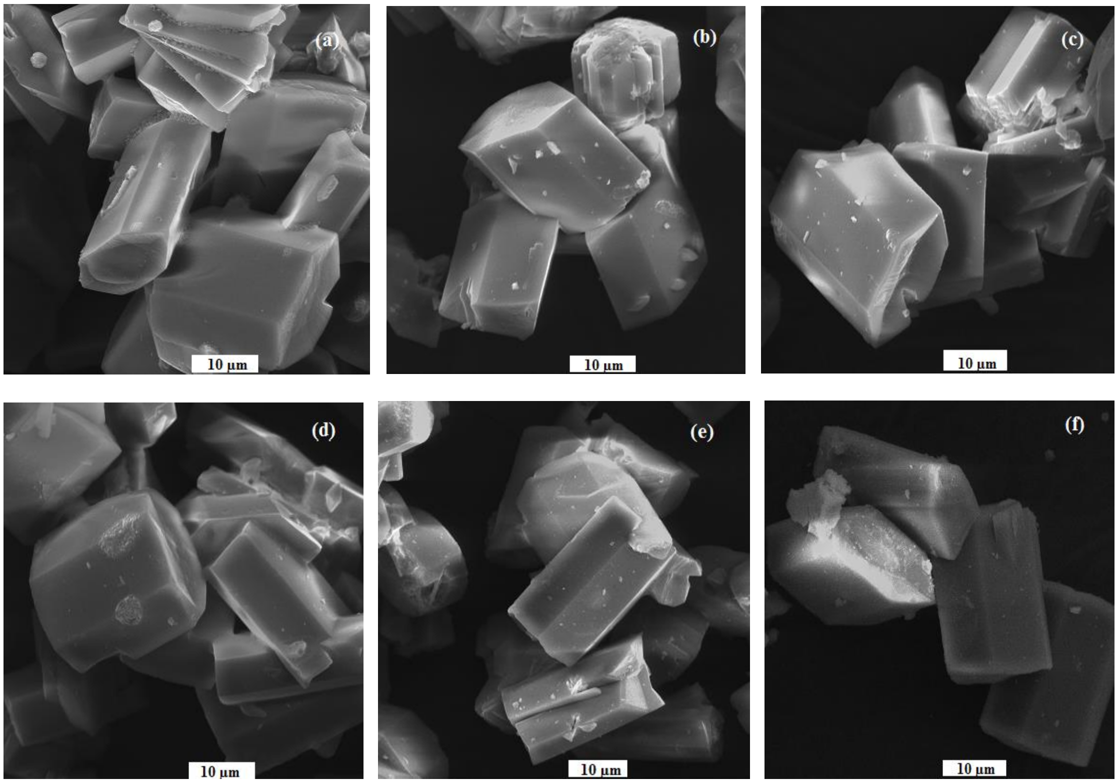

Fig. 4.6 SEM Images of (a) 2wt% La-MOR, (b) 5wt% La-MOR, (c) 10 wt% La-MOR, (d) 2 wt% Ce-MOR, (e) 5 wt% Ce-MOR, and (f) 10 wt% Ce-MOR

Table 4.3 Weight Percent of Elements of Ce-MOR

Material	**Oxygen (wt. %)**	**Aluminum (wt. %)**	**Silicon (wt. %)**	**Cerium (wt. %)**	**Total (100 %)**
2 wt% Ce-MOR	53.46	4.41	39.66	2.47	100
5 wt% Ce-MOR	56.80	4.27	34.09	4.85	100
10 wt% Ce-MOR	51.33	4.20	34.46	10.01	100

The incorporation of La (III) and Ce (III) ions into the framework of the zeolite was also checked by ^{27}Al MAS NMR. ^{27}Al NMR provides information about the environment of the aluminum atoms in zeolite samples. Aluminum atoms tetrahedrally coordinated to the zeolite framework ($Al(OSi)_4$), appears as a peak at chemical shift ~50 ppm, whereas extra-framework aluminum atoms which are octahedrally coordinated to the framework gives a signal around chemical shift ~0 ppm [50]. In strongly dealuminated zeolite samples, a further peak is usually observed between 30 and 50 ppm, and this has been assigned to penta-coordinated aluminum atoms [51] as well as distorted tetrahedrally coordinated aluminum atoms in the extra-framework [52]. The results of the NMR analysis in this study indicates that the two peaks corresponding to the tetrahedral and octahedral aluminum atoms were both obtained for the parent zeolite and the rare earth impregnated zeolites. However, as the metal loading increases, the intensities of the peaks decreases implying that the ratio of the Al atoms have decreased as a result of incorporation of the metals. This is shown in Fig. 4.7.

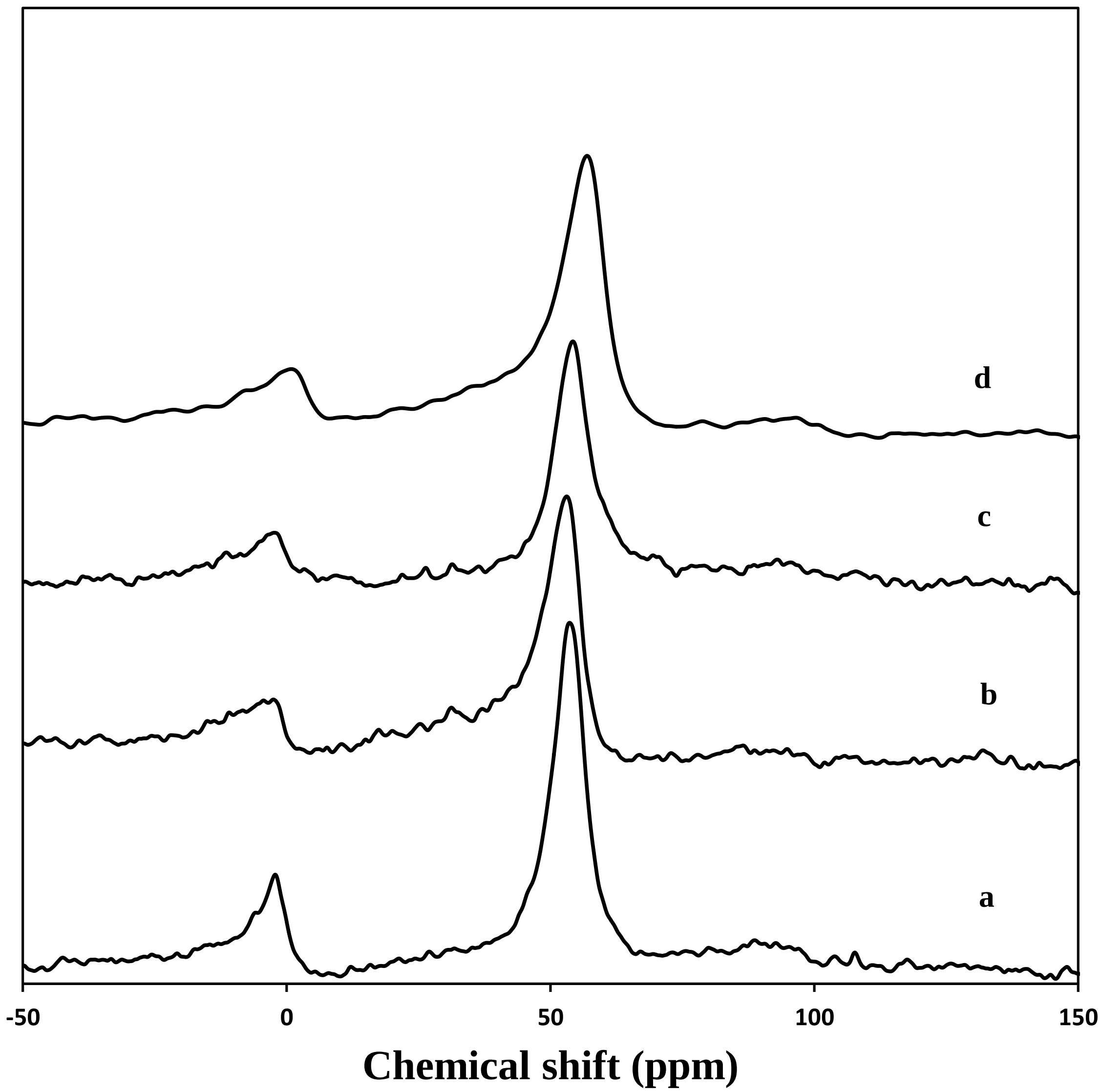

Fig. 4.7 ^{27}Al MAS NMR of (a) MOR, (b) 2wt% La/Ce, (c) 5 wt% La/Ce, and (d) 10 wt% La/Ce-MOR

4.3 Electrochemical Behavior of La/Ce-MOR

4.3.1 Composite Screening

The electrochemical behavior of the La/Ce-MOR was investigated by the construction of La/Ce-zeolite modified carbon paste electrode (La/Ce-ZMCPE) for the square wave anodic stripping voltammetric detection of Pb (II) and Cd (II) ions in aqueous solutions. Preliminary experiments were carried out in order to screen out the electrodes since for every metal (La and Ce), three different loadings were synthesized (2, 5 and 10 wt%). It was therefore necessary to screen out the electrodes in order to obtain the one which gives maximum detection ability. For the preliminary experiments, electrodes were constructed in the ratio 50:25:25 (graphite: zeolite: paraffin) and square wave anodic stripping experiments were carried out in 500 ppb Pb (II) solution in 0.1 M phosphate buffer (pH 4). Fig. 4.8 shows the SWASV obtained at La-ZMCPE. From the results, a remarkable decrease was observed in the peak height as the metal loading increases, with 2 wt% La-ZMCPE having the highest peak height. Another observation made was that of bare carbon paste electrode prepared in the ratio 75:25 (graphite: paraffin) where the peak height was less than those of the modified electrode. This is an indication of an improved sensitivity of the electrode as a result of metal impregnation. In square wave voltammetry, peak height is a function of the concentration of the analyte present in the medium. As such the electrode which gave a better peak height is regarded as being more sensitive to the detection of the analyte. For the La-ZMCPE, 2wt% La-ZMCPE gave the optimum peak current and was therefore employed for the purpose of this study.

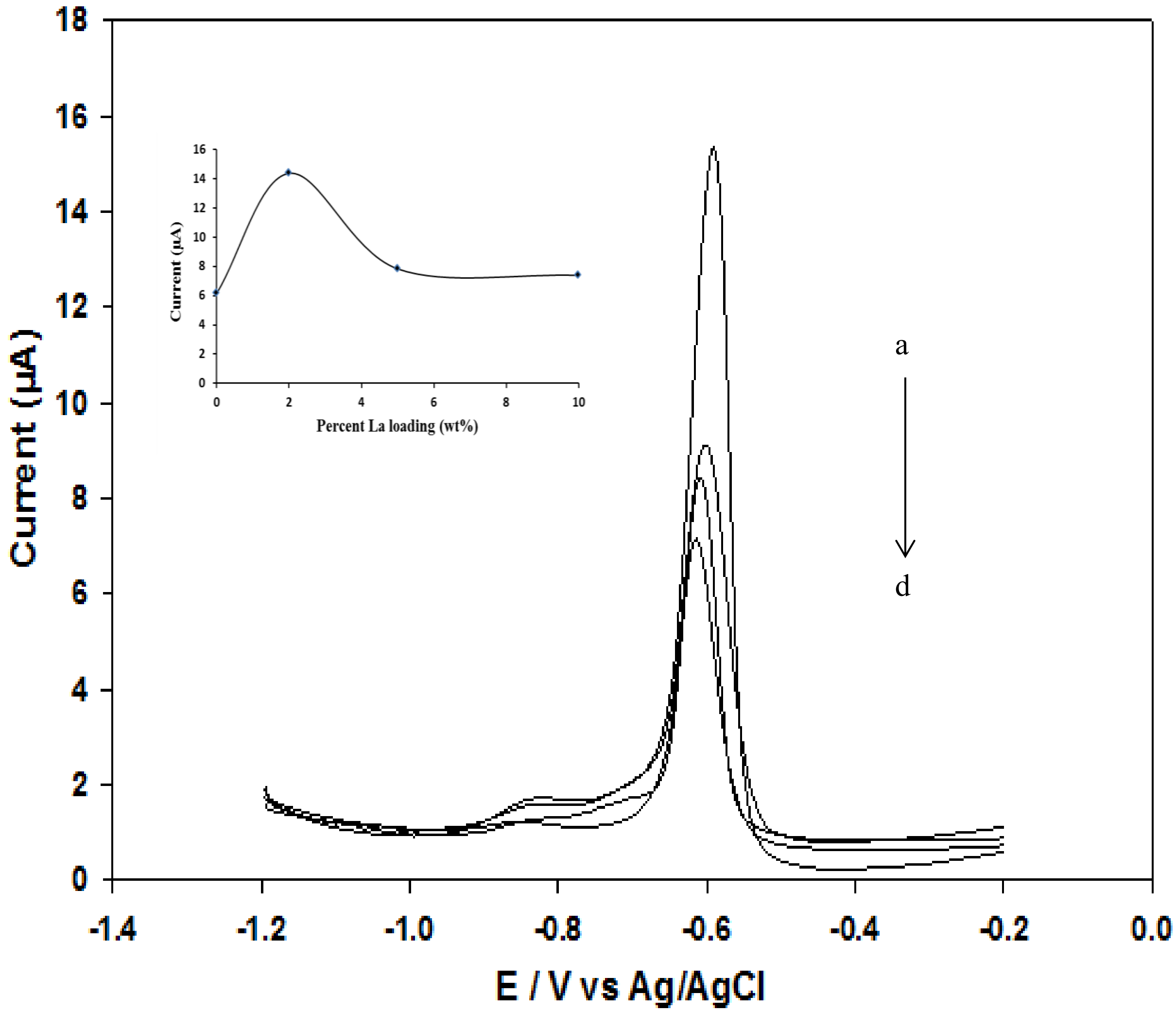

Fig. 4.8 SWASV of 500 ppb Pb (II) in 0.1 M Phosphate Buffer (pH 4) at (a) 2 wt% La, (b) 5 wt% La, (c) 10 wt% La, and (d) Un-Modified Zeolite-Carbon Paste Electrodes in the Ratio 50:25:25 Graphite:Zeolite:Paraffin. (Deposition Potential: -1.2 V; Deposition Time: 120 s; Potential Step: 5 mV; Amplitude: 50 mV; Frequency: 15 Hz. Inset: Plot of Percent La loading)

On the contrary, the electrochemical behavior of Ce-ZMCPE was the reverse of that of La-ZMCPE as the square wave stripping peak increases as the metal loading increases, with 10 wt% Ce having the highest. This is shown in Fig. 4.9. From the results of the preliminary experiments, we observe a reverse characteristic for composites of La and Ce. A quick look into literature reveals no established reason regarding this. However, it was reported elsewhere [53] that the catalytic properties of the two rare earth metals are the reverse of one another as La was reported to be more stabilizing than Ce, and hence less reactive. It was also reported elsewhere[54-56] where the metals were incorporated into various zeolites for applications which include; alkylation of alpha-methyl naphthalene, desulfurization of diesel fuel and cracking of naphtha, that catalysts with low La and high Ce loadings yielded best desired results. A reason for such observations could be due to the ionic sizes of the rare earth metal ions with La having an ionic radius of 1.50 Å and Ce having 1.48 Å. It could therefore be said that, the smaller the metal ion the higher its ability to fit into the zeolitic pores and the higher its catalytic characteristic.

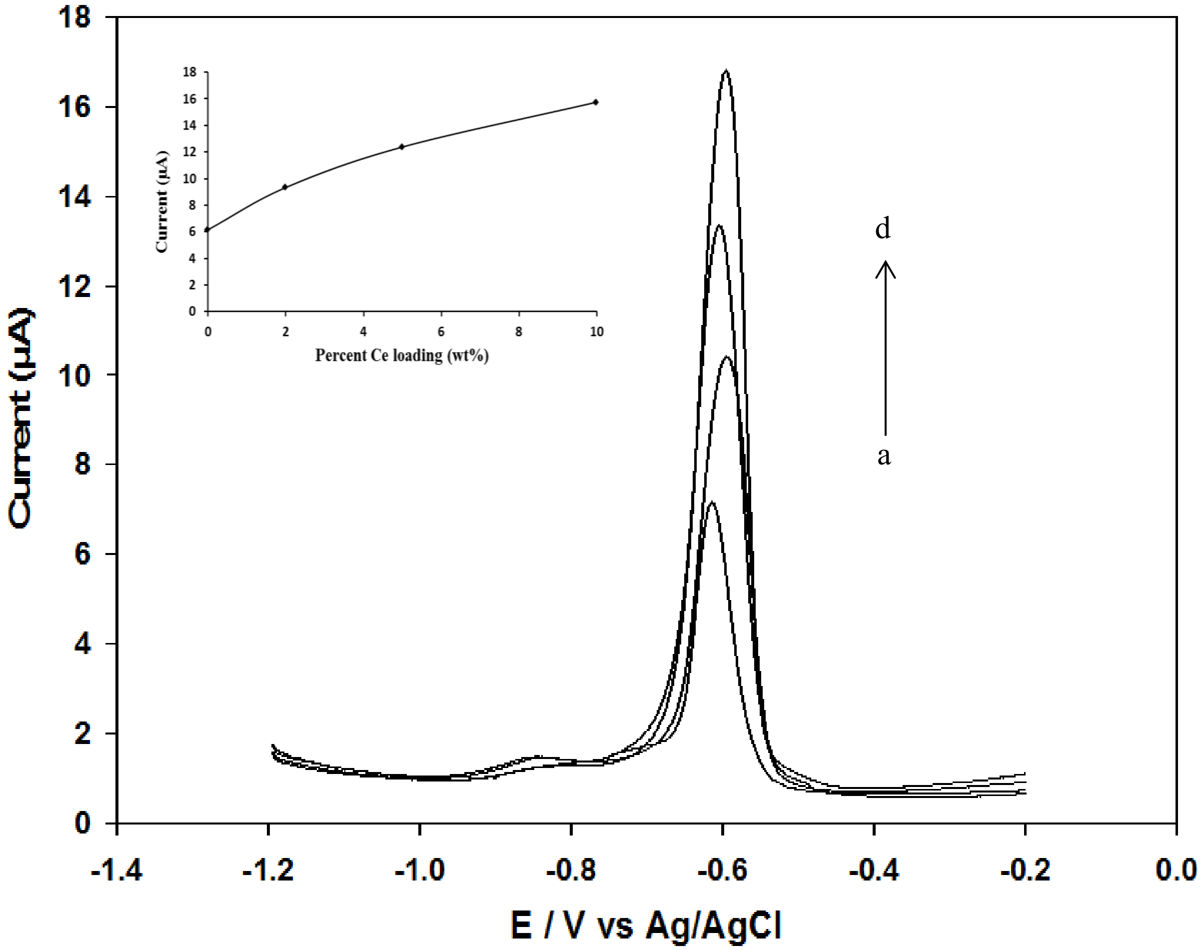

Fig. 4.9 SWASV of 500 ppb Pb (II) in 0.1 M Phosphate Buffer (pH 4) at (a) Un-Modified Zeolite, (b) 2 wt% Ce, (c) 5 wt% Ce, and (d) 10 wt% Ce-Zeolite-Modified Carbon Paste Electrodes in the Ratio 50:25:25 Graphite:Zeolite:Paraffin. (Condition Same as Fig. 4.8; Inset: Plot of Percent Ce Loading)

Having chosen the two composite electrodes (2 wt% La-ZMCPE and 10 wt% Ce-ZMCPE), further screening was carried out by varying the ratio of the composite materials (graphite, zeolite and paraffin oil). Ten composites were fabricated according to Table 4.4. It was observed from the SWASV of 500 ppb Pb (II) solution (Fig. 4.10 and Fig. 4.11) that composite B and G both containing the ratio 65:5:30 gave the optimum peak height in both cases and hence were adopted for the purpose of this study.

Table 4.4 Composite Ratio of 2 wt% La-ZMCPE (A – E) and 10 wt% Ce-ZMCPE (F – J)

Designation	Graphite	Zeolite	Paraffin oil
A	70	0	30
B	65	5	30
C	60	10	30
D	55	15	30
E	50	20	30
F	70	0	30
G	65	5	30
H	60	10	30
I	55	15	30
J	50	20	30

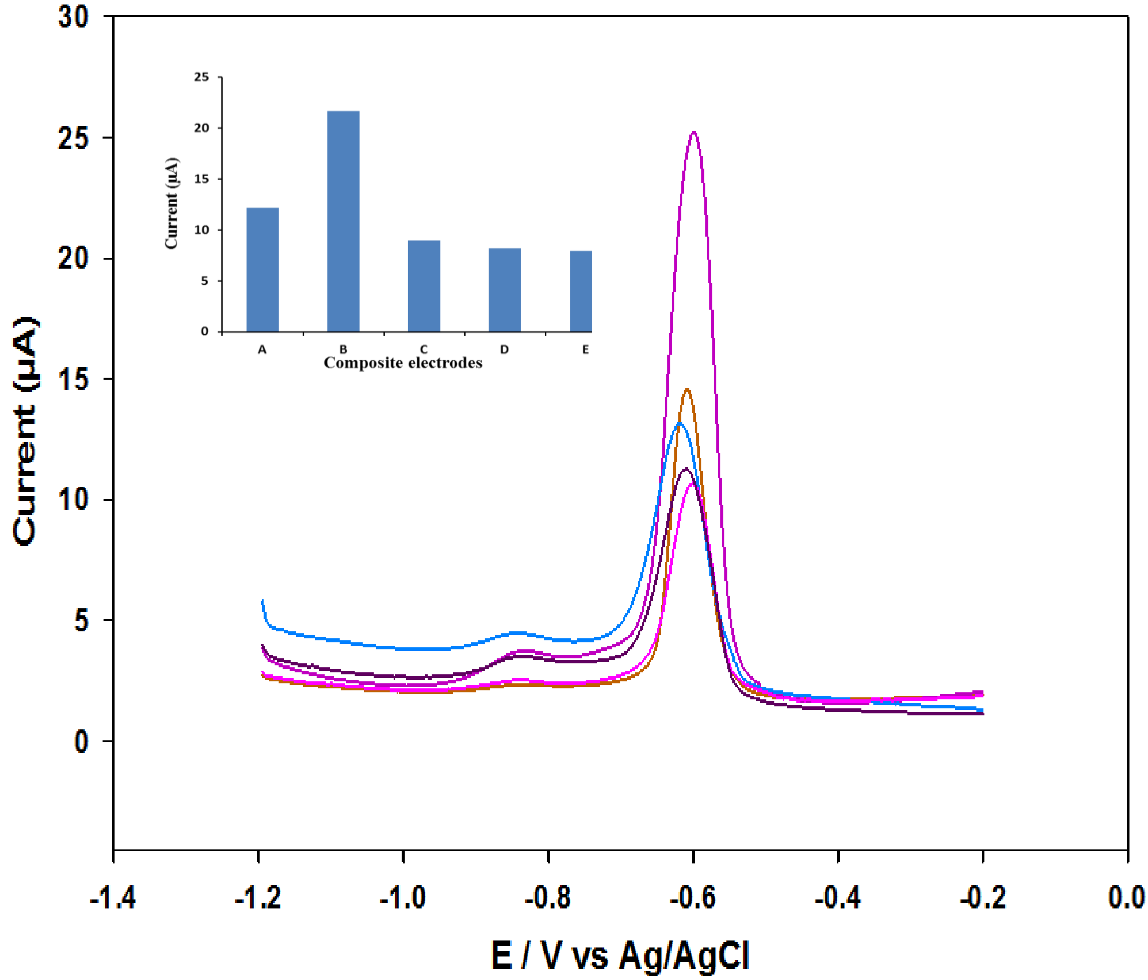

Fig. 4.10 SWASV of 500 ppb Pb (II) Solution in 0.1 M Phosphate Buffer (pH 4) at Composite Electrodes A – E. (Condition Same as Fig. 4.8; Inset: Plot of Current vs Composite Electrodes)

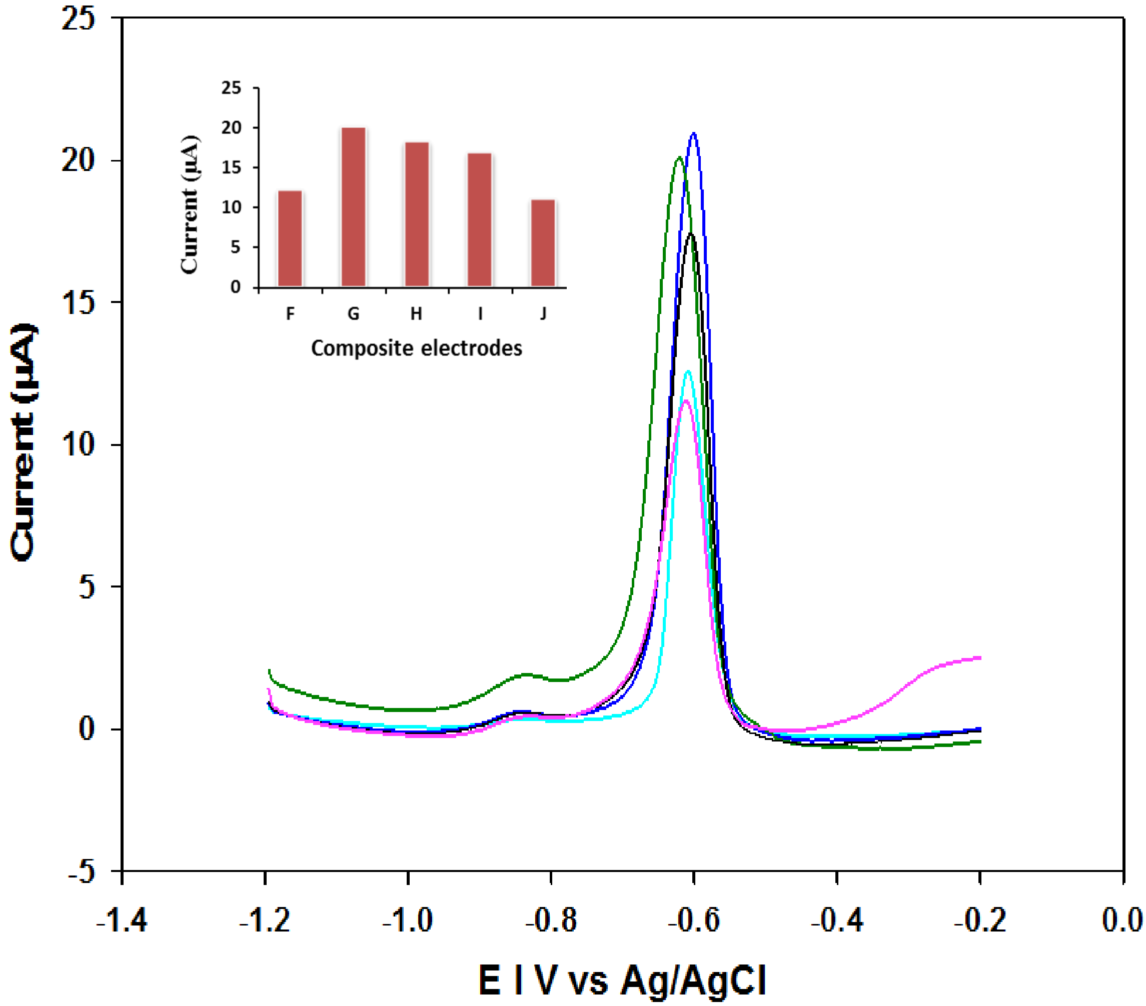

Fig. 4.11 SWASV of 500 ppb Pb (II) Solution in 0.1 M Phosphate Buffer (pH 4) at Composite Electrodes F – J. (Condition Same as Fig. 4.8; Inset: Plot of Current vs Composite Electrodes)

4.3.2 Effect of Supporting Electrolyte and pH

A series of buffer solutions as supporting electrolytes were tested for their suitability in the detection of the analytes in this study. The buffers include; 0.1 M acetate buffer; 0.1 M phosphate buffer; and 0.1 M sulphate buffer all at pH 4. The height and shape of their resulting voltammograms were examined for the choice of the supporting electrolyte. The optimum buffer solution chosen for subsequent studies was 0.1 M phosphate buffer for both composites B and G, as shown in Fig. 4.12 and Fig. 4.13.

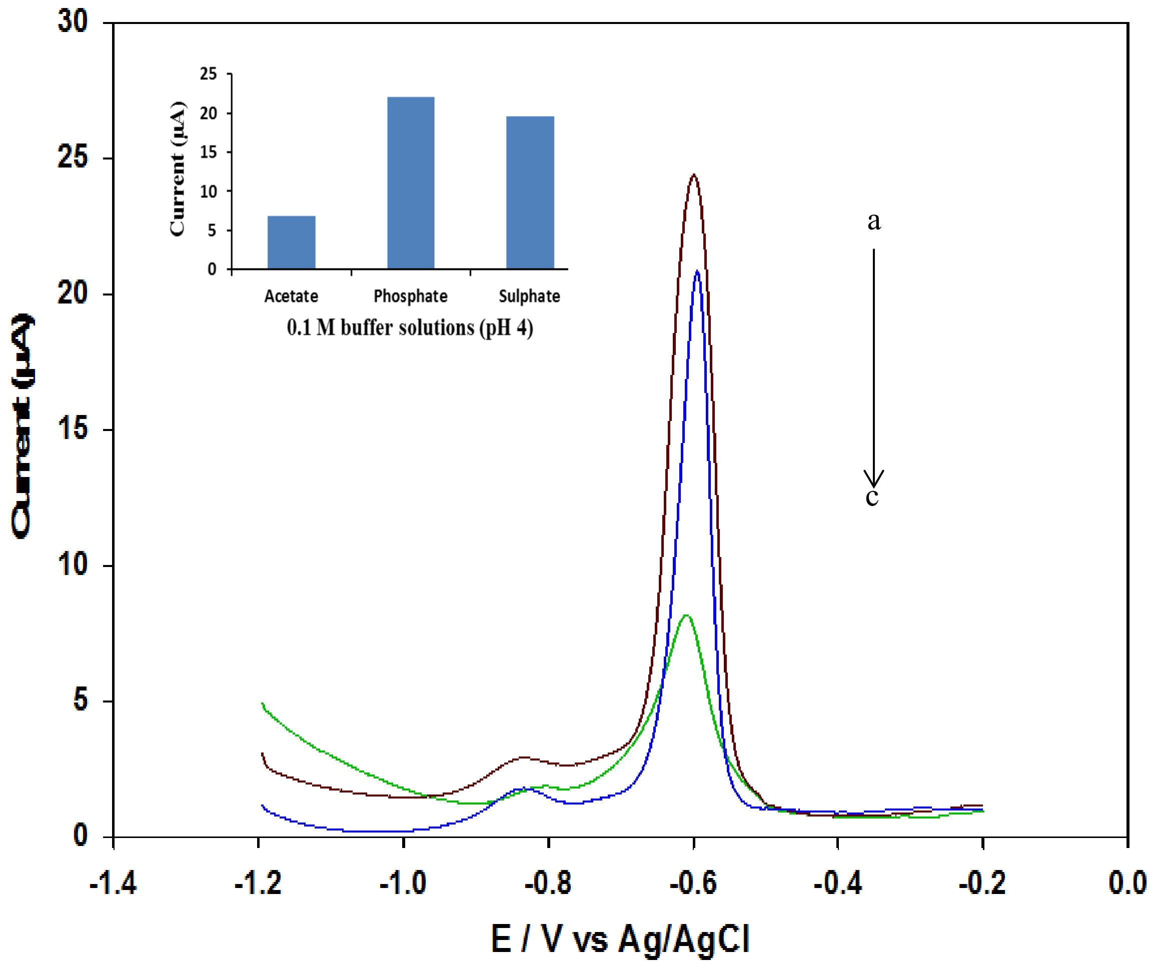

Fig. 4.12 SWASV of 500 ppb Pb (II) Solution in 0.1 M (a) Phosphate, (b) Sulphate, and (c) Acetate Buffer at Composite Electrode B. (Condition Same as Fig. 4.8; Inset: Plot of Current vs 0.1 M Buffer Solutions (pH 4))

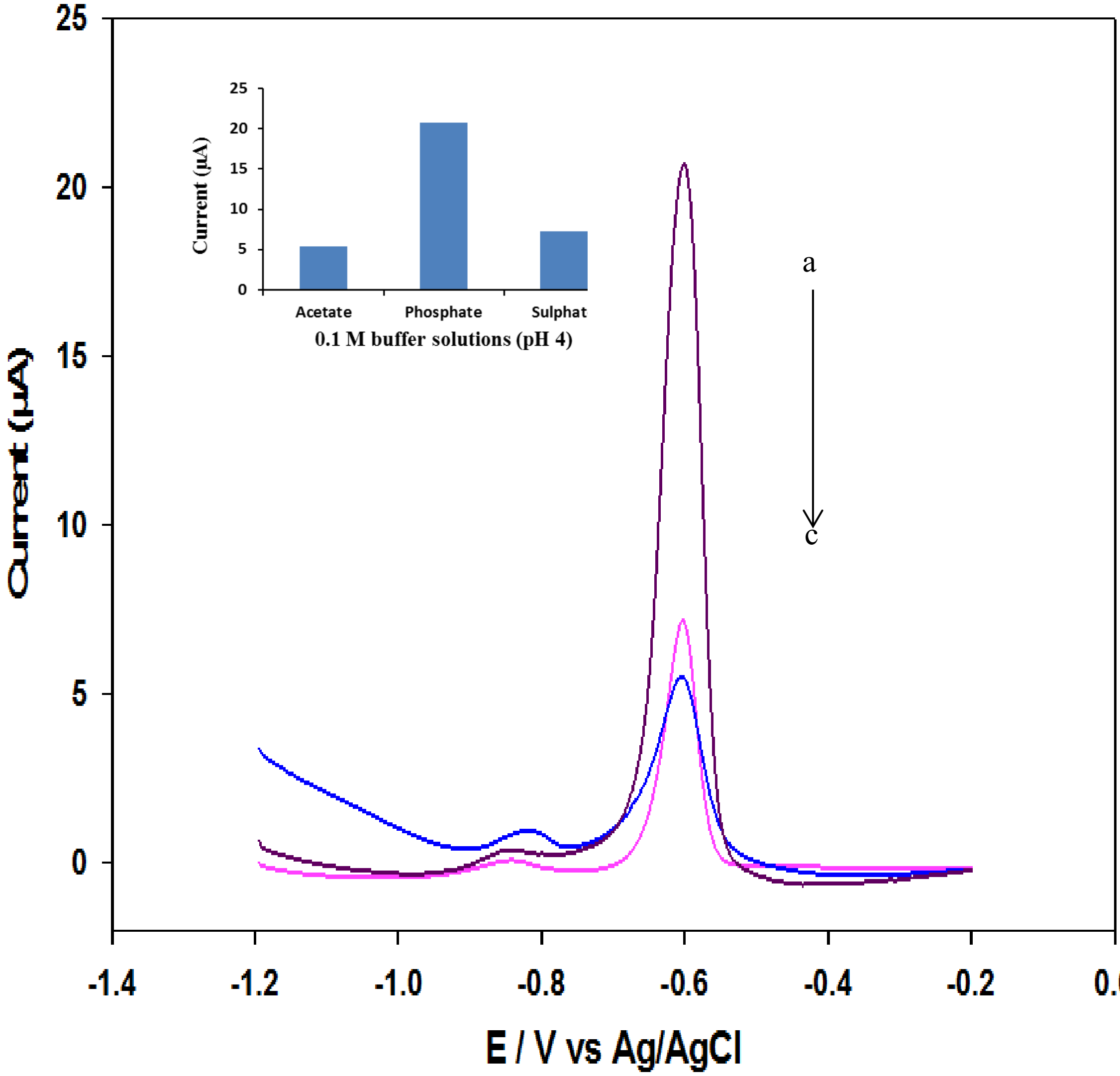

Fig. 4.13 SWASV of 500 ppb Pb (II) Solution in 0.1 M (a) Phosphate, (b) Sulphate, and (c) Acetate buffer at Composite Electrode G. (Condition Same as Fig. 4.8; Inset: Plot of Current vs 0.1 M Buffer Solutions (pH 4))

Square wave stripping voltammograms were also recorded at different pH values in 0.1 M phosphate buffer at composites B and G. The pH was varied between 3 and 8 by adjusting the buffer with H_3PO_4 and NaOH, respectively, until the desired value is reached. The electrolyte's pH plays a crucial role in the electroanalytical behavior of the composite electrodes in this study, and as can be seen from Fig. 4.14 and Fig. 4.15, there was a rise in the peak height going from pH 3 to 4, and then a sudden drop at higher values (5 to 8). The voltammetric signal of Pb at the composite electrodes depends on how well the electrode's surface could sense and detect the presence of free Pb (II) ions in the solution i.e. oxidation process. As a result, the drop observed was attributed to the formation of insoluble $Pb_3(PO_4)_2$ which interferes with the detection of the Pb (II) ions as was observed in the voltammetric cell during the experiment. The peak potential Ep was also found to be pH-dependent as a continuous shift was observed over the varied pH values. This is a characteristic of electrochemical systems in which hydrogen ion is consumed [57]. The optimum pH chosen therefore for subsequent studies was pH 4 for both composites B and G.

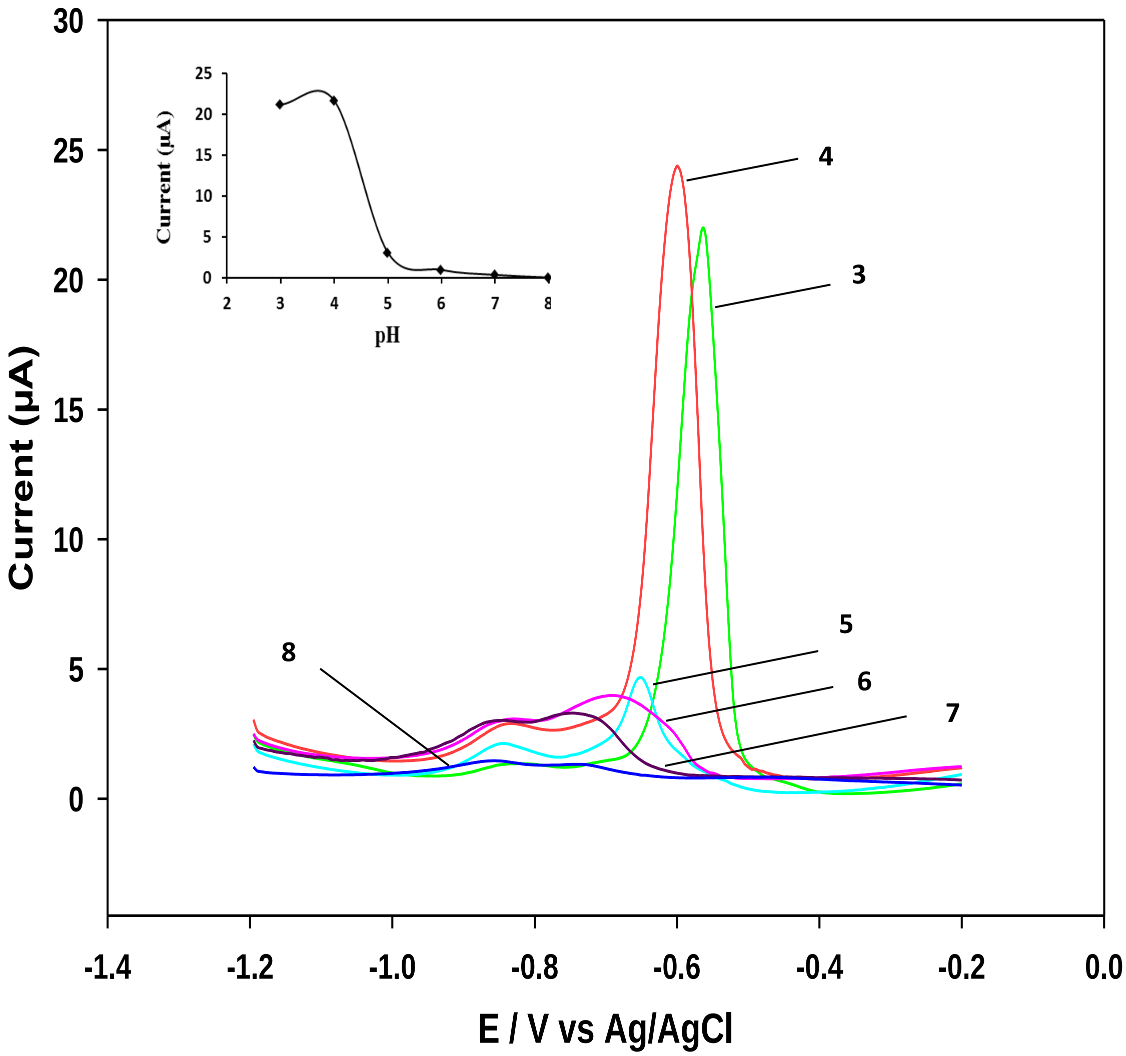

Fig. 4.14 SWASV of 500 ppb Pb (II) Solution in 0.1 M Phosphate Buffer at Composite B; pH 3 to 8. (Condition Same as Fig. 4.8; Inset: Plot of Current vs pH)

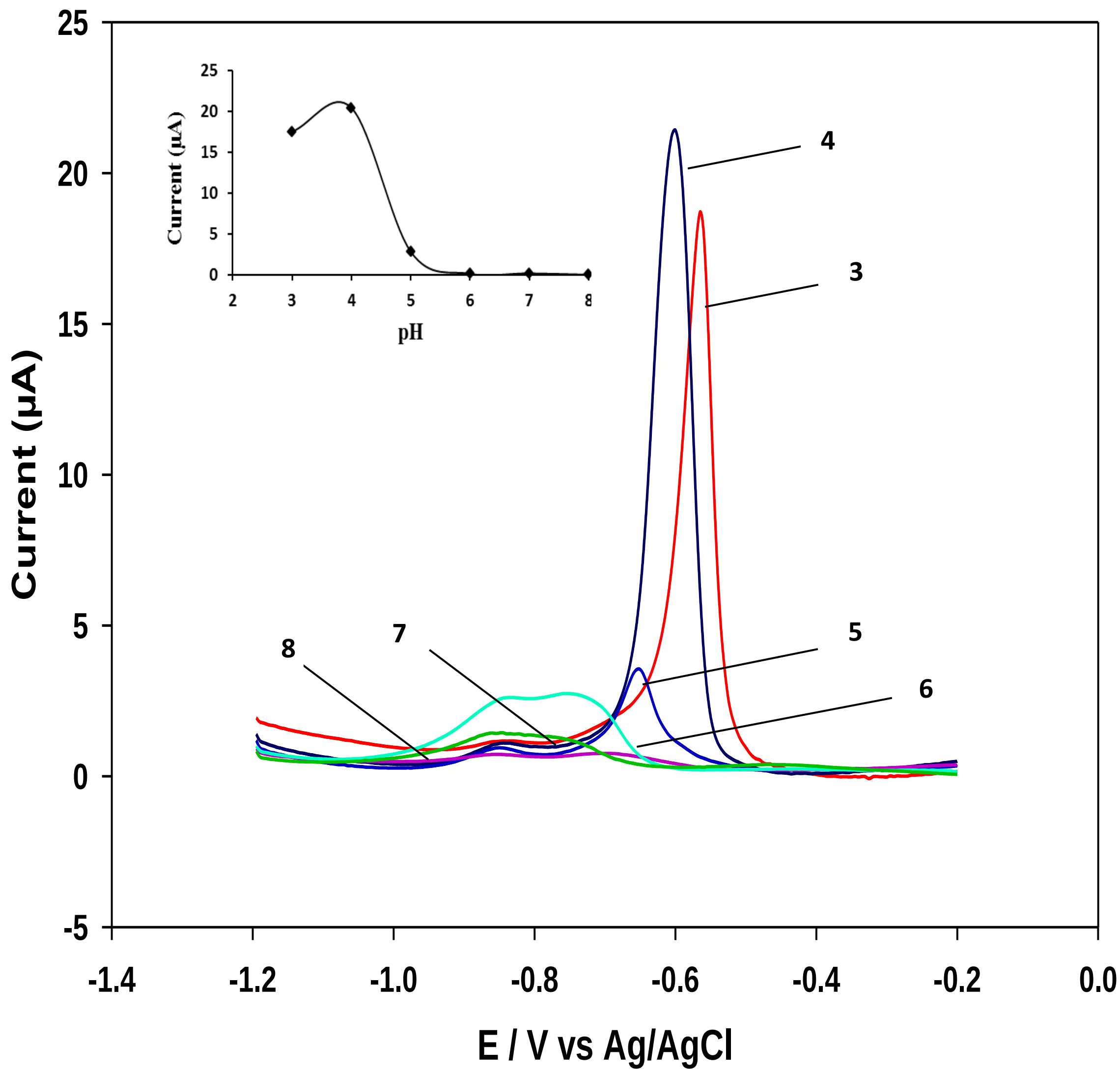

Fig. 4.15 SWASV of 500 ppb Pb (II) Solution in 0.1 M Phosphate Buffer at Composite G; pH 3 to 8. (Condition Same as Fig. 4.8; Inset: Plot of Current vs pH)

4.4 Optimization of Experimental Conditions

4.4.1 Amplitude and Frequency Optimization

In order to maximize the peak current with good resolution and a minimum peak width, the amplitude and frequency of the square wave were optimized. Amplitude was varied from 0.05 V to 0.5 V at both composites B and G, while frequency was varied from 20 Hz to 200 Hz at composite B and 20 Hz to 180 Hz at G. It was observed that as the amplitude increases, the peak current also increases with a slight shift in peak potential until it reaches an apex at 0.3 V at composite B and 0.2 V at G. However, a broadened peak was obtained at those amplitudes. Therefore, a compromise has to be made in order to obtain a good resolution, less broadened peak and a maximum peak current. As a result, amplitudes of 0.1 V and 0.2 V were selected for composites B and G respectively. Fig. 4.16 and Fig. 4.17 show the effect of varying amplitude on peak current for both composites. In the same way when the frequency was varied there was a corresponding increase in the peak current. The results for both composites (Fig. 4.18 and Fig. 4.19) reveals a linear relationship between the current and frequency up to 160 Hz for composite B (y = 0.5122 + 11.736 (n = 8) with R^2 = 0.9959), and up to 140 Hz for composite G (y = 1.7818 + 0.5506 (n = 8) with R^2 = 0.9994), then it increases slowly levelling off at 200 Hz for B and 180 Hz for G. However, at very high frequency the peak current became unstable due to large residual current, thereby giving a broadened peak. Therefore, just as for amplitude, here also a compromise has to be made. As such, an optimal frequency of 60 Hz and 40 Hz were selected for composites B and G respectively.

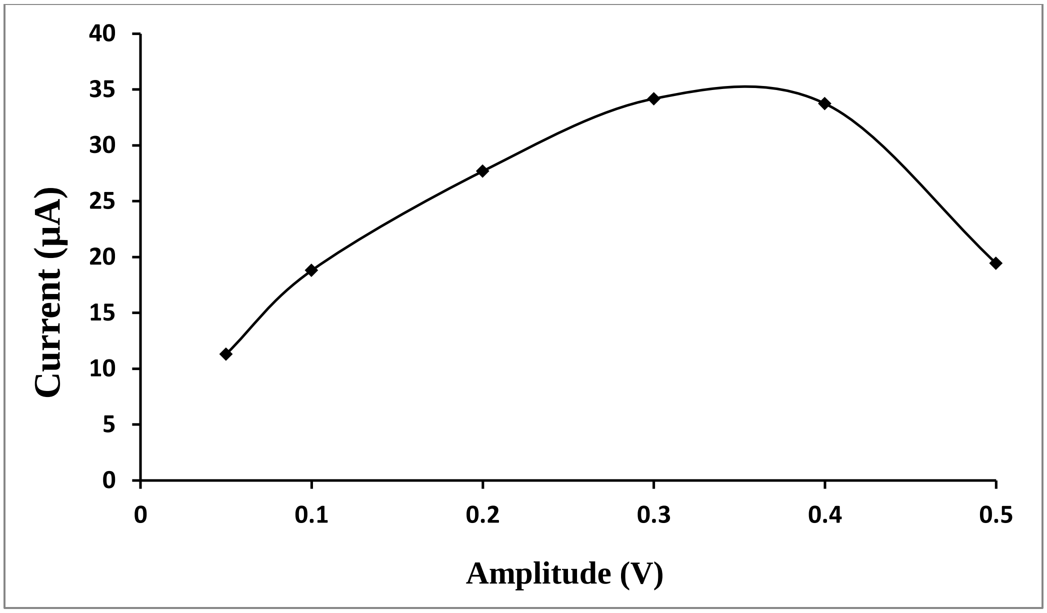

Fig. 4.16 Effect of Amplitude on Peak Current of 500 ppb Pb (II) Solution in 0.1 M Phosphate Buffer (pH 4) at Composite B; Amplitude 0.05 V to 0.5 V. (Other Conditions Same as Fig. 4.8)

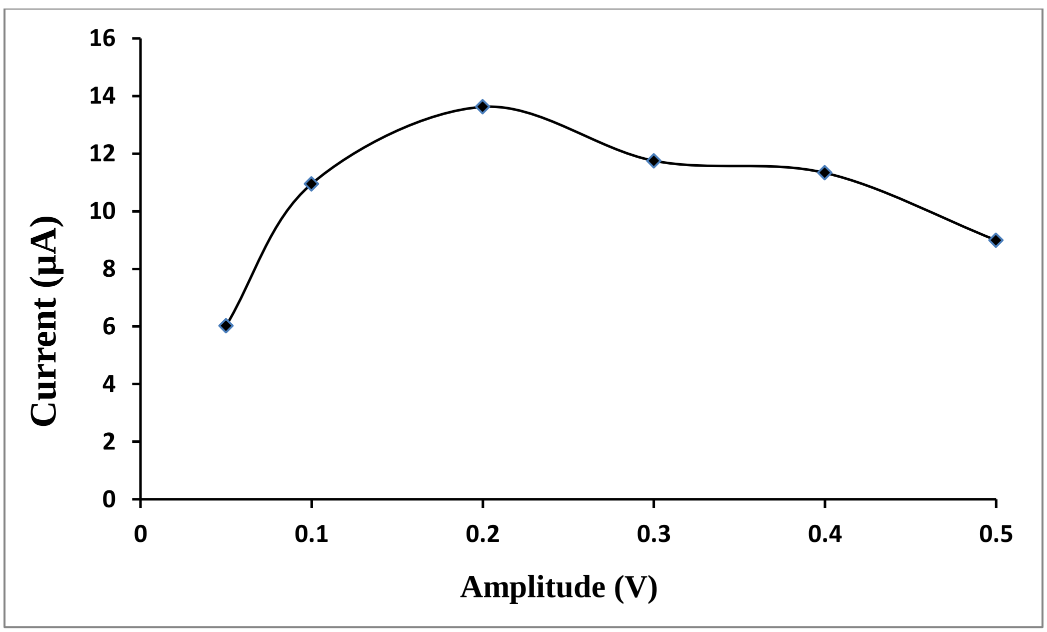

Fig. 4.17 Effect of Amplitude on Peak Current of 500 ppb Pb (II) Solution in 0.1 M Phosphate Buffer (pH 4) at Composite G; Amplitude 0.05 V to 0.5 V. (Other Conditions Same as Fig. 4.8)

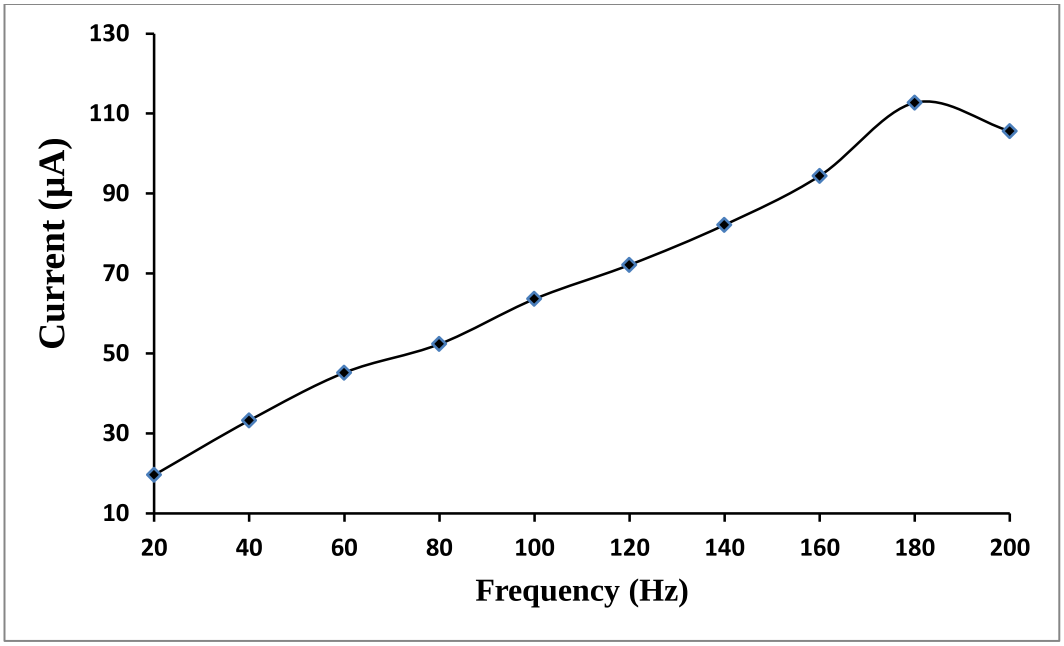

Fig. 4.18 Effect of Frequency on Peak Current of 500 ppb Pb (II) Solution in 0.1 M Phosphate Buffer (pH 4) at Composite B; Frequency 20 Hz to 200 Hz. (Deposition Potential: -1.2 V; Deposition Time: 120 s; Potential Step: 5 mV; Amplitude: 300 mV)

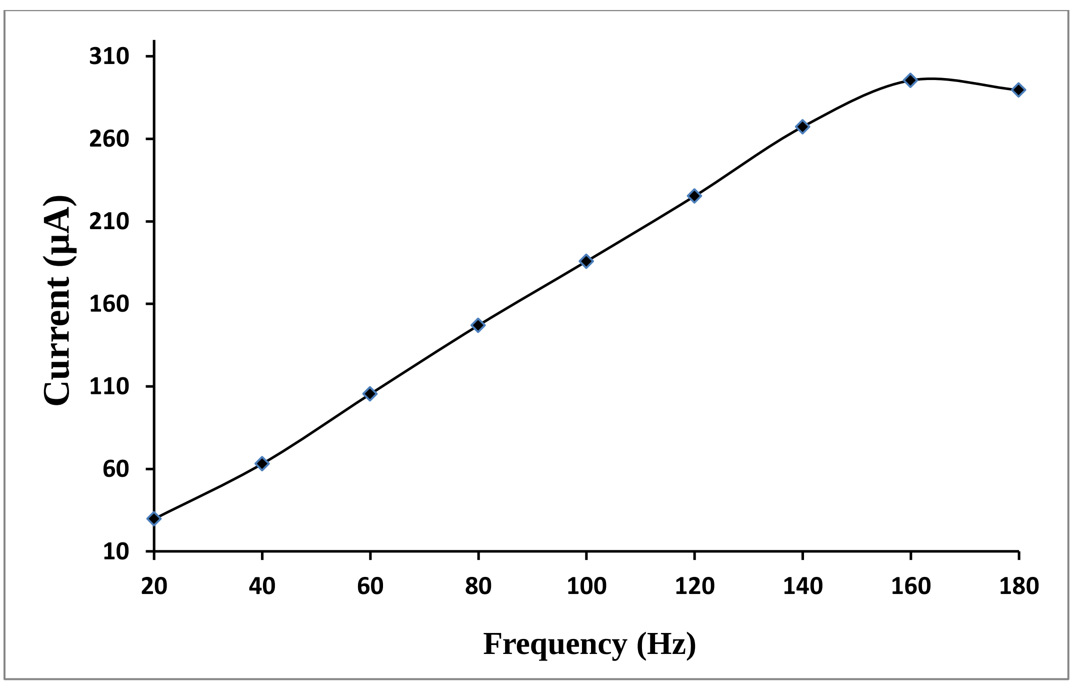

Fig. 4.19 Effect of Frequency on Peak Current of 500 ppb Pb (II) Solution in 0.1 M Phosphate Buffer (pH 4) at Composite G; Frequency 20 Hz to 180 Hz. (Deposition Potential: -1.2 V; Deposition Time: 120 s; Potential Step: 5 mV; Amplitude: 200 mV)

4.4.2 Deposition Potential and Time Optimization

The effect of deposition potential of the analyte onto the surface of the working electrode was evaluated by varying the deposition potential from -1.6 V to -0.4 V at composite B and -1.4 V to -0.4 V at composite G. Deposition potential is one of the essential experimental parameters while carrying out stripping voltammetric determination of analytes such as Pb (II) ions. This is because except an appropriate potential is applied to enable the reduction and deposition of the metal ions onto the surface of the electrode, the sensitivity of the electrode is greatly affected. The effect of deposition potential was studied elsewhere [39], and it was demonstrated that choosing a high potential in the negative direction leads to background hydrogen evolution which interferes with the analyte's signal. At the same time a potential too low is not enough to bring about the reduction of the metal ions. Therefore, the deposition potential needs to be optimized to ensure that no hydrogen evolution occurs while ensuring a reasonable amount of the analyte are deposited on the working electrode before being stripped. From the results of the square wave stripping analysis (Fig. 4.20 and Fig. 4.21), the optimum deposition potential which gave a better pre-concentration of the analyte taking into consideration the peak height, peak shape and peak width was chosen as -1.2 V for both composites.

The deposition time dependence on the peak height was also examined for both composites by varying the deposition time from 20 sec to 180 sec at both composites (B and G). It is generally believed that lower detection limits can be reached with longer deposition time [40]. However, longer deposition time can alter the surface of the electrode thereby affecting its analytical performance, as was evidenced in this study

(Fig. 4.22 and Fig. 4.23). As a result, deposition time of 120 sec for both composites was adopted for this study.

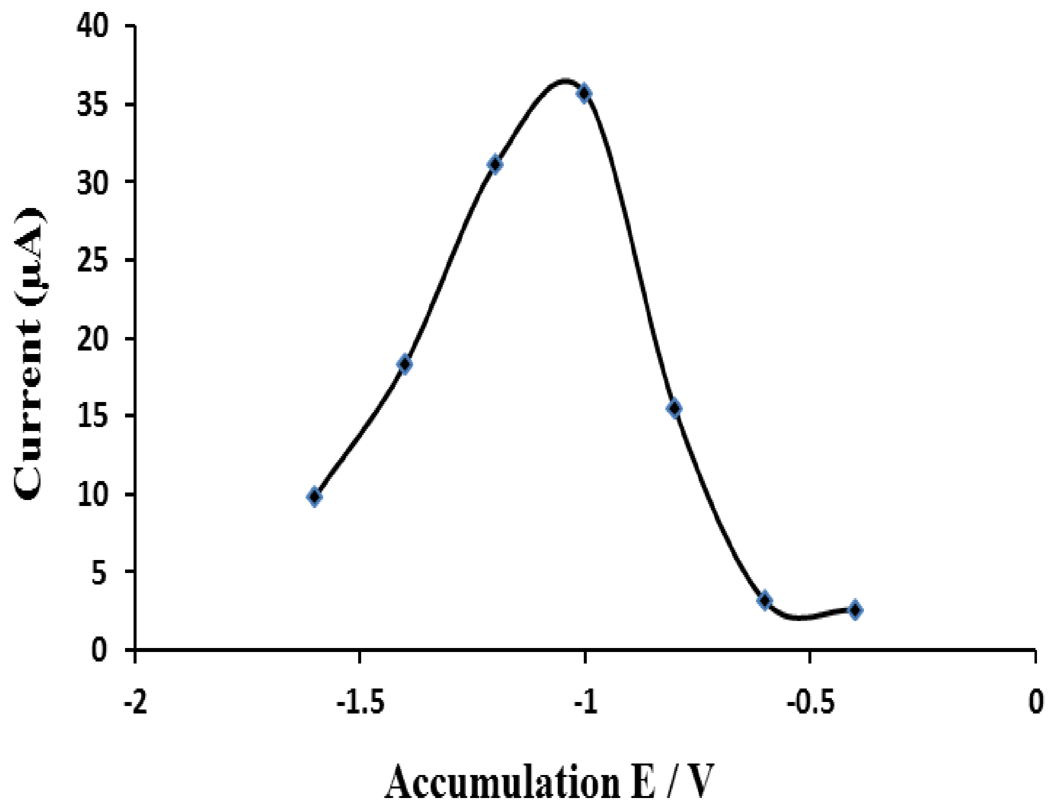

Fig. 4.20 Effect of Deposition Potential on Peak Current of 500 ppb Pb (II) Solution in 0.1 M Phosphate Buffer (pH 4) at Composite B. (Deposition Time: 120 s; Potential Step: 5 mV; Amplitude: 100 mV; Frequency: 60 Hz)

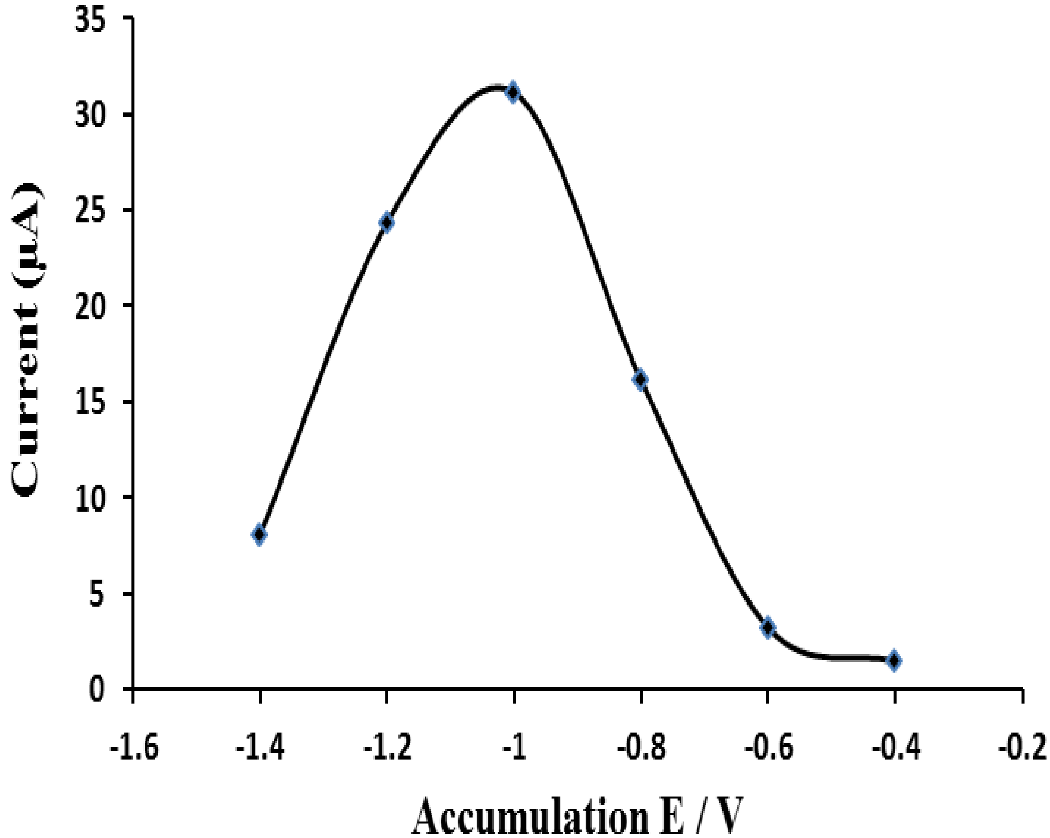

Fig. 4.21 Effect of Deposition Potential on Peak Current of 500 ppb Pb (II) Solution in 0.1 M Phosphate Buffer (pH 4) at Composite G. (Deposition Time: 120 s; Potential Step: 5 mV; Amplitude: 200 mV; Frequency: 40 Hz)

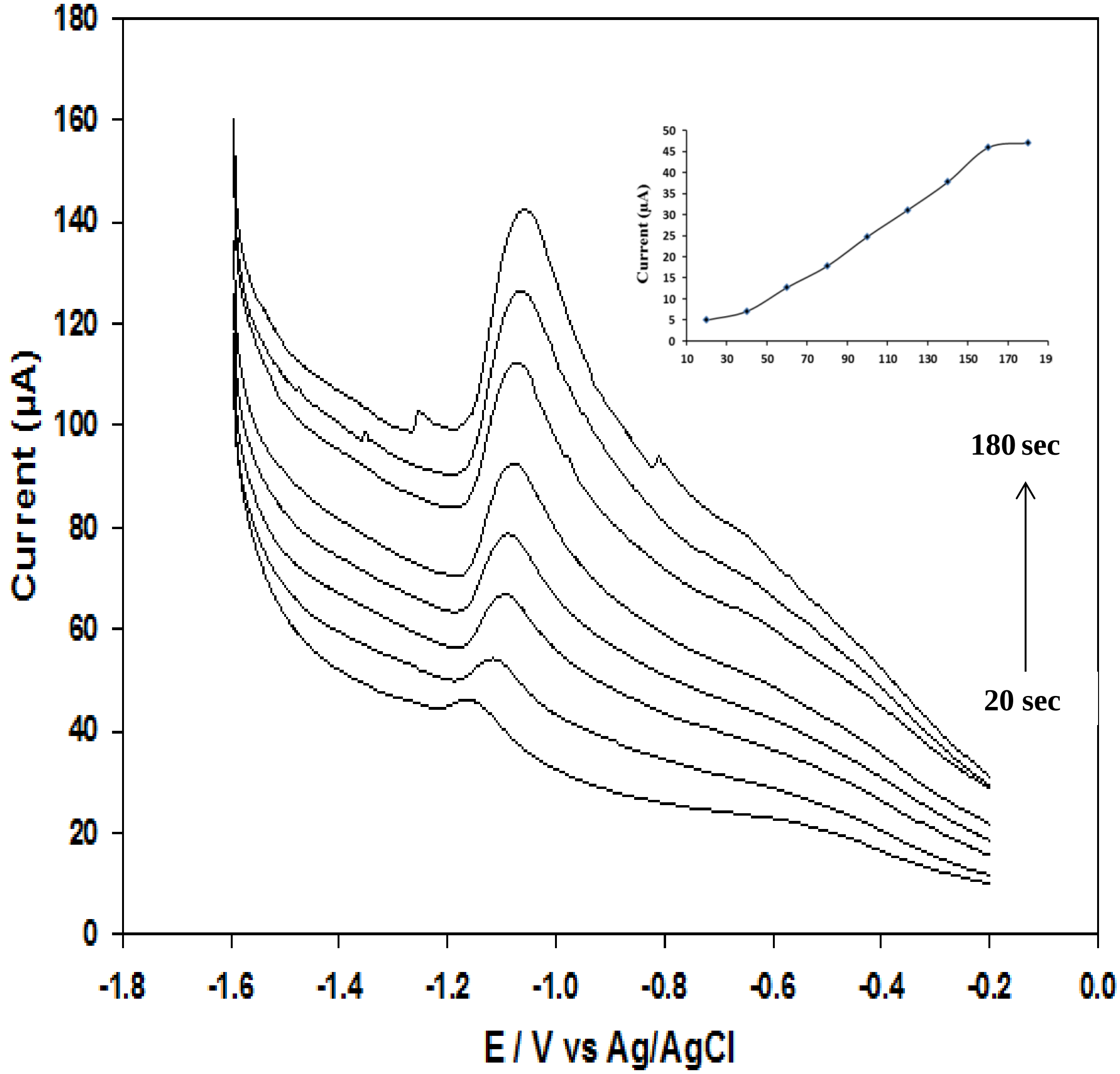

Fig. 4.22 SWASV of 500 ppb Pb (II) Solution in 0.1 M Phosphate Buffer (pH 4) at Composite B with Varying Deposition Time; 20 to 180 s (Deposition Potential: -1.2 V; Potential Step: 5 mV; Amplitude: 100 mV; Frequency: 60 Hz; Inset: Plot of Current vs Deposition Time)

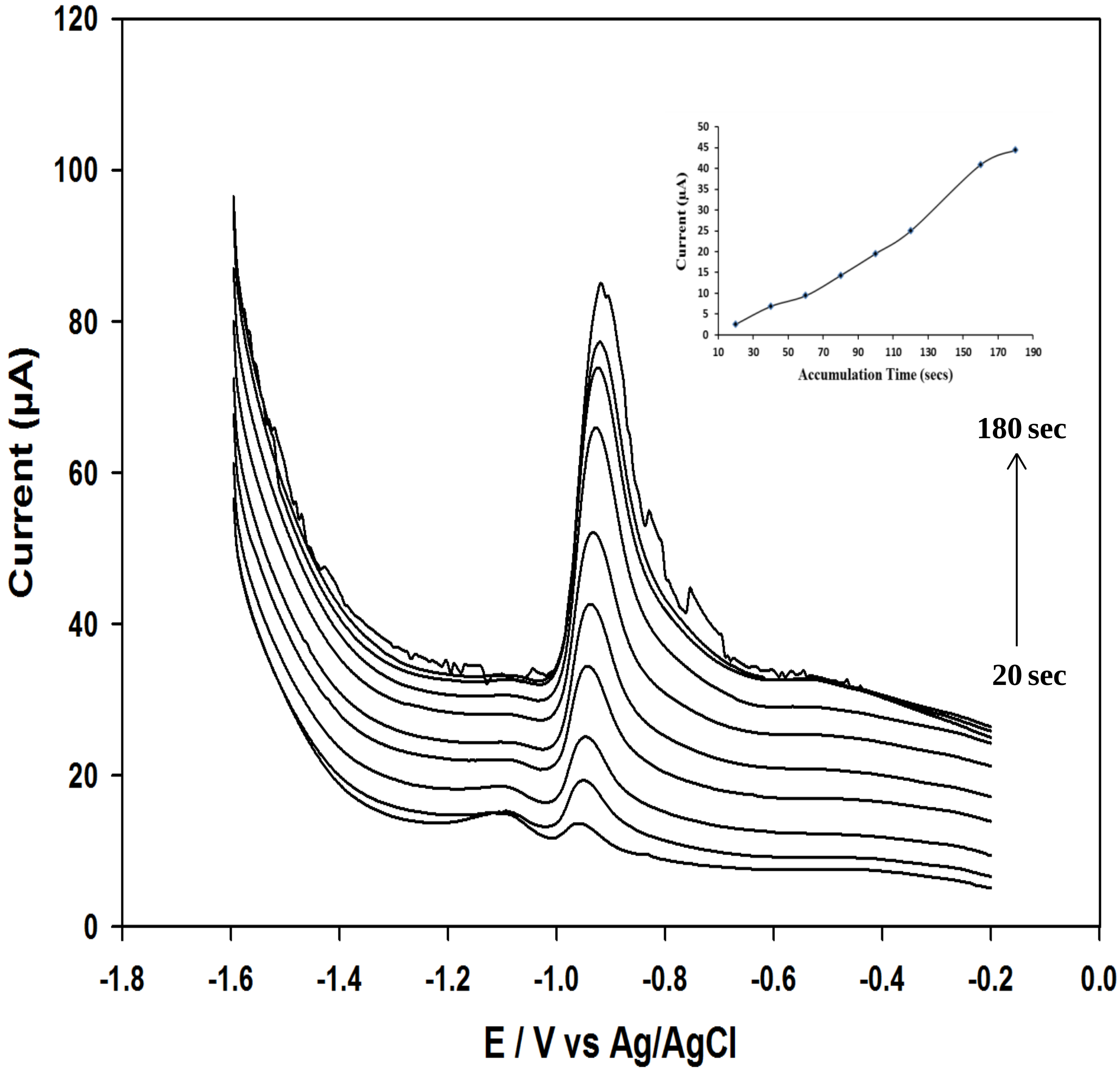

Fig. 4.23 SWASV of 500 ppb Pb (II) Solution in 0.1 M Phosphate Buffer (pH 4) at Composite G with Varying Deposition Time; 20 to 180 s (Deposition Potential: -1.0 V; Potential Step: 5 mV; Amplitude: 200 mV; Frequency: 40 Hz; Inset: Plot of Current vs Deposition Time)

In summary the optimized experimental parameters for the purpose of this study are presented in Table 4.5.

Table 4.5 Summary of Experimental Conditions

Composite	Amplitude (V)	Frequency (Hz)	Deposition Potential (V)	Deposition Time (sec)
B	0.1	60	-1.2	120
G	0.2	40	-1.2	120

4.5 Calibration Curve for Pb (II) Detection

Calibration curves were constructed for anodic stripping voltammetric detection of Pb (II) ion at the composite electrodes over two concentration ranges (50 – 500 ppb and 5 – 50 ppb). The results of the square wave stripping voltammetry (Fig. 4.24 and Fig. 4.25) shows a linear relationship between the stripping current and the concentration of Pb (II) ions at both composite electrodes with R^2 equals 0.9988 and 0.9991 for higher and lower concentration ranges at composite B, while at composite G the values of R^2 were found as 0.9994 and 0.9989 at higher and lower concentration ranges, respectively (Fig. 4.26

and Fig. 4.27). Limit of detection (S/N = 3) for both composites were found as 0.225 ppb and 0.07 ppb for B and G, respectively. The results are summarized in Table 4.6.

Table 4.6 R^2 values, LOD and Slope Values for Pb (II) Detection at La-ZMCPE

Composite	**Analyte**	**R^2**	**LOD (ppb)**	**Sensitivity ($\mu A\ L\ \mu g^{-1}$)**
La-ZMCPE (composite B)	Pb (II)	0.9988 0.9991	0.225	0.051
Ce-ZMCPE (Ce-ZMCPE)	Pb (II)	0.9994 0.9989	0.07	0.047

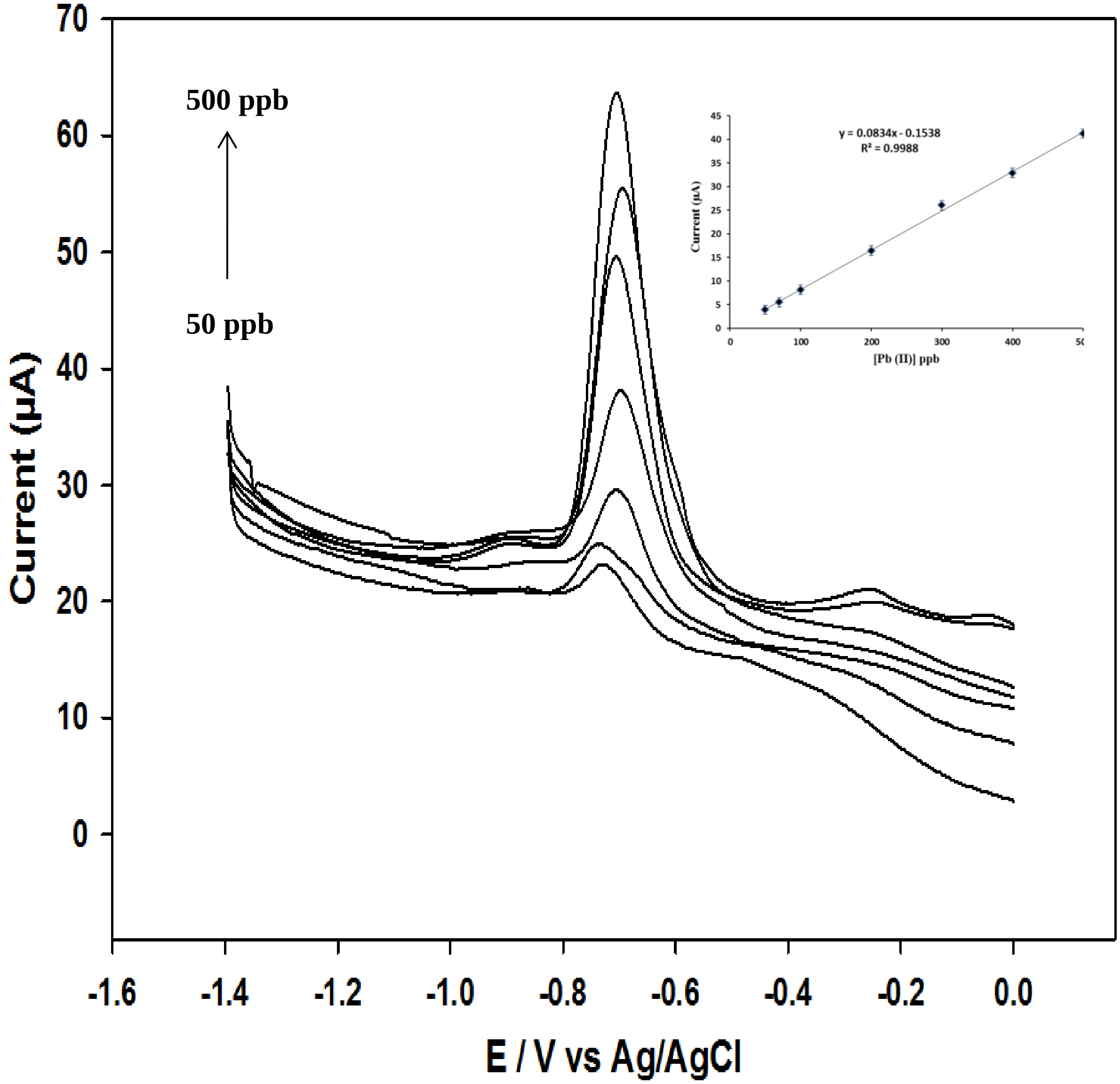

Fig. 4.24 SWASV of Pb (II) (50 – 500 ppb) in 0.1 M Phosphate Buffer (pH 4) at Composite B. (Deposition Potential: -1.2 V; Deposition Time: 120 s; Potential Step: 5 mV; Amplitude: 100 mV; Frequency: 60 Hz; Inset: Calibration Plot of Pb (II))

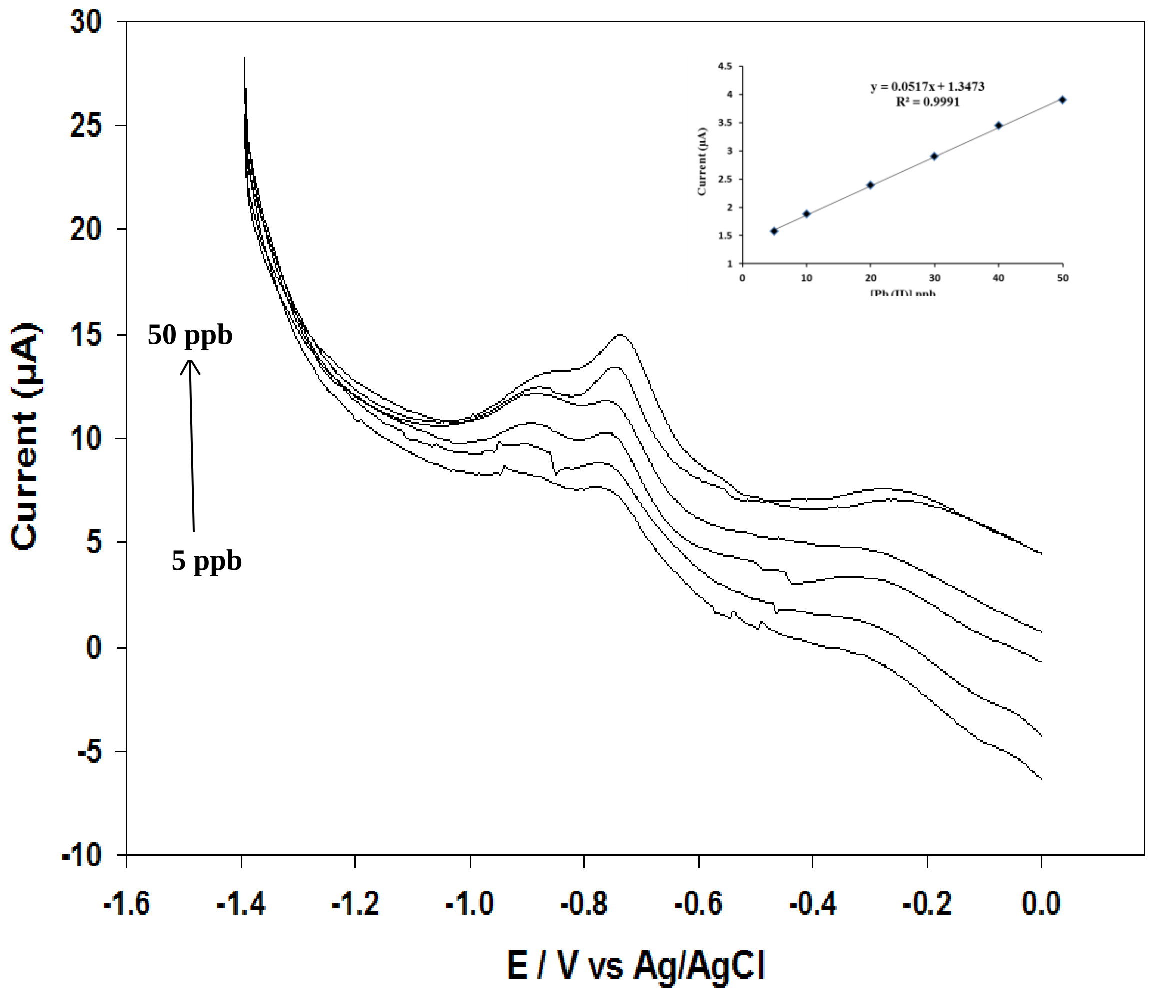

Fig. 4.25 SWASV of Pb (II) (5 – 50 ppb) in 0.1 M Phosphate Buffer (pH 4) at Composite B. (Deposition Potential: -1.2 V; Deposition Time: 120 s; Potential Step: 5 mV; Amplitude: 100 mV; Frequency: 60 Hz; Inset: Calibration Plot of Pb (II))

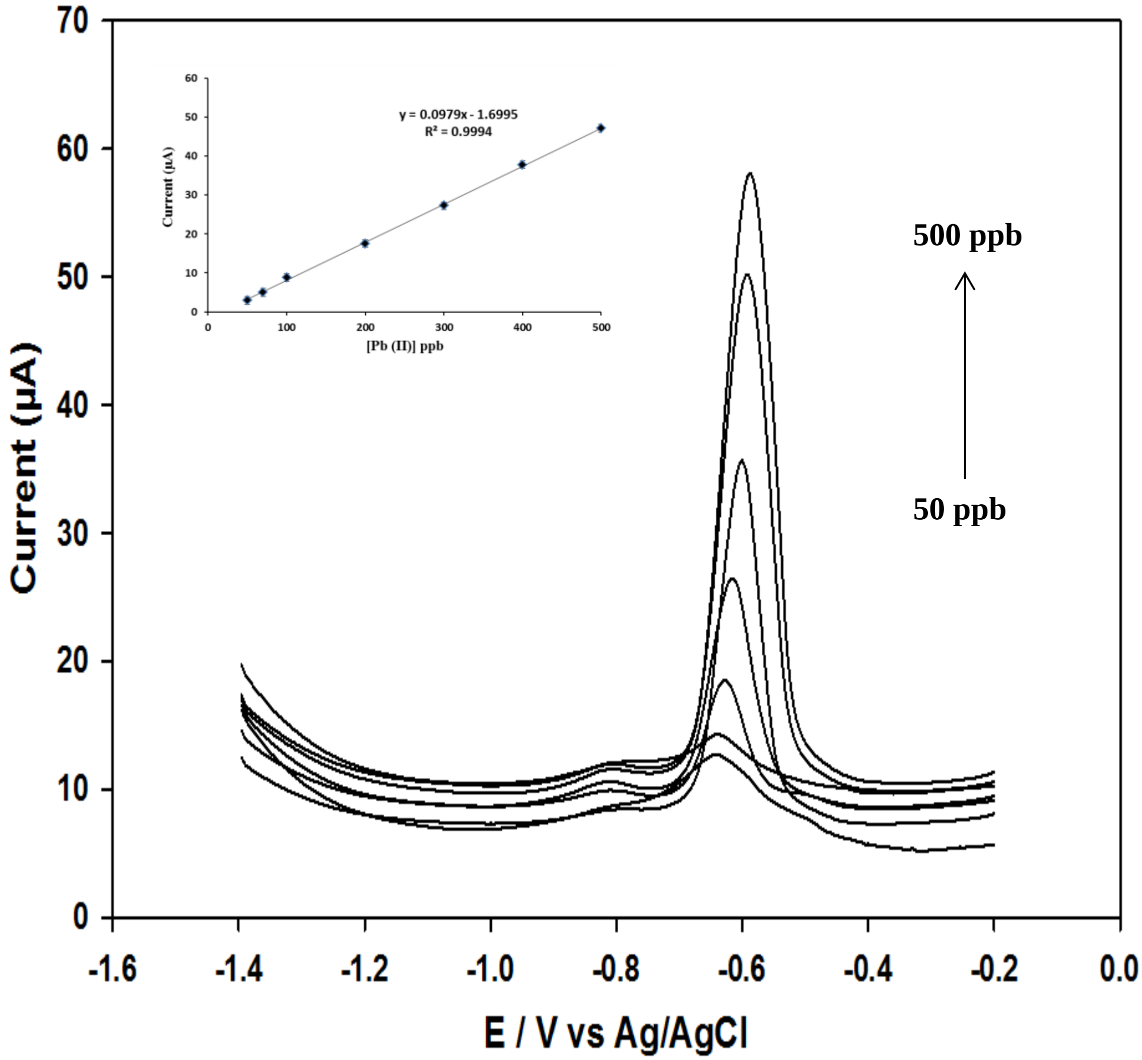

Fig. 4.26 SWASV of Pb (II) (50 – 500 ppb) in 0.1 M Phosphate Buffer (pH 4) at Composite G. (Deposition Potential: -1.2 V; Deposition Time: 120 s; Potential Step: 5 mV; Amplitude: 50 mV; Frequency: 40 Hz; Inset: Calibration Plot of Pb (II))

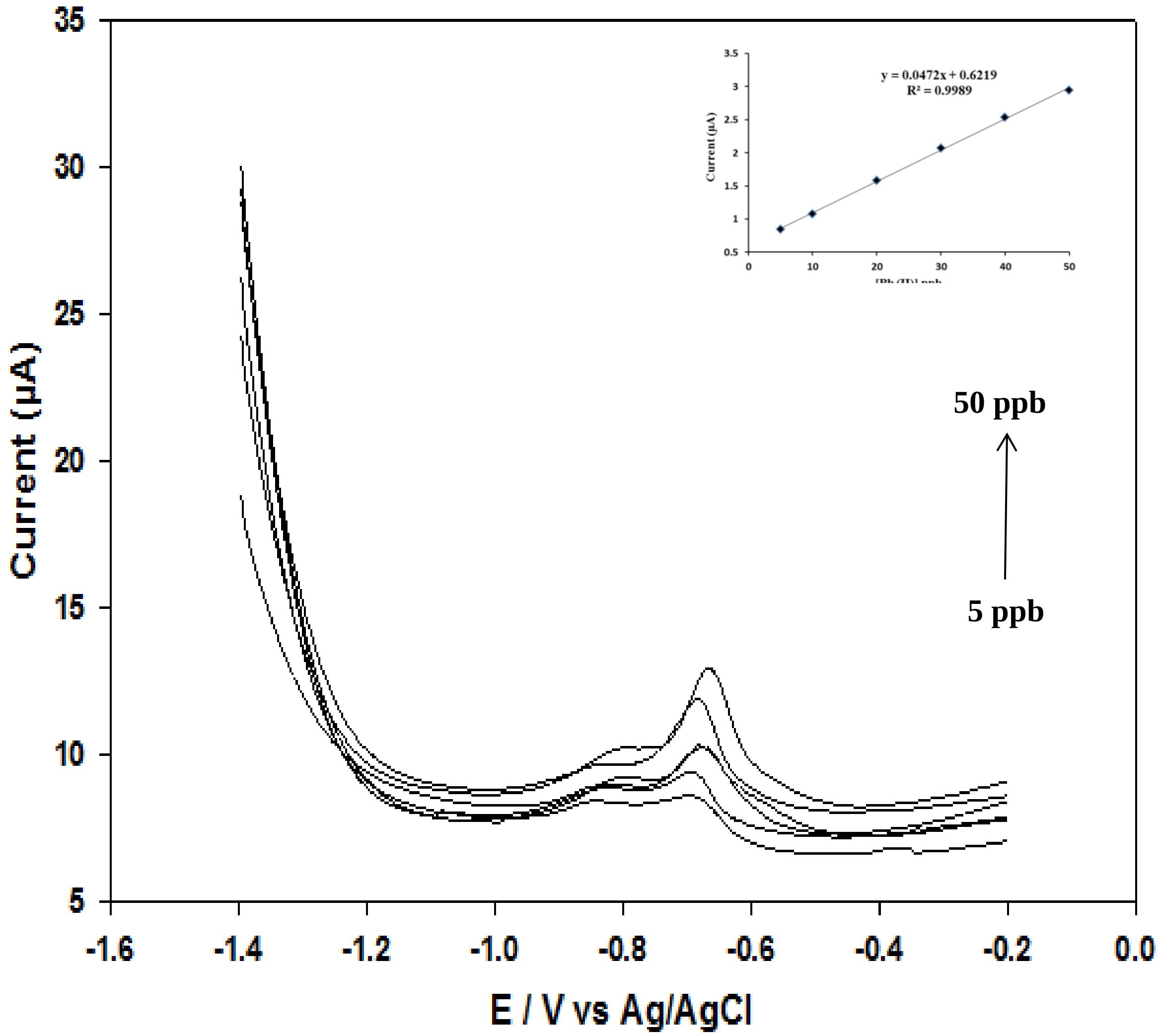

Fig. 4.27 SWASV of Pb (II) (5 – 50 ppb) in 0.1 M Phosphate Buffer (pH 4) at Composite G. (Deposition Potential: -1.2 V; Deposition Time: 120 s; Potential Step: 5 mV; Amplitude: 50 mV; Frequency: 40 Hz; Inset: Calibration Plot of Pb (II))

The results from both composites were subjected to the F test in order to check the precision among them (Table 4.7). F test compares the variances of two methods (or the two composites in this case) and a conclusion is drawn as to whether the results obtained agree with one another. For the composite electrodes in this study, it was found that at 95% confidence level, there was no significant difference between the currents obtained for Pb (II) detection at both composites.

Table 4.7 F Test Results

F-Test Two-Sample for Variances		
	Composite G	**Composite B**
Mean	**12.89**	**12.17**
Variance	**258.24**	**189.52**
Observations	**12**	**12**
Degree of freedom	**11**	**11**
F	**1.36**	
P(F<=f)	**0.308**	
F Critical	**2.81**	

The reproducibility of the stripping analysis of Pb (II) at both composite electrodes was also checked by carrying out five consecutive measurements with a single electrode. The RSD for both composites were found as 3.02% for B and 2.23% at G respectively, implying the reproducibility of the electrodes for Pb (II) detection. When comparing the analytical performance of the electrodes in the current study with other electrodes reported previously, it was found that the composites in this study compares well among other composites reported in the literature [40-46]. Table 4.8 summarizes a comparison of LOD of the composites in this study with other composites from literature.

4.6 Simultaneous Detection of Pb (II) and Cd (II)

To further investigate the sensitivities of the composite electrodes in this study, simultaneous detection of two metal ions Pb (II) and Cd (II) was carried out. The aim of this was to investigate if the detection of a given analyte interferes with the detection of the other analyte. The results of the simultaneous determinations (Fig. 4.28 and Fig. 4.29) give a relatively linear relationship between the current and the concentration of the analyte ions. The results of the R^2 values and LOD are given in Table 4.9. Comparing the results of the individual analysis to the simultaneous analysis, we observed that the detection limits and sensitivities of composite B were affected by the simultaneous analysis, while that of composite G was not greatly affected. Therefore, we conclude that composite G can be applied for either individual determination of Pb (II) or simultaneous determination of Pb (II) and Cd (II) ions in water samples.

Table 4.8 Comparison with Detection Limits of Composites from Literature

S/N	Electrode	Metal detected	Technique	Detection limit (ppb)	Ref.
1	La-ZMCPE Ce-ZMCPE	Pb (II) Pb (II)	SWASV	0.225 0.07	Current study
2	Carbon screen-printed electrode modified by Bi-nanoparticle	Pb (II)	SWASV	0.9	[41]
3	Boron-doped diamond electrode	Pb (II)	DPASV	1.15	[42]
4	Bi-modified carbon paste electrode	Pb (II)	SWASV	0.8	[43]
5	Bi-film electrode	Pb (II)	SWASV	6.9	[44]
6	Nafion-coated Bi-film electrode	Pb (II)`	SWASV	2	[45]
7	Bi nano-powder electrode	Pb (II)	SWASV	0.15	[46]

Table 4.9 R^2 values, LOD and Slope for Simultaneous Determination of Cd (II) and Pb (II)

Composite	Analyte	R^2	LOD (ppb)	Sensitivity (μA L μg^{-1})
La-ZMCPE (composite B)	Cd (II) Pb (II)	0.9985 0.9978	0.122 0.240	0.1785 0.1287
Ce-ZMCPE (composite G)	Cd (II) Pb (II)	0.9976 0.9978	0.046 0.045	0.0861 0.0717

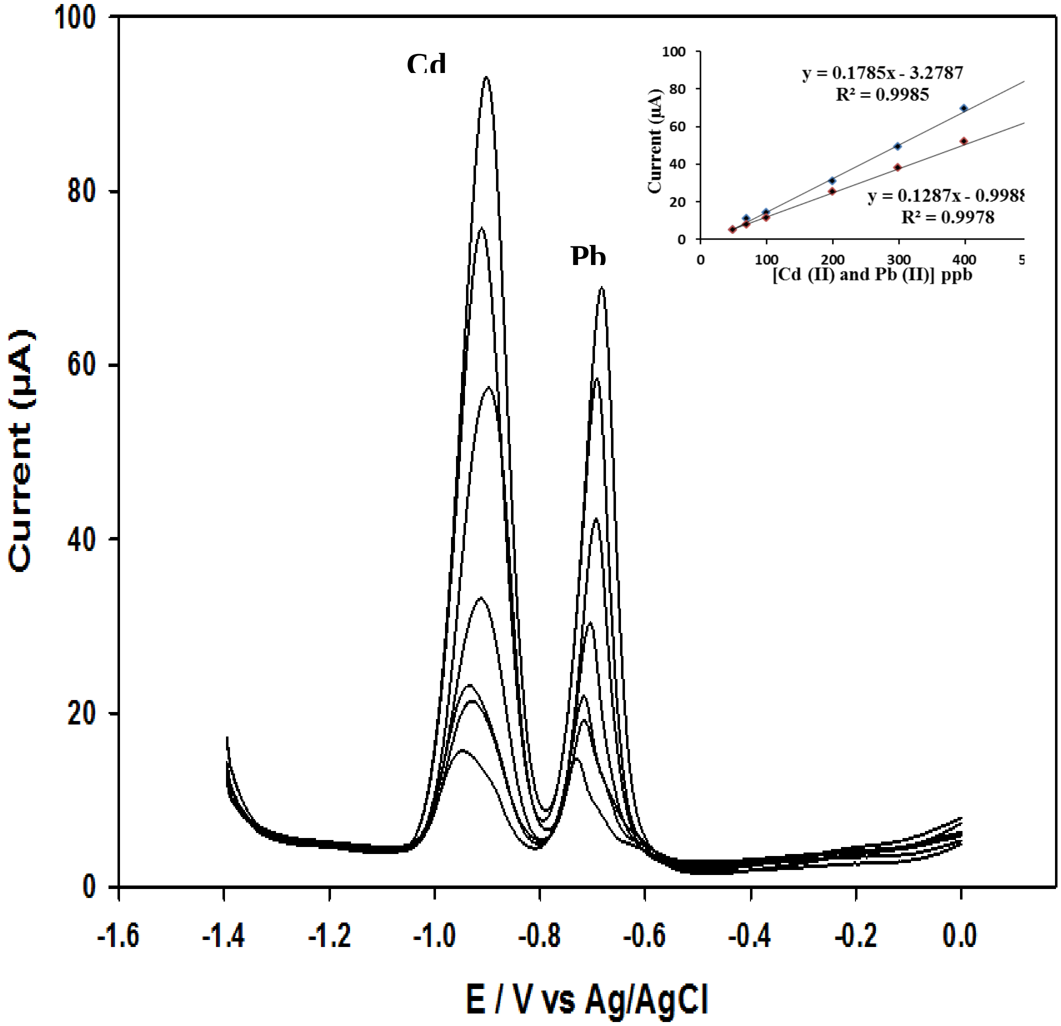

Fig. 4.28 SWASV of Cd (II) and Pb (II) (50 – 500 ppb) in 0.1 M Phosphate Buffer (pH 4) at Composite B. [Deposition Potential: -1.2 V; Deposition Time: 120 s; Potential Step: 5 mV; Amplitude: 100 mV; Frequency: 60 Hz; Inset: Calibration Plot of Cd (II) and Pb (II)]

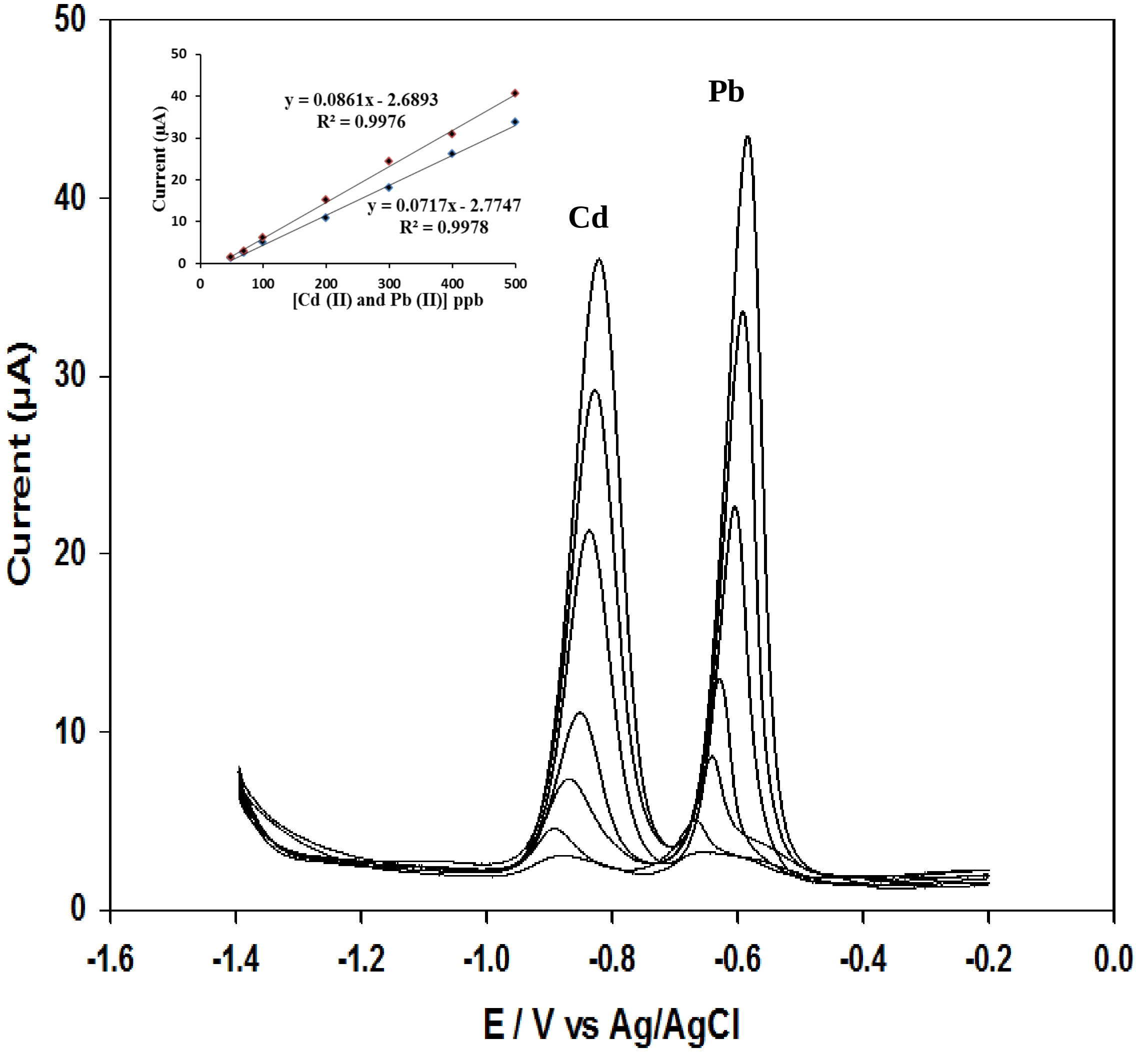

Fig. 4.29 SWASV of Cd (II) and Pb (II) (50 – 500 ppb) in 0.1 M Phosphate Buffer (pH 4) at Composite B. [Deposition Potential: -1.2 V; Deposition Time: 120 s; Potential Step: 5 mV; Amplitude: 200 mV; Frequency: 40 Hz; Inset: Calibration Plot of Cd (II) and Pb (II)]

CHAPTER 5

CONCLUSION AND RECOMMENDATIONS

5.1 Conclusion

Rare earth impregnated zeolite-modified carbon paste electrodes (RE-ZMCPEs) were successfully investigated as an alternative electrode for the anodic stripping voltammetric determination of Pb (II) and Cd (II) ions. Prior to the fabrication of the RE-ZMCPEs, mordenite zeolite with silica to alumina ratio 15 was synthesized and characterized by XRD, SEM, EDX and NMR, the result of which shows that a flat prismic crystal was obtained with an average crystal size 6.8 µm. Preliminary screening of the fabricated electrodes showed that the electrodes with 2 wt% La impregnation and 10 wt% Ce impregnation, and composite ratio 65:5:30 (graphite to zeolite to paraffin) gave the best peak height and were thus adopted for this study. Calibration curves for Pb (II) and Cd (II) gave a linear relationship at both composite electrodes with correlation coefficient 0.9978 and 0.9985 for Pb (II) and Cd (II) at La-ZMCPE, and 0.9978 and 0.9976 at Ce-ZMCPE for Pb (II) and Cd (II), respectively. The reproducibility of the composite electrodes investigated by carrying out five consecutive runs using a single electrode gave a relatively good precision with RSD 3.02% and 2.23% for La-ZMCPE and Ce-ZMCPE for Pb (II) detection respectively. Based on the results of the calibration plots, limits of detection, sensitivities and reproducibility, the composite electrodes in this study demonstrates the ability of being used for the analysis of environmental samples such as drinking water, due to their inexpensiveness and ease of fabrication as well as lack of toxicity compared to mercury-based electrodes used in stripping analysis.

5.2 Recommendations

From the outcomes of the current study, the following recommendations are hereby proposed:

a. Since it was evident that the electroactivity of the electrodes in this study were as a result of the incorporation of the rare earth metals, it is therefore recommended that the rare earth alone should be incorporated into the electrode without the zeolites to compare the performance of the electrode with and without the presence of zeolites.
b. The reproducibility of the electrodes over a long a period of time should be investigated.
c. The analytical performance of the electrodes should be investigated by carrying out real sample analysis and comparing the electrode’s performance to that of conventional detection techniques such as ICP-MS.

References

1. Ivaska, A. and J. Bobacka, *PROCESS ANALYSIS | Electroanalytical Techniques*, in *Encyclopedia of Analytical Science (Second Edition)*, P.W.T. Poole, Editor. 2005, Elsevier: Oxford. p. 309-316.
2. Nagajyoti, P.C., K.D. Lee, and T.V.M. Sreekanth, *Heavy metals, occurrence and toxicity for plants: a review.* Environmental Chemistry Letters, 2010. **8**(3): p. 199-216.
3. Järup, L., *Hazards of heavy metal contamination.* British Medical Bulletin, 2003. **68**(1): p. 167-182.
4. Shams, E. and R. Torabi, *Determination of nanomolar concentrations of cadmium by anodic-stripping voltammetry at a carbon paste electrode modified with zirconium phosphated amorphous silica.* Sensors and Actuators B: Chemical, 2006. **117**(1): p. 86-92.
5. Ng, J.C., J. Wang, and A. Shraim, *A global health problem caused by arsenic from natural sources.* Chemosphere, 2003. **52**(9): p. 1353-1359.
6. Patterson, K.Y., P.R. Pehrsson, and C.R. Perry, *The mineral content of tap water in United States households.* Journal of Food Composition and Analysis, 2013. **31**(1): p. 46-50.
7. Prabakar, S.J.R., C. Sakthivel, and S.S. Narayanan, *Hg(II) immobilized MWCNT graphite electrode for the anodic stripping voltammetric determination of lead and cadmium.* Talanta, 2011. **85**(1): p. 290-297.
8. Mirceski, V., et al., *Square-Wave Voltammetry: A Review on the Recent Progress.* Electroanalysis, 2013. **25**(11): p. 2411-2422.
9. Imisides, M.D., G.G. Wallace, and E.A. Wilke, *Designing chemically modified electrodes for electroanalysis.* TrAC Trends in Analytical Chemistry, 1988. **7**(4): p. 143-147.
10. Walcarius, A., P. Mariaulle, and L. Lamberts, *Zeolite-modified solid carbon paste electrodes.* Journal of Solid State Electrochemistry, 2003. **7**(10): p. 671-677.

11. Walcarius, A., *Zeolite-modified electrodes in electroanalytical chemistry.* Analytica Chimica Acta, 1999. **384**(1): p. 1-16.
12. Ojani, R., et al., *Electrochemical behavior of Ni(II) incorporated in zeolite Y-modified carbon electrode: application for electrocatalytic oxidation of methanol in alkaline solution.* Journal of Solid State Electrochemistry, 2011. **15**(9): p. 1935-1941.
13. Taarning, E., et al., *Zeolite-catalyzed biomass conversion to fuels and chemicals.* Energy & Environmental Science, 2011. **4**(3): p. 793-804.
14. Pophale, R., P.A. Cheeseman, and M.W. Deem, *A database of new zeolite-like materials.* Physical Chemistry Chemical Physics, 2011. **13**(27): p. 12407-12412.
15. Moliner, M., C. Martínez, and A. Corma, *Synthesis Strategies for Preparing Useful Small Pore Zeolites and Zeotypes for Gas Separations and Catalysis.* Chemistry of Materials, 2014. **26**(1): p. 246-258.
16. Davis, M.E. and R.F. Lobo, *Zeolite and molecular sieve synthesis.* Chemistry of Materials, 1992. **4**(4): p. 756-768.
17. Sousa-Aguiar, E.F., F.E. Trigueiro, and F.M.Z. Zotin, *The role of rare earth elements in zeolites and cracking catalysts.* Catalysis Today, 2013. **218–219**(0): p. 115-122.
18. Bartlett, J.R., R.P. Cooney, and R.A. Kydd, *Hydrolysis of europium cations in zeolite X: A fourier transform infrared spectroscopic study.* Journal of Catalysis, 1988. **114**(1): p. 53-57.
19. Pang, X., et al., *Effects of metal modifications of Y zeolites on sulfur reduction performance in fluid catalytic cracking process.* Catalysis Today, 2007. **125**(3–4): p. 173-177.
20. Gu, J., et al., *Hydrothermal incorporation of Ce(La) ions into the framework of ZSM-5 by a multiple pH-adjusting co-hydrolysis.* Journal of Porous Materials, 2013. **20**(1): p. 7-13.
21. Zhan, W., et al., *Current status and perspectives of rare earth catalytic materials and catalysis.* Chinese Journal of Catalysis, 2014. **35**(8): p. 1238-1250.

22. Aly, H.M., M.E. Moustafa, and E.A. Abdelrahman, *Synthesis of mordenite zeolite in absence of organic template.* Advanced Powder Technology, 2012. **23**(6): p. 757-760.
23. Sano, T., et al., *Synthesis of large mordenite crystals in the presence of aliphatic alcohol.* Microporous and Mesoporous Materials, 2001. **46**(1): p. 67-74.
24. Li, X., R. Prins, and J.A. van Bokhoven, *Synthesis and characterization of mesoporous mordenite.* Journal of Catalysis, 2009. **262**(2): p. 257-265.
25. Lu, B., et al., *Direct synthesis of high-silica mordenite using seed crystals.* Microporous and Mesoporous Materials, 2004. **76**(1–3): p. 1-7.
26. Fernandes, L.D., et al., *Ethylbenzene hydroisomerization over bifunctional zeolite based catalysts: The influence of framework and extraframework composition and zeolite structure.* Journal of Catalysis, 1998. **177**(2): p. 363-377.
27. Baerlocher, C., L.B. McCusker, and D.H. Olson, *MOR - Cmcm*, in *Atlas of Zeolite Framework Types (Sixth Edition)*, C. Baerlocher and L.B.M.H. Olson, Editors. 2007, Elsevier Science B.V.: Amsterdam. p. 218-219.
28. Kaur, B., M.U. Anu Prathap, and R. Srivastava, *Synthesis of Transition-Metal Exchanged Nanocrystalline ZSM-5 and Their Application in Electrochemical Oxidation of Glucose and Methanol.* ChemPlusChem, 2012. **77**(12): p. 1119-1127.
29. Mojović, Z., et al., *Carbon monoxide electrooxidation on Pt and PtRu modified zeolite X.* Journal of Porous Materials, 2012. **19**(5): p. 695-703.
30. Guzmán-Vargas, A., et al., *Efficient electrocatalytic reduction of nitrite species on zeolite modified electrode with Cu-ZSM-5.* Electrochimica Acta, 2013. **108**(0): p. 583-590.
31. Raoof, J.B., et al., *Synthesis of ZSM-5 zeolite: Electrochemical behavior of carbon paste electrode modified with Ni (II)–zeolite and its application for electrocatalytic oxidation of methanol.* International Journal of Hydrogen Energy, 2011. **36**(20): p. 13295-13300.
32. Li, Y.-J. and C.-Y. Liu, *Silver-exchanged zeolite Y-modified electrodes: size selectivity for anions.* Journal of Electroanalytical Chemistry, 2001. **517**(1–2): p. 117-120.

33. Cao, L., J. Jia, and Z. Wang, *Sensitive determination of Cd and Pb by differential pulse stripping voltammetry with in situ bismuth-modified zeolite doped carbon paste electrodes.* Electrochimica Acta, 2008. **53**(5): p. 2177-2182.
34. Kaur, B. and R. Srivastava, *Simultaneous electrochemical determination of nanomolar concentrations of aminophenol isomers using nanocrystalline zirconosilicate modified carbon paste electrode.* Electrochimica Acta, 2014. **141**(0): p. 61-71.
35. Hincapie, B.O., et al., *Synthesis of mordenite nanocrystals.* Microporous and Mesoporous Materials, 2004. **67**(1): p. 19-26.
36. Mao, Y., et al., *Morphology-controlled synthesis of large mordenite crystals.* New Journal of Chemistry, 2014. **38**(7): p. 3295-3301.
37. Barras, J., J. Klinowski, and D.W. McComb, *27Al and 29Si solid-state NMR studies of dealuminated mordenite.* Journal of the Chemical Society, Faraday Transactions, 1994. **90**(24): p. 3719-3723.
38. Hassaninejad-Darzi, S. and M. Rahimnejad, *Electrocatalytic oxidation of methanol by ZSM-5 nanozeolite-modified carbon paste electrode in alkaline medium.* Journal of the Iranian Chemical Society, 2014. **11**(4): p. 1047-1056.
39. Kokkinos, C., et al., *Lithographically fabricated disposable bismuth-film electrodes for the trace determination of Pb(II) and Cd(II) by anodic stripping voltammetry.* Electrochimica Acta, 2008. **53**(16): p. 5294-5299.
40. Castaneda, M.T., et al., *Sensitive stripping voltammetry of heavy metals by using a composite sensor based on a built-in bismuth precursor.* Analyst, 2005. **130**(6): p. 971-976.
41. Rico, M.Á.G., M. Olivares-Marín, and E.P. Gil, *Modification of carbon screen-printed electrodes by adsorption of chemically synthesized Bi nanoparticles for the voltammetric stripping detection of Zn(II), Cd(II) and Pb(II).* Talanta, 2009. **80**(2): p. 631-635.
42. El Tall, O., et al., *Anodic Stripping Voltammetry of Heavy Metals at Nanocrystalline Boron-Doped Diamond Electrode.* Electroanalysis, 2007. **19**(11): p. 1152-1159.

43. Švancara, I., et al., *Recent Advances in Anodic Stripping Voltammetry with Bismuth-Modified Carbon Paste Electrodes.* Electroanalysis, 2006. **18**(2): p. 177-185.
44. Siriangkhawut, W., et al., *Sequential injection monosegmented flow voltammetric determination of cadmium and lead using a bismuth film working electrode.* Talanta, 2009. **79**(4): p. 1118-1124.
45. Kefala, G. and A. Economou, *Polymer-coated bismuth film electrodes for the determination of trace metals by sequential-injection analysis/anodic stripping voltammetry.* Analytica Chimica Acta, 2006. **576**(2): p. 283-289.
46. Lee, G.-J., H.-M. Lee, and C.-K. Rhee, *Bismuth nano-powder electrode for trace analysis of heavy metals using anodic stripping voltammetry.* Electrochemistry Communications, 2007. **9**(10): p. 2514-2518.
47. Mohamed, M.M., et al., *Synthesis of high silica mordenite nanocrystals using o-phenylenediamine template.* Microporous and Mesoporous Materials, 2005. **84**(1–3): p. 84-96.
48. Edwards, A.J., *H.P. Klug and L.E. Alexander, x-ray diffraction procedures for polycrystalline and amorphous materials : Wiley-Interscience, New York, 2nd edn., 1974, xxv+966 pp. price £ 18.55.* Analytica Chimica Acta, 1975. **77**(0): p. 349.
49. Bor, T.C., et al., *Simulation of X-ray diffraction-line broadening due to dislocations in a model composite material.* Materials Science and Engineering: A, 2001. **309–310**(0): p. 505-509.
50. Müller, M., G. Harvey, and R. Prins, *Quantitative multinuclear MAS NMR studies of zeolites.* Microporous and Mesoporous Materials, 2000. **34**(3): p. 281-290.
51. Gilson, J.-P., et al., *Penta-co-ordinated aluminium in zeolites and aluminosilicates.* Journal of the Chemical Society, Chemical Communications, 1987(2): p. 91-92.
52. Samoson, A., et al., *Quantitative high-resolution 27Al NMR: tetrahedral non-framework aluminium in hydrothermally treated zeolites.* Chemical Physics Letters, 1987. **134**(6): p. 589-592.

53. Thomas, B., B.B. Das, and S. Sugunan, *Rare earth exchanged (Ce3+, La3+ and RE3+) H–Y zeolites as solid acid catalysts for the synthesis of linear alkyl benzenes.* Microporous and Mesoporous Materials, 2006. **95**(1–3): p. 329-338.
54. Zhao, Z., et al., *Alkylation of α-methylnaphthalene with long-chain olefins catalyzed by rare earth lanthanum modified HY zeolite.* Journal of Molecular Catalysis A: Chemical, 2006. **250**(1–2): p. 50-56.
55. Subhan, F., et al., *High desulfurization characteristic of lanthanum loaded mesoporous MCM-41 sorbents for diesel fuel.* Fuel Processing Technology, 2012. **97**(0): p. 71-78.
56. Taghipour, N., et al., *The effect of key factors on thermal catalytic cracking of naphtha over Ce–La/SAPO-34 catalyst by statistical design of experiments.* Journal of Analytical and Applied Pyrolysis, 2013. **99**(0): p. 184-190.
57. Roque da Silva, A.M.S., et al., *Electrochemical studies and square wave adsorptive stripping voltammetry of the antidepressant fluoxetine.* Talanta, 1999. **49**(3): p. 611-617.

Vitae

Name	Ismail Abdulazeez
Nationality	Nigerian
Date of Birth	25^{th} August 1985
Email	ismailchemist2007@yahoo.com
Address	c/o Chemical Sciences Dept. Federal University Kashere, Gombe State, Nigeria
Education Background	Received B.Tech degree in Industrial Chemistry (first class honor) from Abubakar Tafawa Balewa University, Nigeria in 2010.
	Received MS degree in Chemistry from King Fahd University of Petroleum and Minerals, Saudi Arabia in 2015.
Conferences	Participated in the 23^{rd} Annual Saudi-Japan Symposium (KFUPM 2013)
	Theme: Catalysts in Petroleum Refining and Petrochemicals.
	Attended the 3^{rd} Saudi International Nanotechnology Conference (SINC) Riyadh, Saudi Arabia in 2014.